



QEX

\$5

November/December 2016

www.arrl.org

A Forum for Communications Experimenters

Issue No. 299



W8MQW L-network Matchbox uses a stepper-driven vacuum capacitor and a roller inductor.

ARRL
The national association for
AMATEUR RADIO
225 Main Street
Newington, CT USA 06111-1494 USA



New

APRS® / D-STAR®

TH-D74A 144/220/430 MHz Tribander

Introducing the TH-D74A for the ultimate in APRS and D-STAR performance. KENWOOD has already garnered an enviable reputation with the TH-D72A handheld APRS amateur radio transceiver. And now it has raised the bar even further with the new TH-D74A, adding support for D-STAR, the digital voice & data protocol developed by the JARL, and enabling simultaneous APRS and D-STAR operation – an industry first.



- ▼ APRS compliance using packet communication to exchange real-time GPS position information and messages
- ▼ Compliant with digital/voice mode D-STAR digital amateur radio networks
- ▼ Built-in high performance GPS unit with Auto Clock Setting
- ▼ Wide-band and multi-mode reception
- ▼ 1.74" (240 x 180 pixel) Transflective color TFT display
- ▼ IF Filtering for improved SSB/CW/AM reception
- ▼ High performance DSP-based audio processing & voice recording
- ▼ Compliant with Bluetooth, microSD & Micro-USB standards
- ▼ External Decode function (PC Decode 12kHz IF Output, BW:15 kHz)
- ▼ Free software for Memory and Frequency Control Program
- ▼ Data Import / Export (Digital Repeater List, Call sign, Memory Channel)
- ▼ Four TX Power selections (5/2/0.5/0.05 W)
- ▼ Dust and Water resistant IP54/55 standards

APRS (The Automatic Packet Reporting System) is a registered American trademark of WB4APR (Mr. Bob Bruninga).
D-Star is a digital radio protocol developed by JARL (Japan Amateur Radio League).

KENWOOD

Customer Support/Distribution Customer Support:
(310) 639-4200 Fax: (310) 537-8235

www.kenwood.com/usa



ADS#29016

QEX (ISSN: 0886-8093) is published bimonthly in January, March, May, July, September, and November by the American Radio Relay League, 225 Main Street, Newington, CT 06111-1494. Periodicals postage paid at Hartford, CT and at additional mailing offices.

POSTMASTER: Send address changes to: QEX, 225 Main St, Newington, CT 06111-1494 Issue No 299

Publisher
American Radio Relay League

Kazimierz "Kai" Siwiak, KE4PT
Editor

Lori Weinberg, KB1EIB
Assistant Editor

Zack Lau, W1VT
Ray Mack, W5IFS
Contributing Editors

Production Department

Steve Ford, WB8IMY
Publications Manager
Michelle Bloom, WB1ENT
Production Supervisor
Sue Fagan, KB1OKW
Graphic Design Supervisor
David Pingree, N1NAS
Senior Technical Illustrator
Brian Washing
Technical Illustrator

Advertising Information Contact:

Janet L. Rocco, W1JLR
Business Services
860-594-0203 – Direct
800-243-7768 – ARRL
860-594-4285 – Fax

Circulation Department

Cathy Stepina, QEX Circulation

Offices

225 Main St, Newington, CT 06111-1494 USA
Telephone: 860-594-0200
Fax: 860-594-0259 (24 hour direct line)
e-mail: qex@arrl.org

Subscription rate for 6 issues:

In the US: ARRL Member \$24, nonmember \$36;
US by First Class Mail: ARRL member \$37, nonmember \$49;
International and Canada by Airmail: ARRL member \$31, nonmember \$43;
Members are asked to include their membership control number or a label from their QST when applying.

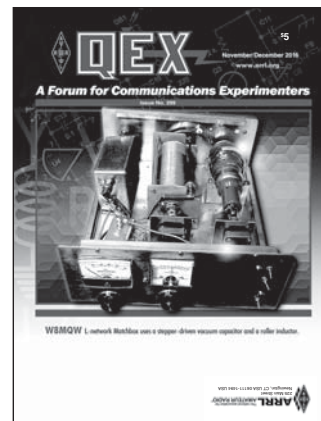
In order to ensure prompt delivery, we ask that you periodically check the address information on your mailing label. If you find any inaccuracies, please contact the Circulation Department immediately. Thank you for your assistance.



Copyright © 2016 by the American Radio Relay League Inc. For permission to quote or reprint material from QEX or any ARRL publication, send a written request including the issue date (or book title), article, page numbers and a description of where you intend to use the reprinted material. Send the request to the office of the Publications Manager (permission@arrl.org).

About the Cover

Charles R. MacCluer, W8MQW, describes a non-iterative two-step matching procedure for an L-network matchbox. The L-network is one of the most common configuration among autotuners. This match box features a stepper-driven vacuum capacitor and a roller inductor.



In This Issue

Features

- 2 Perspectives**
Kazimierz "Kai" Siwiak, KE4PT
- 3 How to Tune an L-network Matchbox**
Charles R. MacCluer, W8MQW
- 5 Determination of Soil Electrical Characteristics Using a Low Dipole**
Rudy Severns, N6LF
- 9 F-Region Propagation and the Equatorial Ionospheric Anomaly**
Jim Kennedy, K6MIO/KH7
- 19 Gray Line Propagation, or Florida to Cocos (Keeling) on 80 m**
Ed Callaway, N4II
- 29 A More Efficient Low-pass Filter**
Gary Cobb, G3TMG
- 36 High-Accuracy Prediction and Measurement of Lunar Echoes**
Joseph H. Taylor, K1JT
- 41 Letters to the Editor**

Index of Advertisers

ARRL	Cover III	Nemal Electronics International, Inc:.....	35
Down East Microwave Inc:.....	40	Quicksilver Radio Products.....	Cover IV
DX Engineering:	25	RF Parts:.....	39, 41
Kenwood Communications:	Cover II	Tucson Amateur Packet Radio:	44

The American Radio Relay League



The American Radio Relay League, Inc. is a noncommercial association of radio amateurs, organized for the promotion of interest in Amateur Radio communication and experimentation, for the establishment of networks to provide communications in the event of disasters or other emergencies, for the advancement of the radio art and of the public welfare, for the representation of the radio amateur in legislative matters, and for the maintenance of fraternalism and a high standard of conduct.

ARRL is an incorporated association without capital stock chartered under the laws of the state of Connecticut, and is an exempt organization under Section 501(c)(3) of the Internal Revenue Code of 1986. Its affairs are governed by a Board of Directors, whose voting members are elected every three years by the general membership. The officers are elected or appointed by the Directors. The League is noncommercial, and no one who could gain financially from the shaping of its affairs is eligible for membership on its Board.

"Of, by, and for the radio amateur," ARRL numbers within its ranks the vast majority of active amateurs in the nation and has a proud history of achievement as the standard-bearer in amateur affairs.

A *bona fide* interest in Amateur Radio is the only essential qualification of membership; an Amateur Radio license is not a prerequisite, although full voting membership is granted only to licensed amateurs in the US.

Membership inquiries and general correspondence should be addressed to the administrative headquarters:

ARRL
225 Main Street
Newington, CT 06111 USA
Telephone: 860-594-0200
FAX: 860-594-0259 (24-hour direct line)

Officers

President: Rick Roderick, K5UR
PO Box 1463, Little Rock, AR 72203

Chief Executive Officer: Tom Gallagher, NY2RF

The purpose of *QEX* is to:

- 1) provide a medium for the exchange of ideas and information among Amateur Radio experimenters,
- 2) document advanced technical work in the Amateur Radio field, and
- 3) support efforts to advance the state of the Amateur Radio art.

All correspondence concerning *QEX* should be addressed to the American Radio Relay League, 225 Main Street, Newington, CT 06111 USA. Envelopes containing manuscripts and letters for publication in *QEX* should be marked Editor, *QEX*.

Both theoretical and practical technical articles are welcomed. Manuscripts should be submitted in word-processor format, if possible. We can redraw any figures as long as their content is clear. Photos should be glossy, color or black-and-white prints of at least the size they are to appear in *QEX* or high-resolution digital images (300 dots per inch or higher at the printed size). Further information for authors can be found on the Web at www.arrl.org/qex/ or by e-mail to qex@arrl.org.

Any opinions expressed in *QEX* are those of the authors, not necessarily those of the Editor or the League. While we strive to ensure all material is technically correct, authors are expected to defend their own assertions. Products mentioned are included for your information only; no endorsement is implied. Readers are cautioned to verify the availability of products before sending money to vendors.

Kazimierz "Kai" Siwiak, KE4PT

Perspectives

Guest Editorial from the President of TAPR

If you are reading *QEX*, you may be a connoisseur of all things technical. That in this hobby of Amateur Radio you enjoy the time on the bench as much as time on the air. Technical connoisseurs enjoy reading and sharing ideas. We love telling others about our journeys.

Sharing comes in many forms. Today, with this marvelous invention called the Internet, information and facts abound. But if the information and facts are not put into the context of a journey, then they are mundane. For it is not the distance from *A* to *B* that we want to read about, it's the path from *A* to *B* with all its side roads and dead ends we wish to hear. It is from the journey that we learn from others.

It has been the mission of *TAPR* to help experimenters on their journey. *TAPR* has helped many experimenters get their projects into the hands and minds of others through funding, technical support — both in development and manufacturing — and the co-production of the Digital Communications Conference with the ARRL.

We have just finished the 35th Annual DCC in St. Petersburg, Florida this past September. The DCC shares information in a printed proceeding and on *YouTube* thanks to Gary Pearce, KN4AQ, for his expert video production. You can view well over one hundred talks at <https://goo.gl/ZMTZCG>.

There are many Amateur Radio technical conferences you can attend — DCC, Microwave Update, Central States VHF Society Conference, and the AMSAT Symposium to name a few. If you have not had the chance to attend one, I highly recommend it. The one element that you can get only from attending a conference is socializing and sharing. That is the one great multiplier when you personally attend. You will come away inspired and energized. You will also be supporting the conference because this is the only way they can survive.

Many of the conferences bounce from city to city in an effort to allow local folk to attend without the expense of an airplane ticket and hotel stay. When one of these conferences comes to your backyard, attend it! See for yourself what a fantastic experience it is.

The grandest way you can support a conference is to tell about your journey on one of your projects. Don't feel that you are not smart enough, or that your project is not significant to present. Nothing is further from the truth. Everyone loves to hear about your journey. Tell the audience about what you learned, the frustration you experienced, about the dirt roads and how to avoid them, and the satisfaction you felt as you completed it. Getting up in front of an audience at a technical conference is most therapeutic if not euphoric!

Share your journey. We are all in this great hobby together and we love a good technical yarn.

Steven Bible, N7HPR,
President, TAPR, www.tapr.org

In This and Future Issues

Our *QEX* authors describe propagation measurements and modes, filter characteristics, and tuning an L-network. Put your favorite topic, or innovative measurement, or technical journey on paper. Share it on these pages with fellow readers. Just follow the details on the www.arrl.org/qex-author-guide web page, and contact us at qex@arrl.org. We value your feedback, comments and opinions about these pages.

In this issue, Joe Taylor, K1JT, describes and tests his new *EMEcho* software to predict and measure Doppler shift, frequency spread, and polarization of EME signals at 144 and 432 MHz using amateur equipment. Gary Cobb, G3TMG compares Zolotarev low pass-band characteristics with the classical Chebyshev designs and shows a universal table of values that can be used in filters for Amateur Radio bands. Ed Callaway, N4II, investigates mechanisms responsible for gray line propagation on the low bands. Jim Kennedy, K6MIO/KH6, describes unique ionization pattern forms in the ionosphere above the Earth's geomagnetic dip equator, that provide for various of F-region propagation at 6 m. Charles MacCluer, W8MQW, describes a non-iterative two-step process for matching an L-network. Rudy Severns, N6LF, explores measurements of soils characteristics in the 80 m band. Flavio Egano, IK3XTV, followed long term observations that suggest long path echoes might propagate with low attenuation by ionospheric ducts.

Please continue to support *QEX*, and help it remain a strong technical publication.

73,
Kazimierz "Kai" Siwiak, KE4PT

How to Tune an L-network Matchbox

W8MQW describes a non-iterative two-step matching for an L-network.

A very common matchbox design is the L-network of Figure 1. It is certainly the most common design among autotuners. Manually tuning such matchboxes is an iterative process, where an initial guess is made for the L and C , then by watching SWR, refinements are made alternately to L and C until SWR has been lowered to an acceptable level. Some autotuners employ simple bisection searches for minimal SWR, or at the other extreme, some use sophisticated frequency sampling equation solving predictor/correctors. But tuning an L-network need not be an iterative process — it can in theory be done in two simple steps if a second parameter in addition to SWR is observed during tuning.

Two-step Matching

Let us first develop these two steps for the special case of matching a pure resistance R greater than $50\ \Omega$. The impedance Z of Figure 1 presented to the transmitter is, by the standard arithmetic of series and parallel impedances,

$$Z = \frac{RX_C^2}{R^2 + X_C^2} + jX_L - j\frac{R^2 X_C}{R^2 + X_C^2} \quad [1]$$

So the obvious approach is to proceed in two simple non-iterative steps.

Step 1. Adjust the capacitor to bring the real part of Z to $50\ \Omega$.

That is, choose X_C so that

$$\frac{RX_C^2}{R^2 + X_C^2} = 50 \quad [2A]$$

This is mathematically possible since the left hand side of [EQ 2A], as an increasing function of X_C , takes on each value between 0 and R exactly once. As an aside, this shows that an L-network has at most one possible matching solution.

Step 2. Adjust the inductor L to bring the reactive part of Z resulting from Step 1 to zero. That is, choose X_L so that

$$X_L = \frac{R^2 X_C}{R^2 + X_C^2} \quad [2B]$$

But is This Doable?

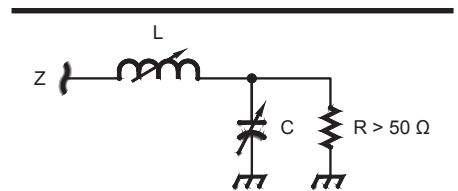
The second step is easy once the first is completed. Merely adjust the inductor for zero return power, i.e., SWR = 1. But is there a method to steer the tuning of the capacitor to accomplish Step 1? Can we, or a CPU, observe some voltage that we may null to achieve Step 1?

Think of the left end of the network of Figure 1 as the beginning of a $50\ \Omega$ transmission line of length zero. If V_f and V_r are the forward and reflected voltages on this line, then because the value of Z is the quotient of the net voltage across it divided by the net current through it, and because the reflected current travels in the reverse direction¹,

$$Z - 50 = \frac{V_f + V_r}{V_f/50 - V_r/50} - 50 = \frac{100V_r}{V_f - V_r} \quad [3]$$

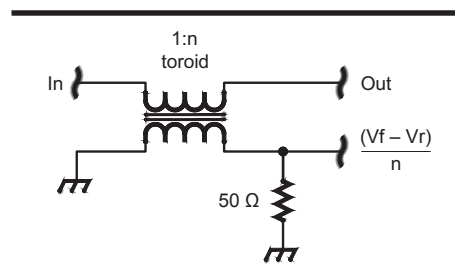
Thus $Z - 50$ is purely reactive exactly when the two voltages V_r and $V_f - V_r$ are in quadrature.

So the crucial voltage to null in order



QX1609-MacCluer01

Figure 1 — A common L-network matchbox that transforms R to Z .



QX1609-MacCluer02

Figure 2 — Forward and reflected currents subtract in this current sampler.

to achieve Step 1 is the dc phase voltage from a phase detector that compares V_r to $V_f - V_r$. This dc voltage will be zero only at a 90-degree phase shift. The reflected voltage V_r is of course obtainable from the reflected port of a tandem coupler, while the difference voltage $V_f - V_r$ is obtainable from a current sampler, such as in Figure 2.

Matching reactive loads

Almost certainly, a matchbox will be asked to match loads with both resistive and reactive parts. Thinking of such a load in its

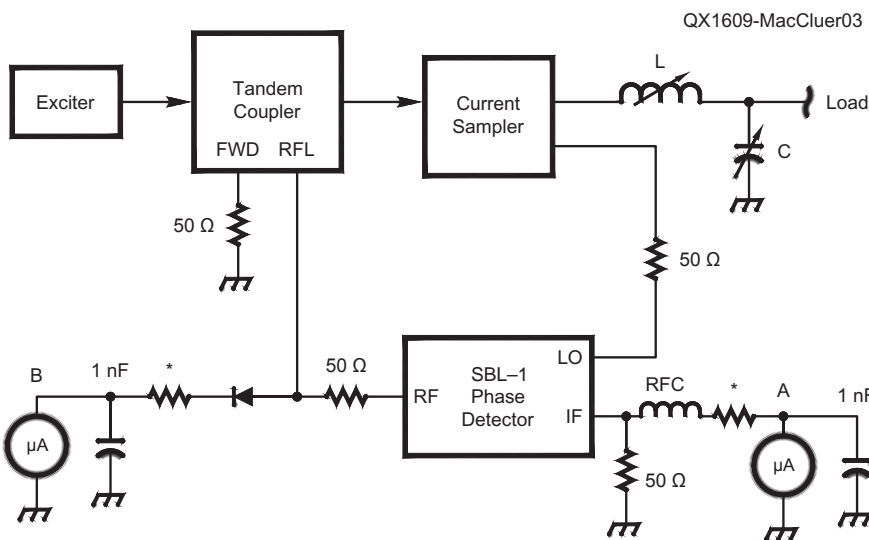


Figure 3 — The matchbox in block form. The user (or CPU) zeros meter A phase voltage by adjusting C, then zeros meter B reflected voltage by adjusting L. Attenuators (not shown) reduce the sampled voltages when operating high power.

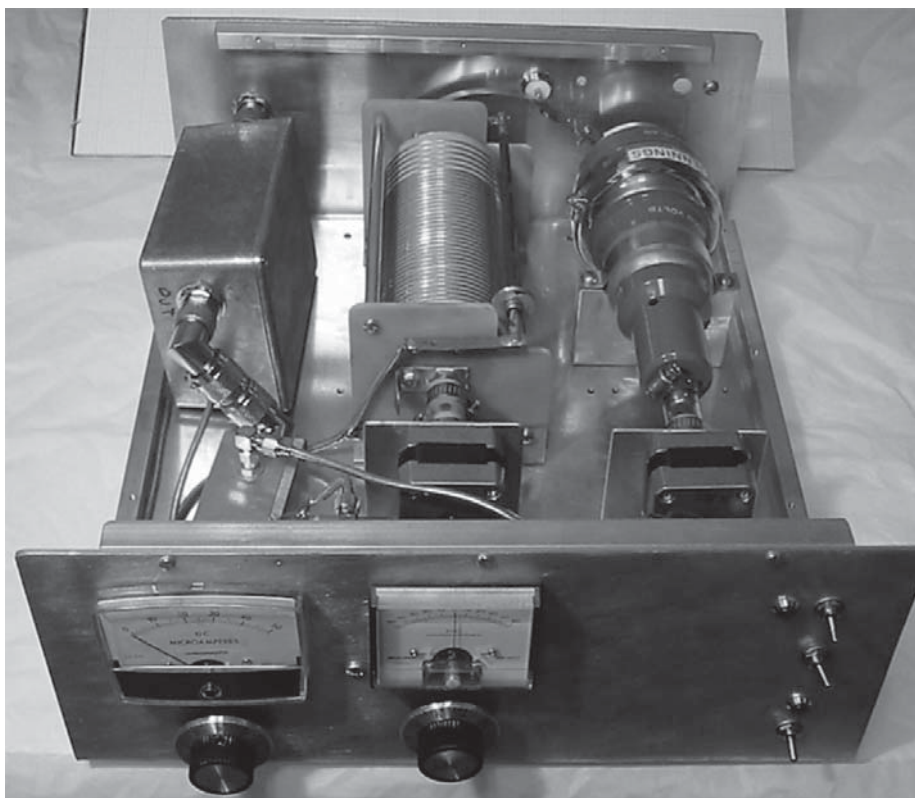


Figure 4 — The L-network matchbox with stepper-driven vacuum capacitor and roller inductor.

parallel equivalent, its reactive part can be thrown onto the shunt capacitive reactance of C, and the algorithm proceeds in two steps as before, as long as the series resistive part exceeds 50 Ω.

To extend the capabilities of any L-network to handle resistive parts less than 50 Ω, the shunt capacitor must of

course be switched from the antenna to the transmitter side of the network. In this case, the algorithm is as before: phase voltage is zeroed by the capacitor, return voltage by the inductor.

Proof of Concept

To verify this simple two-step algorithm, I

built a simple L-network tuner with the block diagram of Figure 3. Referring to this figure, the algorithm therefore becomes:

Step 1. Null out the center-zero meter A by adjusting C.

Step 2. Null the meter B by adjusting L.

Again note that this is a simple two-step process, *not* an iterative process.

The Construction Project Sketched

A 28 μH roller inductor was obtained from Palstar. The capacitor used was a Jennings 1000 pF vacuum variable. Each is turned by a small 28 oz-in stepper motor from Adafruit. The two steppers are directed by an Arduino UNO R3 and an Adafruit motor shield. The Arduino reads the user's intent from two panel-mounted 10 kΩ potentiometers, see Figure 4. These two CPU-controlled stepper motors were used in anticipation of eventually implementing automatic tuning.

The tandem coupler used was the inestimable design by Larry Phipps, N8LP.² The tandem and current sampler of Figure 3 were built in separate cast-aluminum boxes, see Figures 5 and 6.

The phase detector employed was a Mini-Circuits SBL-1, see Figure 7. All the sampled forward and return voltages from the coupler and current sampler are of a level that no active devices are required when tuning with 10 W. Not shown in the block diagram of Figure 3 are attenuator pads that lower sample levels during normal operation after tuning is completed.

Theory Collides with Practice

Alas, in actual operation, the L and C controls interact somewhat, especially on higher frequency bands. On 160 and 80 practice closely matches theory, with the two-step algorithm yielding a match with little post adjustment. But as the frequency rises, the real-world stray L/C/R of the components and wiring begin to induce interaction. Another cause of this divergence from theory is that theoretical performance is predicated on the source being a perfect 50 Ω voltage source, while during matching the reflected currents disturb the characteristics of the source. But the dominant source of this interaction is that phase difference reported by the phase detector depends not only upon the phases, but upon the amplitudes of the two inputs to the detector. To obtain true two-step tuning would require the use of a logarithmic amplifier such as the AD8302 to swamp out this effect from the input amplitudes. When the matching process is observed as a Lissajous display, (V_r against $V_f - V_r$), convergence to a match follows theory.

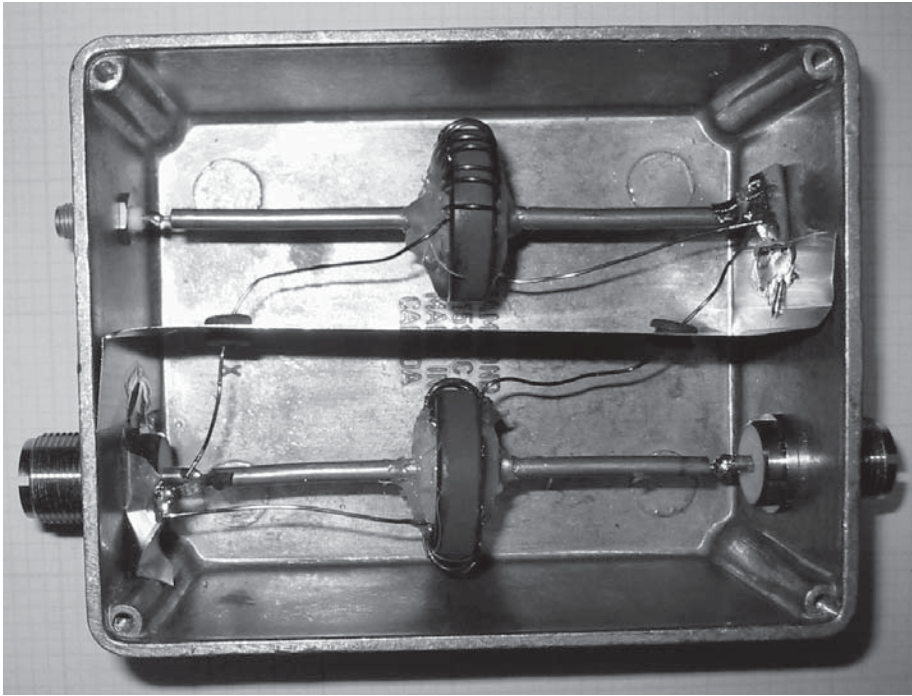


Figure 5 — Tandem coupler design by Larry Phipps, N8LP.

But even with the minor interaction of the L and C controls, convergence to match is much quicker because of the added information available from the phase voltage. If phase voltage is negative, decrease C ; if phase voltage is positive, increase C . Thus the $50\ \Omega$ real part is matched immediately. Then proceed in the usual way to a one-to-one match by adjusting L .

Some Final Thoughts

To save space, the current sampler of Figures 2 and 6 could possibly be incorporated into the tandem coupler of Figure 5 by adding its toroid as a second toroid on the through line. I did not try this.

Both meter A and B can be any $100\ \mu\text{A}$ or smaller ammeters. The meter A must be a center-zero meter since the phase detector reports both positive and negative voltages. Select by trial and error the current limiting resistors, marked ‘*’, for your particular meters. As a starting point try $1\ \text{k}\Omega$.

The fortuitous levels of the sampled voltages require no active devices. This permitted all signals to be piped about with my favorite coax, RG402 semi-rigid coax with SMA connectors, lending a microwave look to the construction.

This algorithm is valid for any L network

matchbox, whether it is a balanced network preceded by a balun or an unbalanced network followed by a balun.

It would be easy to add an outboard current sampler and phase detector plus meter to existing manual L -network tuners to achieve expedited two-step tuning.

Displaying V_r (horizontal input) against $V_f - V_r$ (vertical input) as an oscilloscope Lissajous diagram is an exceptionally efficient aid in finding a match — one adjusts C to rotate the ellipse vertical, then L to shrink the ellipse to a vertical line.

An outboard current sampler/phase detector/meter might also speed T -match tuning.

The above matchbox construction details were merely sketched. Instead the thrust of this note is to reveal that *tuning an L network need not be a tedious iterative process*. It can in theory be done in two steps by carefully observing two simple-to-measure voltages.

Acknowledgements

This project grew from a challenge from Gary Adamowicz, WA1OXT, who is developing a competing approach. I thank Mike Blake, K9JRI, and Chuck Hawley, KE9UW, for their many helpful comments and suggestions.

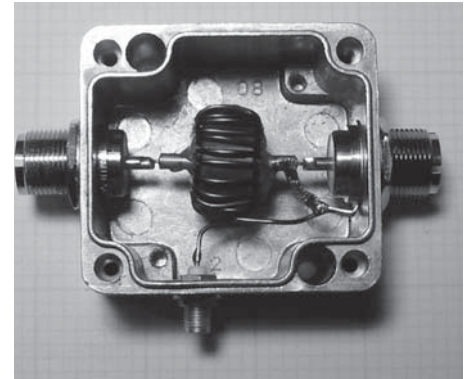


Figure 6 — The current sampler used to sample the difference between forward and reflected voltage.

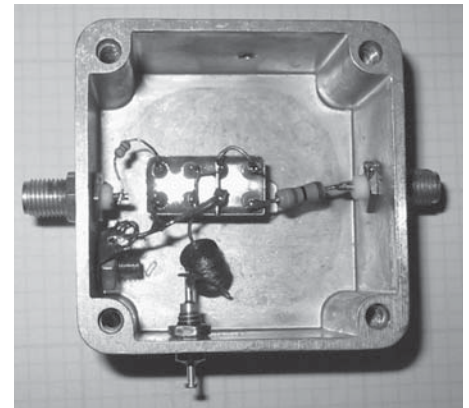


Figure 7 — A phase detector employing a MiniCircuits SBL-1.

Chuck MacCluer, W8MQW, was first licensed in 1952 with the novice call sign WN8MQW, and progressed to Amateur Extra license. He has been very active in EME on 432 and 1296 MHz, and recently is active on SSB, CW, and digital modes on 160, 80, and 40 meters. Chuck received a PhD in Mathematics in 1966 from the University of Michigan and is now Professor Emeritus of Mathematics at Michigan State University. Chuck is a Life member of ARRL, IEEE, SIAM, and ASHRAE.

Notes

¹The intermediate quotient of [EQ 3] is the core computation that underlies the Smith Chart. ARRL item no. 0413, available from your ARRL dealer, or from the ARRL Store, Telephone toll-free in the US 888-277-5289, or 860-594-0355, fax 860-594-0303; www.arrl.org/shop/; pubsales@arrl.org.

²L. Phipps, N8LP, “The LP-100 Wattmeter”, *QEX*, Jan/Feb 2006.

Determination of Soil Electrical Characteristics Using a Low Dipole

N6LF shows how to create a universal chart showing antenna impedance values for a wide range of soils that map to the average values of σ and E_r for the soil over which the antenna is installed.

Rick Karlquist, N6RK, asked on the top-band reflector about placing a dipole on the ground surface to derive soil electrical characteristics — conductivity (σ) and relative dielectric constant (E_r) — from impedance measurements of the dipole. A short discussion of this technique has appeared in the last few editions of *The ARRL Antenna Book*.¹ For some years I've used the ground probe approach² to measure soil characteristics so I hadn't paid much attention, but in some situations this method may have advantages over the soil probes and is worth considering. The probe approach gives the values for a small volume of soil around the probe, down to a depth of 3 ft or so. If you want to map the properties of a large area you need to make multiple measurements at different locations. The low-dipole approach on the other hand intrinsically averages the properties of a much larger area below the

antenna and for a couple of skin depths down into the soil. The *ARRL Antenna Book* discussion was pretty limited so I decided to expand on it using antenna modeling software combined with a spreadsheet.

If you have a program that accurately models the soil-antenna interaction (such as NEC4) then you can use the antenna of your choice at whatever frequency you are interested in, see Example 2. Most amateurs don't have this software but the technique can still be used. With some prompting from Rick, N6RK, I realized that if the antenna dimensions — length, height, wire size, etc. — and measurement frequency are predefined then it is possible to create a universal chart with contours showing values of R_i and X_i for a wide range of soils. If the antenna is fabricated as specified, and impedance is measured at the specified frequency, the measured impedance can be

plotted directly on the graph yielding a good estimate of the average values of σ and E_r for the soil over which the antenna is installed. As a practical matter the reference antenna needs to be something easy and inexpensive to build. For that purpose a low dipole works well, and details of a suggested design are given in Example 1. From a practical point of view it is necessary to have a predefined antenna for each band. In this article I've chosen 80 m for demonstration purposes.

What frequency, lengths and heights?

The height above ground z and test antenna length L will depend on the frequency of interest. At what frequency within the band should we make the measurement or do we need to measure across the band? Figures 1 and 2 show examples of actual measured values for σ and E_r at my home site using soil probes.

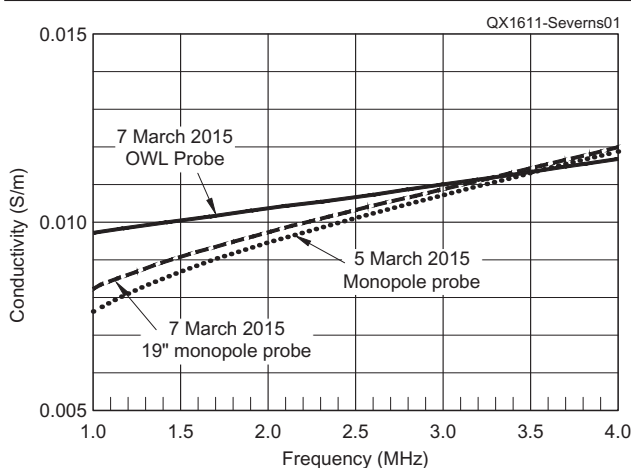


Figure 1 — Soil conductivity σ at N6LF.

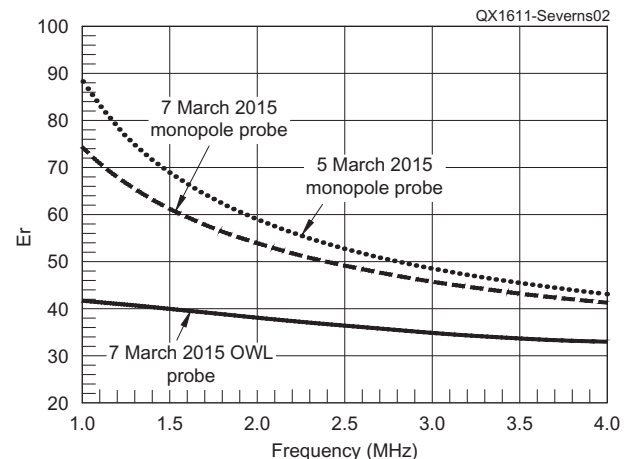


Figure 2 — Soil relative permittivity E_r at N6LF.

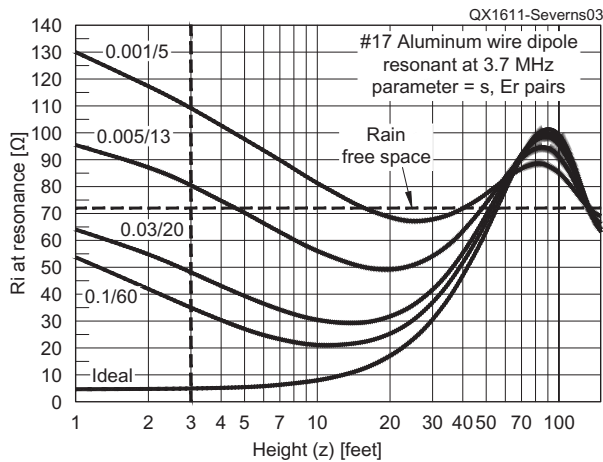


Figure 3 — R_i at resonance versus z for typical σ, E_r pairs.

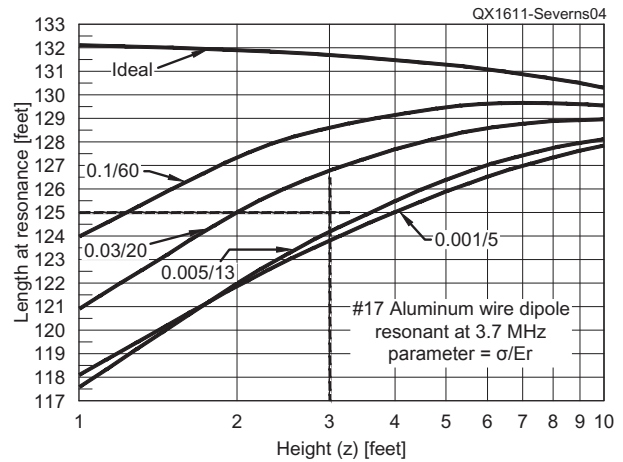


Figure 4 — Effect of height and ground constants on resonant length at 3.7 MHz.

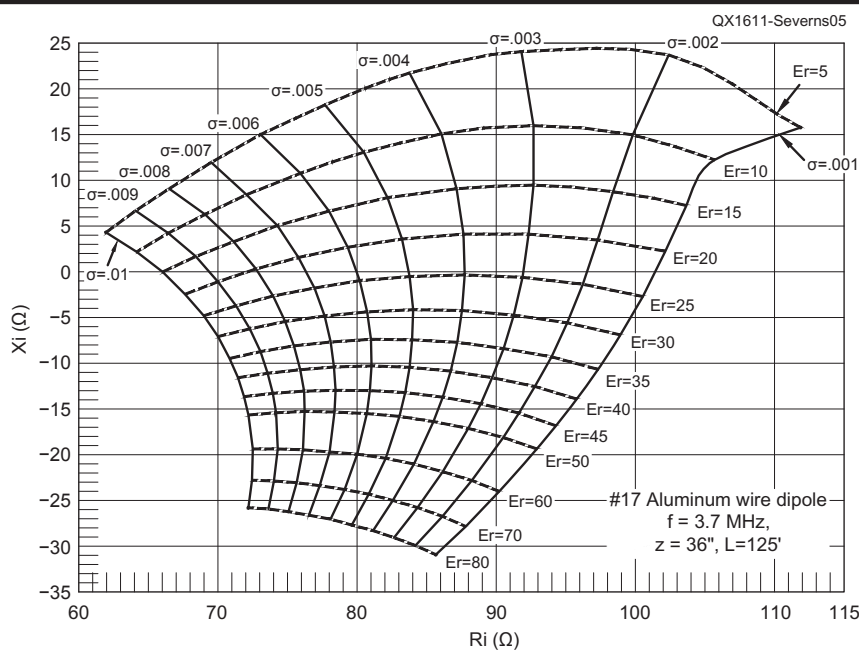


Figure 5 — X_i versus R_i for $0.001 < \sigma < 0.01$ and $5 < E_r < 80$.

Over the 80 m band (3.5-4.0 MHz), conductivity is $0.011 < \sigma < 0.012$ S/m and relative permittivity is $41 < E_r < 43$. This is a pretty small range and a measurement near mid-band, say 3.7 MHz, should be more than accurate enough. Remember, we are not trying for 1% accuracy, $\pm 20\%$ will do just fine. The modest change of values shown over the 80 m band is typical of most soils. Other bands are much narrower in percentage of center frequency so the changes are even smaller. A single frequency measurement is adequate for each band.

Strictly speaking, the test antenna does not have to be resonant but there are practical measurement advantages to not being too far from resonance. As you move away from resonance the values for R_i and X_i will

begin to change fairly rapidly. Many of the instruments used to measure impedance don't handle very well impedances less than 10 Ω or greater than a few hundred ohms. The impedance values are smaller close to series resonance.

The next question is "how high"? Figure 3 shows the effect of various soils (typical σ and E_r pairs) at a range of heights when the antenna is tuned to resonance at each point. For heights between 1 and 10 ft the contours are well separated, promising reasonable resolution for variations in σ and E_r . However, at greater heights the contours begin to tighten up making resolution a problem. It looks like any height z between 1 and 10 ft should work. I chose 36 in because it's a very convenient working height. Since

standard electric fence hardware is well suited for this kind of field measurement, 36 in corresponds to a standard insulated electric fence post — a practical detail passed to me by N6RK.

For a given height and resonant frequency, the resonant length will depend on the values for the ground constants as shown in Figure 4. For calculations at 3.7 MHz with $z=36$ in, $L=125$ ft is a reasonable compromise.

A universal graph for 80 m

If we have a physical description of the antenna in terms of height above ground z , length L , wire size, etc., we can model the antenna at a single frequency f using a wide range of values for σ and E_r . This will give us values for the feed-point impedance $Z_i = R_i + jX_i$ at a given frequency for each pair of σ and E_r values. Using a spreadsheet we can then graph R_i versus X_i — which are the quantities we can actually measure on a test antenna — as functions of σ and E_r , with R_i on the x -axis and X_i on the y -axis, where σ and E_r are parameters defining the contours. After measuring the feed-point impedance at f we can plot the measured R_i and X_i pair as a point on the graph. I used EZNEC pro³ with NEC4.2 and an Excel[®] spreadsheet software, AutoEZ⁴, to automate the calculations and graph them. From earlier work I did on verifying the accuracy of NEC4 for wires close to ground I found that the fitting at the feed point has a shunt capacitance of about 6 pF. This has been added to the model.

With $L=125$ ft, $z=36$ in and $f=3.7$ MHz we graph X_i versus R_i as functions of σ and E_r (Figures 5 and 6). The dashed contours represent $5 < E_r < 80$ and the solid contours represent $0.001 < \sigma < 0.01$ S/m (Figure 5), and $0.01 < \sigma < 0.03$ S/m (Figure 6). This range of values should cover most common soils that amateurs are likely to encounter. If this doesn't work for your site then you can use the

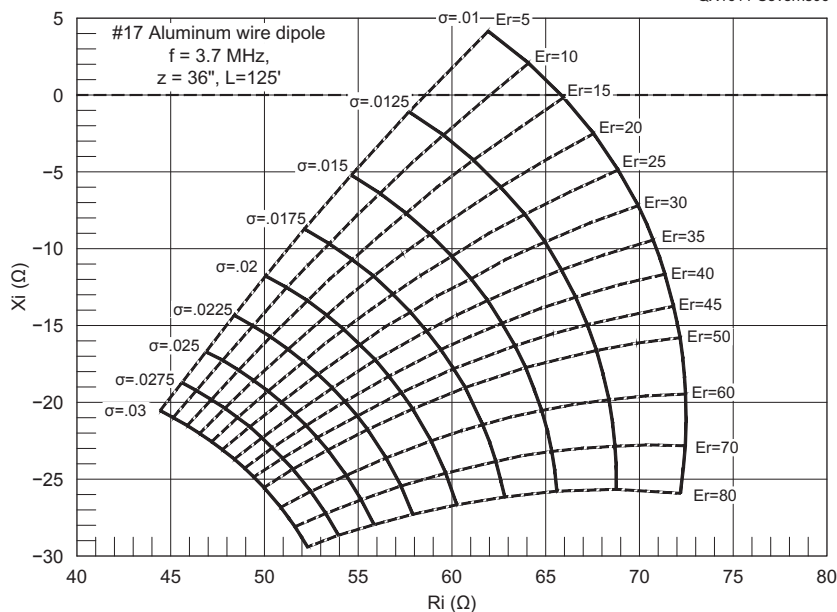


Figure 6 — X_i versus R_i for $0.01 < \sigma < 0.03$ and $5 < E_r < 80$.

procedure described in Example 2 to generate your own graph using NEC4 software.

Note that I've cut Figure 6 off for σ greater than 0.03 S/m. As the conductivity increases the scale compresses rapidly. In fact if we push σ all the way to infinity (perfectly conducting soil) Z_i converges to a single point at $Z_i = 4.2 - j76.5 \Omega$. Most amateurs are not blessed with soil of this high conductivity so this limitation is not that serious. For higher conductivity soils ground probe measurements are probably a better method.

Example 1

Figures 7 and 8 are photos of the mechanical arrangements for typical test antenna using standard #17 AWG aluminum electric fence wire and hardware widely available in hardware and farm stores. The electric fence wire is suspended at 36 in on fiberglass (F/G) wands, with yellow plastic wire clips that slide up/down the wands for height adjustment. The wands were spaced 10 to 20 ft apart and the wire is anchored at the ends to steel fence posts 6 to 10 ft away from the ends of the wire. Multiple support points and significant wire tension kept the droop to less than 0.25 in. High quality insulators and non-conducting Dacron line were used at the wire ends. Figure 7 shows the Budwig center connector and the common mode choke (balun) at the feed-point. The center connector and choke introduce approximately 6 pF of shunt capacitance across the feed point, which must be added to the model. The steel fence post at the midpoint shown in Figure 8 was replaced with the F/G wand shown in Figure 7.

The measured impedance of the common mode choke is shown in Figure 9. The choke comprises two Fair-Rite 2631665702 type

31 cores taped together to form a binocular core. The winding is six turns of RG174/U 50 Ω mini-coax.

Example 2

If NEC4 based software is available then you can create your own charts using your choice of antenna, as follows. We assume a horizontal center-fed dipole made with #17 AWG aluminum wire at a height z of 36 in. After tuning to resonance at 3.5 MHz the length L is 131.11 ft. The measured feed-point impedance Z_i at 3.5 MHz is $80.26 + j0 \Omega$. From this we can determine the values for σ and E_r at 3.5 MHz. First create the NEC4 model using #17 AWG aluminum wire 131.11 ft long and 36 in above ground. Since we do not know the values for σ or E_r , we'll run the model repeatedly with a range of possible values for σ and E_r . If we're too far off in our choice of values the process should point the



Figure 7 — Center connector and feed-point support. [Rudy Severns, N6LF, photo.]

way to go. In this case the trial values will be $0.001 < \sigma < 0.01$ S/m and $1 < E_r < 50$. Running the model repeatedly, we can determine Z_i for a matrix of σ and E_r values. A spreadsheet, sample included in the *QEXfiles*, is a good way to keep track of results.⁵

Using the spreadsheet we can graph a more restricted set shown in Figure 10. The measured value of Z_i for the antenna at 3.5 MHz is $80.26 + j0 \Omega$. A dot with a label has been placed at that value on the graph. We see our matrix of values has bracketed this value nicely. The $\sigma = 0.005$ S/m line passes right through Z_i . Also, Z_i lies between the $E_r = 10$ and $E_r = 15$ lines, right around $E_r = 13$. We could repeat the process for multiple values of E_r around 13 to refine the answer further, but from a practical point of view we're already close enough. With $\sigma = 0.005$ S/m and $E_r = 13$, we have average soil.



Figure 8 — Test antenna supported with F/G wands. [Rudy Severns, N6LF, photo.]

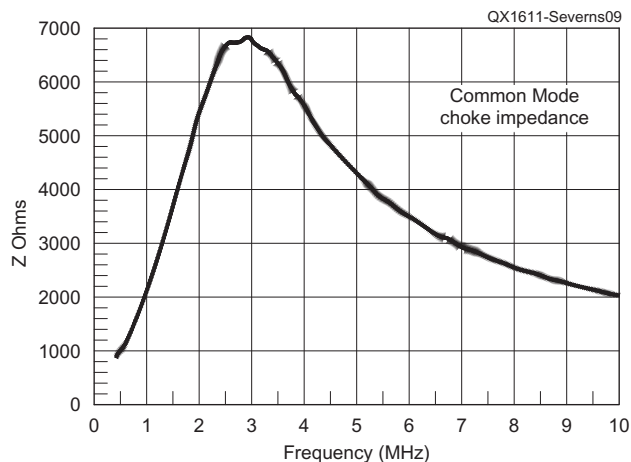


Figure 9 — Common mode choke impedance.

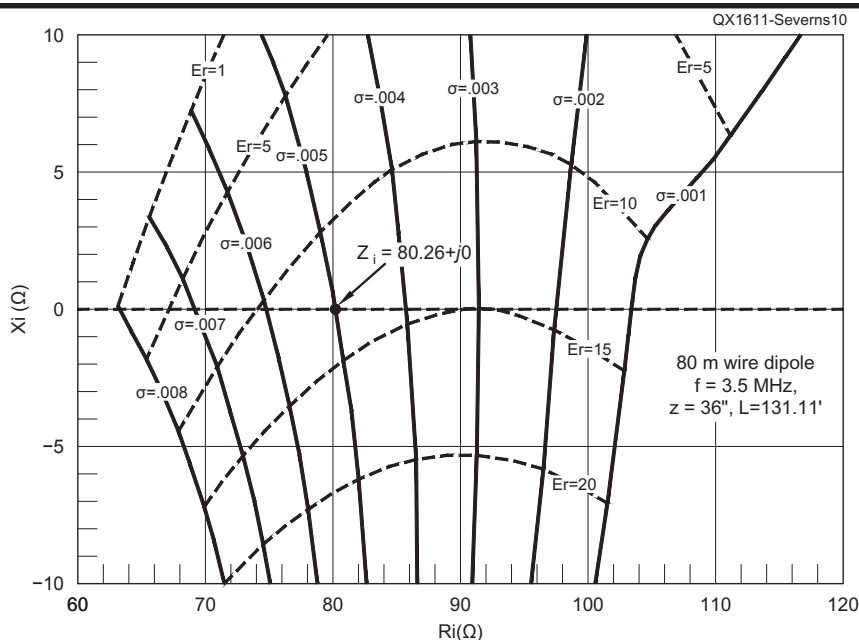


Figure 10 — Graph of R_i versus X_i for a range of σ and E_r values at 3.5 MHz.

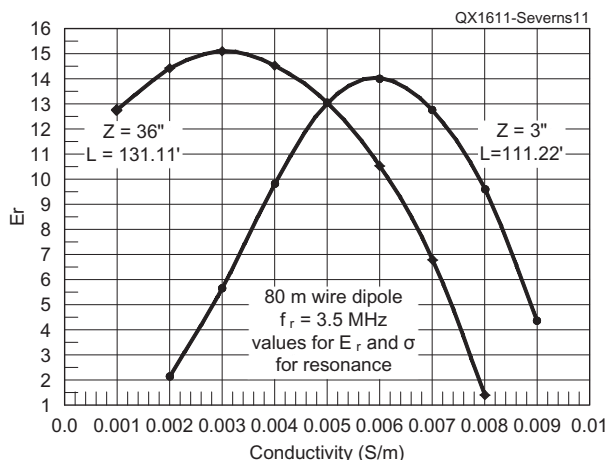


Figure 11 — Values for σ and E_r that result in the resonant lengths shown at 3.5 MHz.

Example 3

If you have the requisite modeling software but not the impedance measuring equipment it is possible to determine σ and E_r by resonating the antenna at a given frequency at two different heights and then, modeling these two configurations — trying different L and z — and graphing the values for σ and E_r that correspond to the same resonant frequency. Figure 11 shows the procedure. Here $f=3.5$ MHz, and at $z=3$ in length $L=111.11$ ft, while at $z=36$ in $L=131.11$ ft. The two curves intersect at $\sigma=0.005$ S/m and $E_r=13$.

Summary

There are several ways to use a low dipole to determine soil electrical characteristics. However, you will need either NEC4 software or a good impedance measuring instrument or both to do this. The ground probe method does not rely on modeling but it does require a reasonably good impedance measuring instrument capable of showing R and X as well as the sign of X . Low dipole measurements have the advantage of giving a realistic average of the soil characteristics over a substantial area and down a few skin depths into the soil. Ground probe measurements generally give the characteristics over a small volume of soil, and multiple measurements are required to cover a large area. Each has advantages and limitations but both will work.

Acknowledgements

I would like to acknowledge the help that Rick Karlquist, N6RK, provided by reading my early drafts and asking many questions that needed some thought to answer. My thanks to George Cutsogorge, W2VJN, for relaying Ricks original top-band query.

Rudy Severns, N6LF, was first licensed as WN7AWG in 1954. He is a retired electrical engineer, an IEEE Fellow and ARRL Life Member.

Notes

¹Pages 3-31 to 3-33 in, *The ARRL Antenna Book*, 22nd edition, 2011. Available from your ARRL dealer or the ARRL Bookstore, ARRL item no. 6948. Telephone 860-594-0355, or toll-free in the US 888-277-5289; www.arrl.org/shop; pubsales@arrl.org.

²R. Severns, N6LF, "Measurement of Soil Electrical Parameters at HF", *QEX* Nov/Dec 2006, pp 3-9. Available at www.antennasbyn6lf.com.

³Several versions of EZNEC antenna modeling software are available from developer Roy Lewallen, W7EL, at www.ez nec.com.

⁴AutoEZ for EZNEC, see www.ac6la.com.

⁵See www.arrl.org/qexfiles.

F-Region Propagation and the Equatorial Ionospheric Anomaly

Unique ionization patterns form in the ionosphere above the Earth's geomagnetic dip equator, which provide several variations of F-region propagation recently displayed on 6 m.

A version of this article appeared in the Proceedings of the 48th Annual Conference of the Central States VHF Society, Austin, Texas, July 24-27, 2014.

The 6-m band has always been a fascinating place to study radio propagation. This is partly because ionospheric propagation is relatively rare, at least compared to lower frequency bands. As a result, when something does happen, usually it's easier to determine *what* happened. Despite the poor solar activity numbers, the long-awaited peak of the Sun's southern hemisphere has created a — perhaps brief — bump in 6-m F-layer propagation. This was especially obvious in the upsurge of DX paths during the northern fall of 2013 and spring of 2014. Much of this flurry of activity involved the geomagnetic equator and the *Equatorial Ionospheric Anomaly* (EIA).

The EIA is a unique set of ionization patterns that forms in the E layer above the Earth's geomagnetic equator, specifically the *dip* equator. The dip equator is a line around the Earth showing where the Earth's magnetic field is exactly parallel to the Earth's surface.

The ionization patterns that form along this line provide for a number of variations of F-region propagation, including Transequatorial Propagation (TEP). These propagation types have been around for years. But for some, they are not broadly recognized as distinct forms, and though commonly referred to as TEP, not all of them are TEP. Nevertheless, like balls on a billiards table, the EIA and its effects can really bounce things around. Recently, 6 m has displayed a number of these modes, and

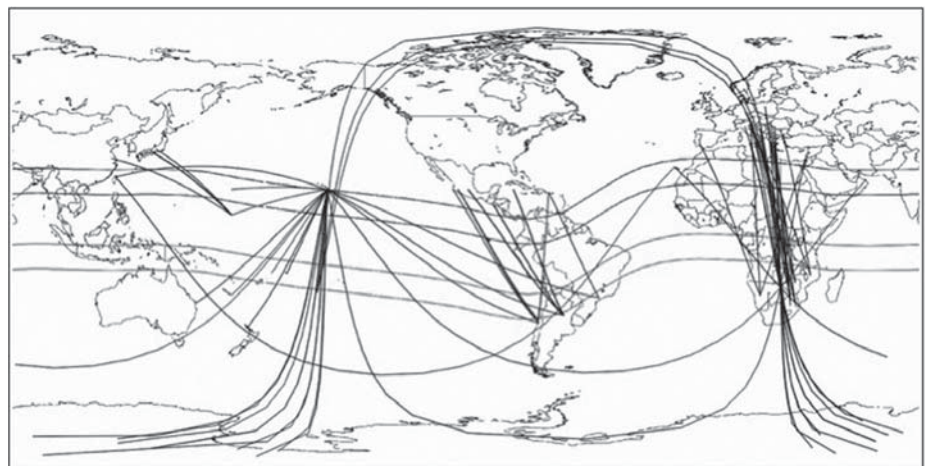


Figure 1 — Several distinct F-layer paths are rooted in the Equatorial Ionospheric Anomaly. Five are shown: aTEP, eTEP, 1- and 2-hop F2, and transpolar long path (TPL). [G.Projector map and overlays.]

a few examples are shown in Figure 1.

If the gloomy outlook for the next coming solar Cycle 25 comes to pass, as predicted by a number of prominent solar physicists, then some of the lessons learned at 6 m may well become relevant, not only to 6 and 10 m, but also 12, 15, and 17 m, and maybe even 20 m. The good news is that there are quite a variety of related, but different, F-region skip modes that vitally hinge on the rather special ionospheric conditions that occur in the general vicinity of the dip equator.

Basic Ionospheric Skip

The following review points out a few of the key components that make ionospheric propagation work, and which are important to understanding some of the propagation puzzles.

Ionization

The F2 region lies above about 250 km and goes upward beyond 1500 km. The ionization of the F layer is due primarily to extreme ultraviolet (EUV) radiation from the Sun. When a solar EUV photon collides with a neutral gas atom in the F layer — mostly single oxygen atoms — the photon knocks one of the outer electrons off the atom, leaving a rather heavy oxygen atom with a positive charge of one, and a very light free electron with a negative charge of one. From a radio propagation perspective, the key part is the light, very mobile, free electron. Of course, with more solar activity there are more free electrons.

If a radio wave is sent up into the ionosphere, when it encounters the free electrons, the oscillating electric field of the

passing wave causes the electrons to move back and forth at the same frequency as the radio wave. Electronically, these oscillating electrons behave like an antenna, except the electrons are wiggling back and forth in nearly empty space, rather than on a metal wire. This means that a certain fraction of the up-going wave energy will be reradiated back downward towards the Earth by this “free-electron antenna”. If the electron density is greater than a certain number, the *entire* radio wave will be reradiated back down, and skip occurs. The amount of ionization required to do this depends on the *frequency* of the upcoming wave, and the *angle* between the wave and the ionosphere itself.

Taking the simpler case first, suppose that a signal is sent straight up, vertically, to the ionosphere directly overhead. If N_e is the free-electron number density, the *maximum* frequency (in MHz) that can be bounced *straight back down* is given by:

$$f_c[\text{MHz}] = (9 \times 10^{-6}) \sqrt{N_e}$$

$N_e = \text{electrons/m}^3$

The *highest* frequency that a straight up signal can bounce straight back down — the *critical frequency* — depends on the square root of the electron density N_e and a known constant.

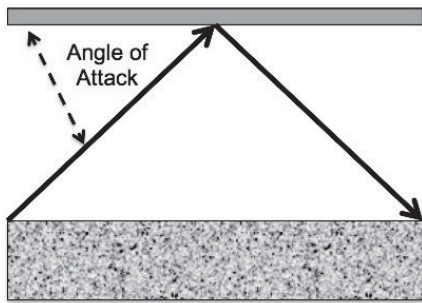


Figure 2 — Es produces mirror-like reflections. Note also that the smaller the angle of attack the higher the MUF for a given electron density N_e .

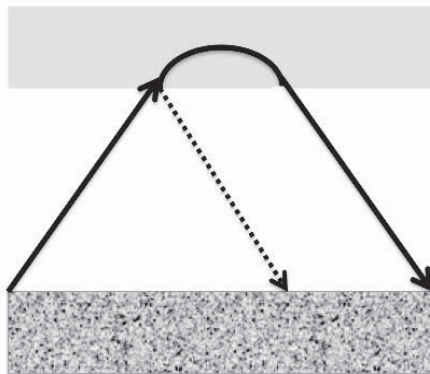


Figure 3 — The large vertical extent of the F2 layer skips a signal by more gradual bending, or refraction. Refraction can provide longer skip distances than the specular reflection (dotted arrow shows reflection).

M Factor and the Angle of Attack

Aiming signals straight up won't produce much DX. One aims at the horizon and that changes the angle with which the signal hits the ionosphere. With a shallower angle there is a higher maximum usable frequency (MUF) and the longer the skip distance. The angle between the wave and the ionosphere is the angle of attack α shown in Figure 2. The increase in the MUF is related to the cosecant of α , called the *M Factor*, and it directly multiplies the effect of the critical frequency f_c . The MUF is,

$$f_{MUF}[\text{MHz}] = f_c \text{cosec}(\alpha)$$

With M replacing cosec(α),

$$f_{MUF}[\text{MHz}] = M (9 \times 10^{-6}) \sqrt{N_e}$$

Under normal circumstances M depends on the height of the ionospheric layer. With an antenna aimed at the horizon, the typical F2 hop has M near 3.4. However, M and

therefore the MUF can be much higher under the right conditions.

Specular Reflection

In an elementary picture of ionospheric skip, one imagines that the ionosphere presents a hard-surfaced radio mirror (Figure 2). A radio wave simply bounces off the layer and returns to Earth. This is fairly accurate with sporadic E (Es) skip. In Es a very thin layer of very dense ionization produces a nearly mirror-like, or “specular” reflection. However, this is not the usual case for F-layer propagation.

Refraction

F-region ionization spreads over a large vertical expanse, extending upwards hundreds of kilometers. As a result, the signals are not skipped by a mirror-like bounce, but rather they are gradually bent until they point back downward again, if the MUF is high enough (Figure 3).

Since the F layer is three or more times

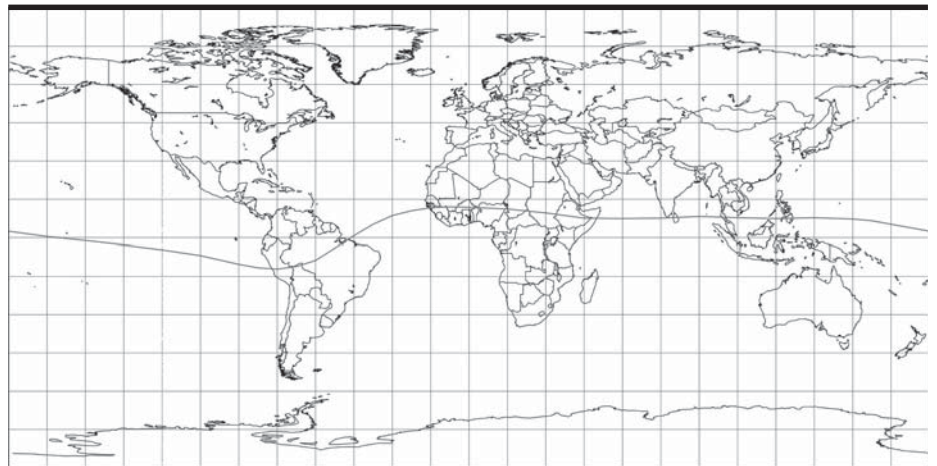


Figure 4 — The wavy line near the geographic equator is the geomagnetic dip equator. The geomagnetic field center is displaced from the geographic center toward the Pacific side, leaving the odd “bump” over the Atlantic. [G.Projector map and overlays.]

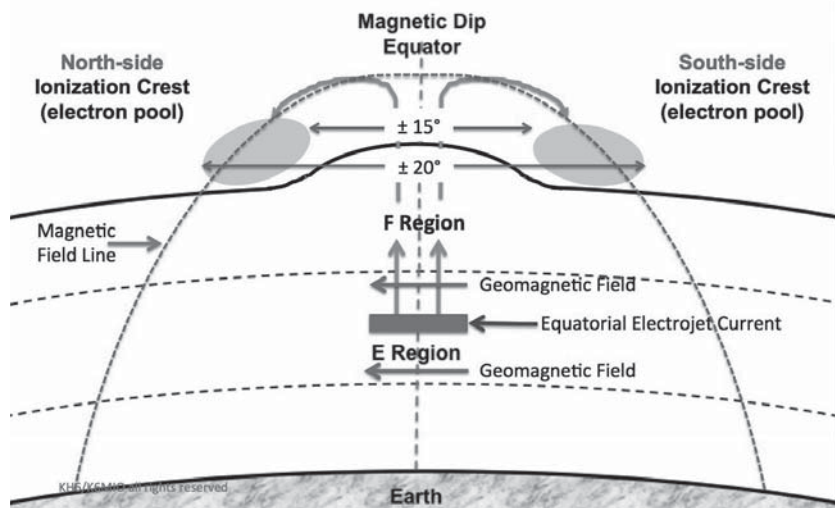


Figure 5 — The daytime fountain produces two regions of enhanced ionization near the dip equator, one centered at about 15° – 20°N and the other about 15° – 20°S.

higher than the E layer, it naturally provides a much longer single-hop skip distance than Es. In addition, once in the F layer, the signal can travel horizontally quite some distance while the refractive bending is taking place. Refraction can provide a longer skip distance than a specular reflection for the same layer height. Frequency is a factor as well. A single F2 hop at HF is about 4000 km. At 6 m it can be as much as 20% longer.

Ionospheric Environment

Simplified views often show the ionosphere as a smooth flat layer. But, the ionosphere is *neither* flat nor smooth. It is not even spherical. These realities have significant impact on the fine details of radio propagation — providing communications opportunities that would not otherwise exist. Making sense of them requires a little deeper look at our planet and how it behaves.

Geomagnetic Field

The Earth's geomagnetic field interacts with the ionized electrons within the various layers, and this produces a range of interesting effects. The simplest pictures of the magnetic field can hide some of its most important characteristics. An important feature is that the Earth's magnetic field is misaligned with the Earth's rotational axis by about 10°. As a result, there are two different longitude-latitude systems. One — the *geographic* system — is based on the Earth's rotation axis. The other — the *geomagnetic* system — is based on the orientation of the geomagnetic field axis. Of course, the rotation axis determines the time of day and the seasons of the year.

Adding complication, the magnetic field is also off center. The center of the magnet is not at the center of the Earth but rather, several hundred kilometers from the center — toward the Pacific side. This weakens the field over the South Atlantic Ocean off Brazil, and causes an abrupt glitch in the geomagnetic dip equator.

The interaction between the offset field center with the Earth's interior structure also leads to distortions in the overall field, so that the magnetic field is not a true dipole. Some maps do show a magnetic-dipole longitude-latitude scheme, but this approximation is not at all realistic for propagation purposes. Figure 4 shows the location of the geomagnetic dip equator — the line of shows where the magnetic field lines are parallel to the Earth's surface. The abrupt distortion on the dip equator is clearly seen over the South Atlantic near Brazil.

Equatorial Electrojet

During the local daytime, in the E-layer around 100 to 110 km, directly over the dip equator, there is a very intense electric current called the Equatorial Electrojet (EEJ). This ribbon of flowing electrons is quite thin and confined to a very narrow north-south range across the dip equator at approximately +3° to -3°. The EEJ is primarily driven by the Sun, which ionizes the daytime E layer and also drives a wind of neutral gases in an east-to-west direction, dragging the free electrons along with them. The interaction with the equatorial geomagnetic field, which is parallel to the Earth's surface, produces the ribbon of current. The current follows the dip equator throughout the year, even though the place-to-place, day-to-day, even hour-to-hour, strength of the current can vary strongly with the season, F10.7 solar flux, diurnal atmospheric tides, lunar tides, and perhaps even vertical drafts caused by tropospheric weather.

Daytime Electron Fountain

When a current flows at right angles to a magnetic field, as it is here, the electrons — and positive particles — are subjected to electromagnetic forces. Within the EEJ, these forces push electrons from the E and F1 layers upwards, at times more than 1500 km, to F2-region heights where the electrons have

much longer lifetimes.

As in the E layer, when the daytime Sun heats the F region, it drives the daytime neutral wind patterns. The F2 winds flow outward from the warmed area over the dip equator, and to the cooler regions toward the nearest pole. These neutral winds carry the upcoming electrons with them. As a result, the electrons that are on the northern side of the dip equator are carried further northward, while those on the south side are carried further southward.

Going north and south of the dip equator, the Earth's magnetic field lines gradually tilt downwards toward the Earth, and the fountain electrons follow these field lines. So, as they go north and south, they also descend to lower F2 levels. Finally, the electrons collect in two ionization pools, often referred to as "crests" — one centered around 17° north, and the other centered around 17° south — of the dip equator at altitudes from 300 to over 450 km (Figure 5). Figure 6 shows how these same features show up on a USU-GAIM rendering. USU-GAIM is an ionospheric model developed at Utah State University that uses a wide range of measured data to recreate the state of the ionosphere in 3-D at a given time.¹

Nighttime Bubble Fountain

When the Sun sets on the E and F2 layers, the electrojet current drops dramatically to the much lower nighttime levels. However, just before the daytime fountain fails there is a brief, but very significant upward surge in the fountain, called the *Pre-reversal Enhancement* (PRE). At this time, the vertical pipeline of daytime ionization is still full from the E layer to the high F region.

The shock of the PRE impulse is believed to trigger a set of atmospheric gravity waves, rather like ocean waves, within the standing vertical electron column. These gravity

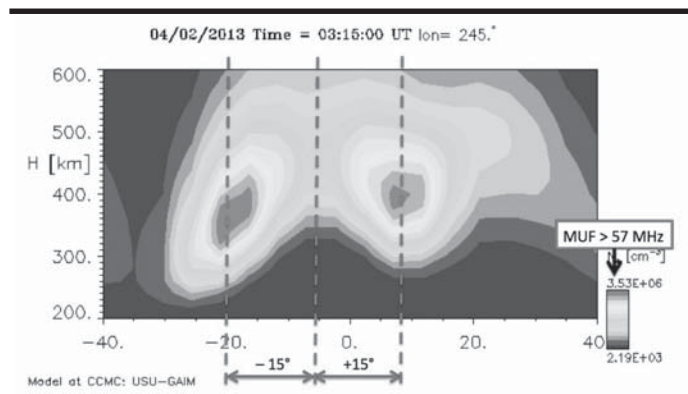


Figure 6 — This electron density map, for 0315 UTC on April 2, 2013 at 85°W (Geomagnetic Equator 5°S), shows both EIA pools have MUFs of about 57.5 MHz at about 390 km. Compare this with Figure 5. [USU-GAIM ionosphere.]

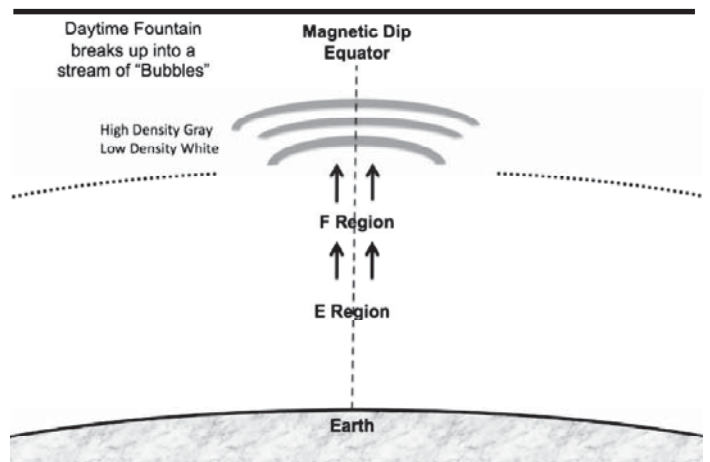


Figure 7 — The dying daytime electron fountain is shocked into a series of standing waves of alternating high and low ionization. The stacked layers are buoyant and float upward.

waves then produce a series of low-density ionization “bubbles” in the otherwise dense vertical column.²

These bubbles are 50 to 350 km thick sheets of low-density ionization, called depletions. They are sandwiched in between layers of the original high-density plasma.³ These *Equatorial Plasma Bubbles* (EPB) can be more than 2000 km wide in latitude.

Like bubbles in a glass of water, these depletions are buoyant and begin to rise, pushing up the denser ionization layers lying above them. Figure 7 shows a portion of this multilayer stack of alternating low- and high-density ionization layers as they float upward — as a nighttime fountain effect — typically between about 1900 and 0000 local solar time (LST). During periods of high solar activity, the bubbles have lifetimes of about three hours, increasing to as much as seven hours during lower solar activity.⁴ In latitude, the bubbles span a region from about 20° north to 20° south on the dip equator, with the bulk occurring between about 16° north and south.⁵

Seasons, Times, and Ionization

Since ionospheric free electrons are initially produced by the Sun’s EUV radiation, the more directly the Sun is shining down on a given place, the more the ions are produced. If the local time were noon at that place, then having the Sun directly overhead would produce the most ionization. Of course, the Sun’s high-noon angle depends on the latitude of that place and the local season.

As the Earth goes through its seasons, the noontime ionospheric Sun angle at a specific point slowly changes, as each of the Earth’s two geographic poles alternately tips toward and then away from the Sun. This leads to the cycle of the seasons being reversed between the geographical northern and southern hemispheres.

Summer and Winter

Since the Sun’s noontime angles in a given hemisphere are greatest during the hemisphere’s local summer, more free electrons are produced in the summertime. If the story stopped right there, then one would expect that the local summer season would be the best for F2 propagation. However, while more ions are produced in the summer ionosphere, another summertime effect in the F-layer chemistry causes these ions to have shorter lifetimes. The electrons are recombined with the positive ions at a much higher rate than in the wintertime. There are fewer net free electrons in the local summer than in the winter, so at mid latitudes, F2 propagation is best in the local wintertime.

The real discussion starts with propagation in the geomagnetic equatorial latitudes,

and in particular, paths traveling across the geomagnetic dip equator.

Spring and Fall

In contrast to the extremes of summer and winter, the Sun shines more or less equally on both the northern and southern electron pools during the spring and fall. Even though the Sun angle is not optimum for either the northern or southern side, but the balanced makes skip across the dip equator much more likely. Since spring in one hemisphere is fall in the other hemisphere, there are two times a year when this kind of propagation peaks.

Dates of Seasons

The dip equator sits at an angle to the geographic equator. Going around the world, the peak-to-peak latitude variation between the two equators is about 24° (Figure 4). Furthermore, the warped magnetic field leads to the geomagnetic equator being north of the geographic equator for two-thirds of its way around the Earth. This asymmetry has a subtle effect on the calendar dates of the “propagation season”, depending one’s geographic longitude.

Strictly speaking, the geomagnetic equinox at a given geographic longitude occurs when the Sun is positioned directly over the geomagnetic dip equator, not the geographic equator. This happens on different dates at different geographic longitudes. So, the magnetic seasons are not exactly the same as the geographic seasons. Given the angle between the dip equator and the geographic equator, this also means that on any given day, the magnetic season changes during the day, as the Sun passes over the various longitudes.

Referring back to Figure 4, stations in the northern hemisphere located at geographic longitudes between the middle Atlantic eastward to the east coast of Australia have their dip equator between 8° and 12° north. As a result, their spring magnetic equinoxes occur 20 to 30 days later than the geographic equinoxes, and their fall equinoxes are 20 to 30 days earlier. Of course, stations at these same longitudes in the southern hemisphere have these same equinoxes at the same dates, but the names of the seasons are reversed.

The northern hemisphere stations located between geographic longitudes corresponding to the central United States eastward to the tip of Nova Scotia have their dip equator between 8° and 12° south. Their fall equinoxes occur 20 to 30 days earlier than the geographic dates, and their spring equinoxes are 20 to 30 days later. In the Southern hemispheres, the dates are the same, but again the seasons are reversed.

In principle, these equinox date shifts affect which weeks of the year are the best for propagation, based on one’s longitude.

However, there are also many other factors that influence when exactly propagation occurs, including short-term solar activity.

Times of Day

The Sun is the source of the ionization that drives the EEJ, which in turn provides the resulting propagation. The relevant time is at the points in the ionosphere where the skip actually takes place, and not either of the endpoints. That is, the time is the actual Local Solar Time (LST) at the skip points.

On mostly north-south paths, the skip points will be at near the same longitude. These times are essentially the same, and one can talk simply about the path midpoint time. However, there are important cases where the paths have strong east-west differences and the different skip-point times have to be dealt with separately.

Many Flavors of Equatorial Ionospheric Anomaly F2

Let’s take a look at some of the many different ways that the EIA can result in interesting F2-based propagation. Notice first that many things routinely called TEP are really several different phenomena. In one way or another, they involve the Anomaly, and some aren’t TEP at all. The following breaks these down to basic forms, but there is no doubt that this still is not the complete picture.

Classical Transequatorial Propagation (TEP)

This is perhaps the most commonly known form of Equatorial Ionospheric Anomaly F2 propagation. TEP involves skip paths that cross over the geomagnetic dip equator. It was discovered in late August 1947, as hams returned to the airwaves following World War II, and in the US, on 6 m for the first time. The first contact may have been between W7ACS/KH6 at Pearl Harbor Hawaii and VK5KL.⁶

There are two main types of classical TEP, the afternoon and evening types. They have similarities, but actually work somewhat differently. In both, signals are first propagated up into the F2 layer on the nearside of the dip equator. Then, the signals propagate more or less horizontally across the dip equator, completely within the F region, without coming back to Earth in between. Finally, some distance from the far side of the dip equator, the signals leave the F2 layer and returned to Earth.

The total distance travelled, including through the F2-layer, corresponds to about an F2 “hop and a half”, so the total distance between the north and south ground endpoints can be a good deal greater than 5,000 km. It is also a low-loss path. Since the signal doesn’t come down at the midpoint, it avoids two passes of D-layer absorption

(negligible at 6 m, but a factor at HF) and any mid-path ground effects that a normal double hop would have encountered.

Afternoon TEP (aTEP)

As the world turns, the Sun progressively illuminates the daylight side of the Earth under it. This starts the Daytime Fountain Effect. The Fountain pumps electrons upward from the E and F1 layers into the upper F2 region. This produces two regions where the ionosphere is systematically tilted and the free-electron density is enhanced by the pooling of electrons descending from the top of the fountain.

Generally, the morning hours are spent building up the amount of ionization transported into the F region. When the TEP crests or pools are sufficiently charged up, an upcoming radio wave hitting the tilted corner of the enhanced nearside ionization pool arrives at a shallower angle of attack than if it were a strictly spherical layer. So, not only are the electron densities higher than normal,

the M Factor is also higher than the usual 3.4. Both factors conspire to produce much higher MUFs than the surrounding F2 layer. This happens again as the signal skips off the curved surface on the other side of the dip equator and heads back to Earth (Figure 8).

Around the spring and fall *equinoxes*, the solar ionization is more or less equal in both the northern and southern TEP pools. This balanced amount of ionization is favorable to aTEP propagation. Although there are some subtler details, aTEP is much more common around the equinoxes.

Ionization Lanes

For aTEP to work by the afternoon, both the north and south F2 skip points that straddle the dip equator must be ionized at or above the effective MUF required for the frequency involved. These two ionization pools move around the Earth following the Sun. This leads to two lanes or pathways that the ionization pools follow, day after day, on the daylight side of the planet. These lanes lie

mostly between 10° and 20° north of the dip equator, and between 10° and 20° south of the dip equator (Figure 9).

Common Paths

The aTEP paths are largely magnetic north-south paths. They usually cross the dip equator within ±15° of the perpendicular, and can reach out to distances of about 7500 km. Figure 10 shows the general appearance of these paths and some of the common geographical regions where they are found. Although, there are some paths that have significant east-west components, these are special cases that will be discussed in later sections.

Times of Day

As aTEP ionization builds up in the morning daylight hours, it often reaches high enough levels for propagation in the early afternoon. This propagation mode then collapses shortly after the path midpoint E-layer sunset, because the daytime electron Fountain shuts down. So, the aTEP time period is about 1300–1900 path midpoint LST.

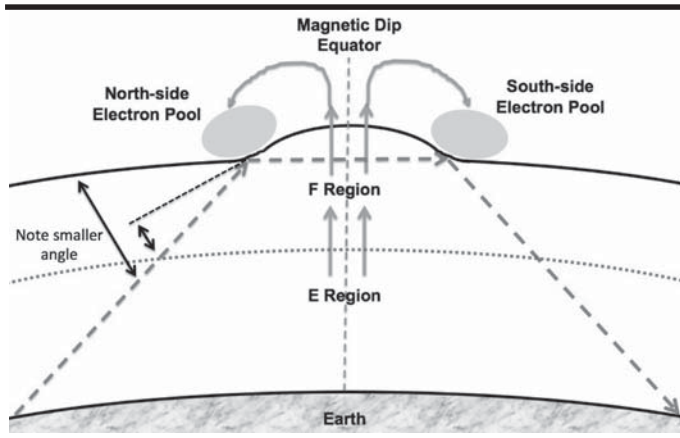


Figure 8 — This shows a transequatorial chordal hop off the tilted north and south skip points. The points are centered between about 15° and 20° north, and south, of the Earth's magnetic equator and cause nighttime TEP in the magnetic tropics.

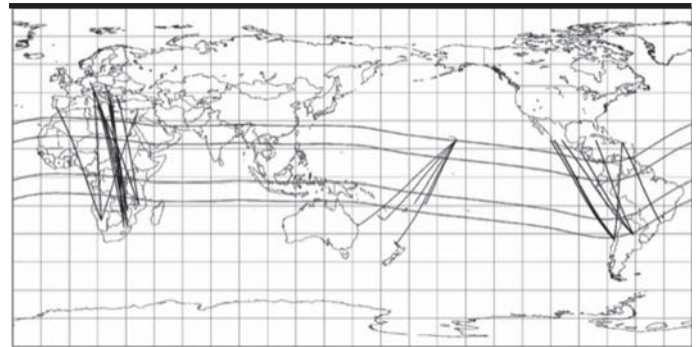


Figure 10 — Both afternoon TEP (aTEP) and evening TEP (eTEP) can produce paths that are approximately perpendicular to the dip equator. These are common examples of these mostly north-south paths. [G.Projector map and overlays.]

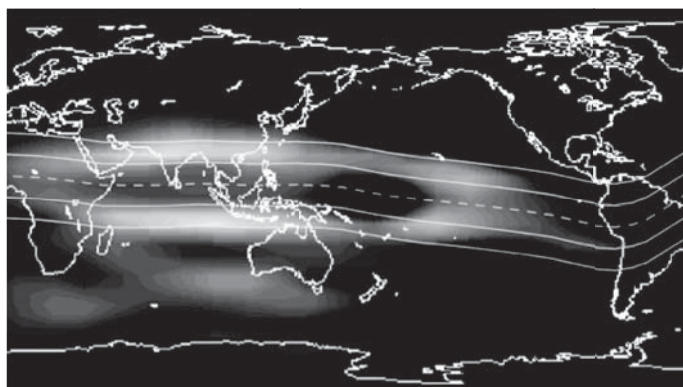


Figure 9 — The daytime northern and southern F2 ionization pools are seen near the centerline, at 315 km at 0915 UTC, March 20, 2013 (March Equinox). Solid lines show the daily paths/lanes they follow from east to west. The central peaks, left of center, show strong north and south electron levels. These are afternoon TEP peaks (aTEP). Two weaker peaks, right of center, are the evening TEP peaks (eTEP). The maximum MUFs were 53 MHz, over India and the Indian Ocean. [USU-GAIM ionosphere; G.Projector overlays.]

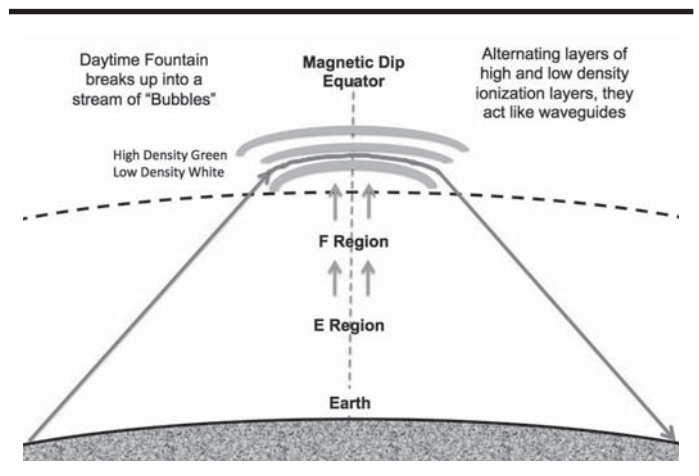


Figure 11 — Stacked layers of weakly conducting regions sandwiched in between highly conductive regions form ducts guiding upcoming radio waves through the dip-equator F region, and back down to the ground. If more than one duct is illuminated, even strong signals can show noticeable multipath effects.

Seasons

Since aTEP works best with equal ionization on both sides of the dip equator, it normally occurs during the two annual spring-fall equinox seasons. This usually peaks during March and April, and then again during October and November. The exact dates may be earlier or later, or longer or shorter, depending on the location of the dip equator, the timing and amount of solar activity, and other effects.

Evening TEP (eTEP)

Evening TEP is the second classical form of TEP. After the Sun sets on the path midpoint E layer, the daytime fountain shuts down, and the nighttime fountain begins producing bubble layers. The bubbles consist of sheets of high density ionization separated by very weakly ionized sheets called depletions. These sandwiched combinations of high — then very low — then high conductivity plasma layers are the key to making eTEP work.

The north and south ends of the depletion layers have openings on each side of the dip equator (Figure 11). A radio signal approaching the bubble stack will find it difficult to penetrate the highly conducting layers, but find it quite easy to enter the low ionization depletion layers. As a result, the depletion layers can act like signal ducts or tunnels through the bubble stack.

Instead of skipping the signal from a dense cloud on one side of the dip equator, to another cloud on the far side of the dip equator (like aTEP), a depletion duct carries the signal in a continuous curved path through the F layer bubbles, following the Earth's magnetic field lines.⁷ Once a radio wave enters the duct, it slides along making very high M-Factor grazing incidence skips off

the top wall of the duct that guide the signal around its curvature until the signal exits the duct on the other side of the dip equator.

Since the bubble stacks can extend from about 20° north to about 20° south of the dip equator, the general locations of the entrance and exit regions are similar to skip points seen in aTEP.

Since the vertical span of the individual ducts are in the 50 to 350 km range, the ducts are fully capable of transporting signals from at least as high as 432 MHz, and then well on down into the HF range.

With the family of bubbles being stacked up vertically, an upcoming signal can enter more than one guided path at the same time. So, there can be many paths over the dip equator. As a result, even with strong eTEP signals, there are often obvious, profound multipath effects, including deep fading, and echoes.

Common Paths

Usual eTEP paths include the mostly north-south paths, as also seen in aTEP (Figure 10). The observed maximum range is a bit longer than aTEP, going out to about 8800 km. There are at least two other modes that have some characteristics of eTEP, but are or may not be eTEP, as will be discussed shortly in the section on Oblique TEP and Single-Lane F2.

Times of Day

The evening bubble fountain gets underway shortly after the path midpoint sunset and the collapse of the daytime fountain. Various studies of the equatorial plasma bubbles themselves suggest that their active periods are about 2000-2300 LST at the path midpoint. However, propagation observations indicate that they can be

effective from about 1900-0100 LST, and in some cases, even later. It is not uncommon to encounter north-south paths that are open in the mid-path afternoon with aTEP, and then later after mid-path sundown, pick up again in the evening hours by eTEP.

Seasons

The eTEP and aTEP seasons are about the same, spring and fall in both hemispheres. Both are facilitated by roughly equal ionization of the E and F layers on both sides of the dip equator.

Oblique TEP

The classical picture of aTEP and eTEP outlined above applies to paths that are largely oriented magnetically north-south. In these cases, there is only modest east-west difference in magnetic longitude, and this presents no mystery. However, paths that cross the dip equator at very large oblique angles must be much longer than nearly north-south paths. Even though the latitude differences between the stations about the dip equator are about the same, the longitude differences can be very large. These include recurring paths between Hawaii and South America. Figure 12 shows common examples of several of these paths. The longest is over 13,000 km, the shortest over 10,000 km, and most are over 11,000 km.

Figure 12 also shows an overlay of a typical USU-GAIM ionization map for that time of day and season. The dashed ovals show the path northern aTEP (left) and southern eTEP (right) skip-point ionization pools at 400 km. Their corresponding southern aTEP and northern eTEP pools are also visible.

These longer paths pose at least two interesting challenges. The first is that the distance in between the near side lane skip point and the far side lane skip point is simply too long for a chordal or ducted hop. This middle segment would have to be about 5400 km for the shortest path, and about 8500 km for the longest. The basic problem is that the curvature of the Earth would cause the signal path to run into the ground about 2300 km downstream, destroying the path. Even under the most ideal conditions, the paths are 900 km to 4000 km short of the mark.

Getting the Distance Right

The challenge of going long distances around the curvature of the Earth, without hitting the ground has come up in other contexts. At least some types of 50 MHz long-path propagation show evidence that the very long central portion of the path has one or more segments — some perhaps longer than 11,000 km — that never come back to Earth.⁸

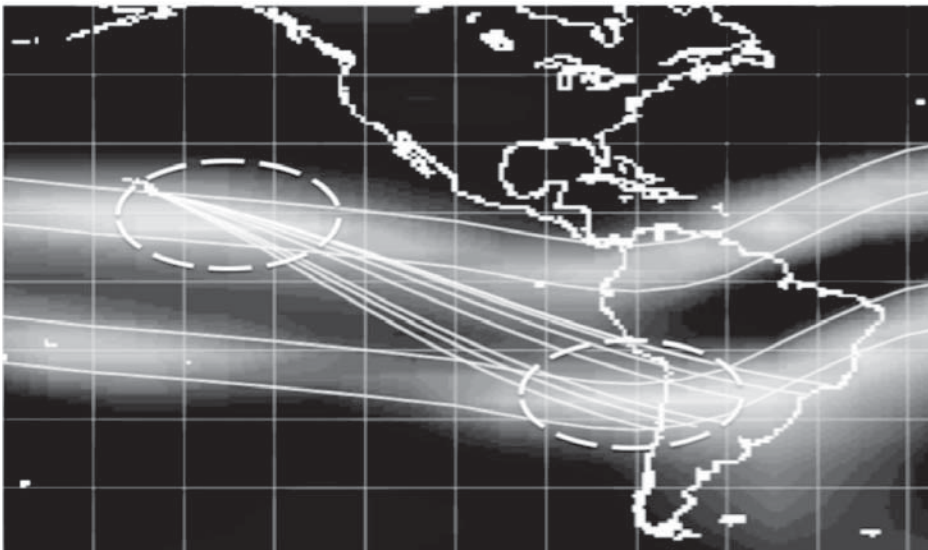


Figure 12 — Dashed ovals show the north aTEP (left) and south eTEP (right) ionization peaks. The lane boundaries are also shown. The southern aTEP (left) and northern eTEP (right) peaks are visible, but not involved in shown the path. [USU-GAIM ionosphere; G.Projector overlays.]

One possibility is a variation of the guided wave scenario. In this hypothesis, the signal skips off, say, the west-end ionization peak as an aTEP hop, and then goes into the region between the two lanes. There it starts nearly parallel to the Earth's surface, and going forward, the horizon moves up to meet it. However, long before it hits the ground, it encounters the topside of the E layer at grazing incidence. MUFs resulting from such skips are typically twice that of normal skips.⁹

This skip sends the signal further on down the path, edging upwards toward the F layer again. From there, F-layer refraction along the path eventually returns the signal path back downward again, to either another topside E skip, or carrying the signal all the way to the east end TEP peak, and from there back to the ground at the end of the path.

A simpler variation of this scheme might be to propose that F-layer refraction simply bends the signals around the curvature of the Earth, from one end to the other, all the way to the east-end TEP peak. Whatever the case, the paths do occur, and do so frequently when TEP is around. The above effects have been observed on other contexts, and they offer plausible explanations here as well. There may be other explanations as well.

Oblique aTEP and eTEP

In addition to path length, the time of day patterns raise another question. The extended paths separate the two end-point stations by five or six time-zone hours — so their Local Solar Times are very different. The observed propagation usually occurs during the west-end mid afternoon, while it is evening at the east end. Adjusting for first and last skip points, the west is still in the afternoon TEP regime and the east is well into the evening TEP regime. The simplest conclusion is that the west end is getting an aTEP hop and the east end is getting an eTEP hop. That may well be what's happening. If so, it is interesting that the two different mechanisms, which work in rather different ways, seem to make such a good connection.

The issue here is that aTEP requires a separate hop on each side of the dip equator, while the usual view of eTEP is that signals are piped all the way across the whole space from the north lane to the south lane, while buried inside the depletion ducts. So, the question would be, how did the aTEP signal from the north side — traveling in between the two lanes — get into the middle of a closed eTEP depletion duct, in order to get over to the south side lane and down to Earth?

The most likely answer is that as the bubbles rise, they also have open edges pointed into the region between the north

and south lanes. Recalling that in eTEP all the guiding of the wave comes from high-M skips off the ceiling of the duct. In other contexts, eTEP has been observed to “leak” signals out the bottom of the ducts. So, if a signal coming from the north side can find a hole in the bottom of a duct, or a duct without a bottom altogether, then it could complete the journey on the south end as an eTEP hop.

Common Paths

Highly oblique paths are very common in the Pacific region during the TEP seasons. They may occur in other regions as well, though the combination of the hook-shaped dip equator region over South America, followed by a rather straight, gently northward flowing line out toward Asia may play a role in the frequency of its appearance there.

Times of Day

On the west end they occur during the local afternoon. On the east end they occur in the local evening.

Seasons

Like other true TEP forms, the path seems to favor the equinoxes. The span, from the beginning to ending date, seems somewhat shorter than some other paths.

Single-Lane F2

While much attention has been given to TEP propagation across the dip equator, there is another EIA propagation mode that is simply east-west F2 occurring off only one of the two ionized lanes. The dip equator is not crossed and the far side lane is not involved at all in a given path.

What many don't realize is how high the MUF can be for this mode. The USU-GAIM model shows that the east-west MUF can be well over 66 MHz, without any special angles and M-Factor values. It also need not be near an equinox. The models also show high local wintertime values. In this last regard, the Wake Island (KH9) beacon was into Hawaii almost daily from October 2013

until late April 2014.

Of course, taking advantage of this form of propagation generally requires that the two end-point stations must be on within about 2000 km of the same ionization lane peak. If the path is north-south, then they have to be on opposite sides of the lane. If they are more or less aligned along the lane, then double hop also occurs. That places a lot of constraints on where one has to be and whom one will be able to talk. Nevertheless, this mode happens quite frequently in certain parts of the world, where there are landmasses in the right positions for the required end-point station alignments. Figure 13 shows some actual examples from the western Pacific and the central Atlantic during March and most of April 2014.

Common Paths

From Hawaii these paths go westward toward the northern hemisphere islands including Wake, Guam, Taiwan, the Philippines, Japan, and mainland China. As can be seen in Figure 13, these kinds of paths show up in between the northern part of South America and its maritimes, and northwestern Africa, and martimes, and southern Europe.

Times of Day

The midpoint time in that example was about 1800. While midpoint times seem to run from 1330-0000 for single hop and 1330-2000 for double hop, earlier times have been seen.

Seasons

Equinoxes generally are best, if not for the positive impact of Fountain ionization, then at least because more people are on the air. Those associated with the northern spring seems to perform better, but the amount of data is small.

There is some evidence suggesting that this sort of propagation should be available in seasons no one is expecting it, such as local winter.

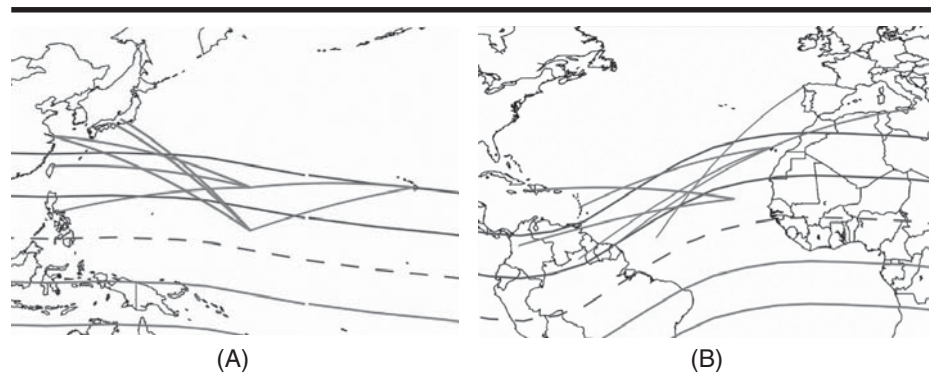


Figure 13 — These are examples of single- and double-hop Pacific, and Atlantic, F2 paths along, and across, just the north lane alone, during evening TEP hours. Note that the skip points all fall within the north lane. [G.Projector map and overlays.]

Non-Great Circle Paths

Nature is an equal-opportunity propagation provider. She is not restricted to using any one propagation mode to move a signal between point *A* and point *B*. It is perfectly possible to have one kind of propagation mechanism hand over a signal to some other kind of propagation mechanism.

In some cases, this results in paths that do not appear to follow a single Great Circle path from end to end. Rather, each of the different modes follows a Great Circle, but not necessarily the same one as the other, due to the different character of the two or more modes involved in the end-to-end path.

Skewed Paths

Of course, there is nothing new about skewed paths, but it is interesting to look at how they might come about. Understanding the possibilities is often hampered if one takes the simplified 2-D skip pictures too seriously, because the ionosphere is a 3-D world. So, not every reflection, refraction, skip, or hop occurs in the vertical plane. Things can be bent or bounced sideways as well.

The EIA is, by its very nature, a 3-D structure. All sorts of interesting things can occur. Whether the lanes are viewed from the side (north-south) or down along their long dimension (east-west), they provide a family of high electron density surfaces that skip signals at many different angles — not just straight ahead — but to the side as well.

Even a small deflection of the signal direction can make a profound difference in the signal path that then follows. When this happens, hybrid paths can be generated that, in the whole, are not Great Circle paths, even though the segments that make them up may well be. Figure 14 shows two examples of this effect.



Figure 14 — Both skew paths start as south-lane TEP and then are redirected upon entering a later lane (circles). The path from CE then does a 2F2 hop in the north lane to BA. The FK8 path crosses the north lane and runs into it again, and is redirected to EA8. [G.Projector map and overlays.]

The first is a variation of a path that, although completely a surprise when it first showed up decades ago (SA-JA), has continued to create excitement under good conditions. This recent example occurred on February 22, 2014 at 0052 UTC with an opening between several LU/CE and BA/BV stations. They are represented here as a single CE-BA path for clarity. The dashed line that runs down toward the South Pole shows the equivalent Great Circle path. However, these were not the directions that the antennas were aimed.

The first path segment from SA westward took almost exactly the same frequent eTEP path from SA to KH6 seen in Figure 12. As in that path, it occurred during the local SA evening. The path from the near side lane to BA very closely follows a known single-lane double-hop F2 path from KH6 to BA/BV. The circle on the plot shows the approximate point that the new path appeared to deviate from the other. The deflection angle is to the left about 14°. The deflection was away from the centerline between the two lanes, suggesting that refraction might have played a role.

The other example is the contact between FK8 and EA8 on November 10, 2013 at 0055 UTC. Again, the plot shows a reasonable estimate of the path actually followed, and also the normal great circle route, this time up toward the North Polar regions. As before, the key information was the station beam headings. FK8 was beaming east and did actually swing the beam looking for the best signal direction.

One interesting thing here is that the local time in FK8 was about 1300, which is consistent with the first segment starting as an aTEP link, looking toward later times to the east. Plotting a Great Circle for this segment suggested that the path appeared to first make a TEP hop to the northern side of

both lanes.

Due to the abrupt northward swing of the dip equator over the SA, a little farther downstream it then encountered the north side lane a second time, this time in from the north. From there, it seems likely to have deflected to the left — as was the case in the CE-BA path above. The deviation point in that path's circle is about 13°, and as in the previous example, to the left, away from the lane centerline. After the deflection, the path is consistent with a single-lane one-half-hop F2 path down to EA8.

Common Paths

These are the only two paths for which data are currently available.

Times of Day

Both involved very oblique eTEP hops in the night near longitude 75° W.

Seasons

One occurred in late northern fall and the other in the early northern spring seasons.

TransPolar Long-path (TPL)

Late evening on 9 October 1988, on the rapidly rising leading edge of Cycle 22, a 6-m station in Greece (SV1DH using the special 6-m call, SZ2DH) worked JG2BRI in Japan. What was especially amazing was that it was nearly midnight in Greece and SV1DH was beaming southwest, away from Japan, toward the southeastern reaches of South America! The Japanese station was beaming southeast, at the other side of the south end of South America.

The two stations completed a nearly 31,000 km long-path contact from north of the magnetic equator southwestward encroaching on the Antarctic near the South Pole, and then back north across the magnetic equator again and landing in Japan. The actual signal traveled about three-quarters of the way around the world!¹⁰

There were many TPL openings from KH6 to the Mediterranean and southern Europe near the Cycle 23 solar cycle



Figure 15 — Various transpolar long paths are shown between KH6 and the Med and A45; KH8 and 5H3; E51 and ZS; and BV and EA8. [G.Projector map and overlays.]

maximum, and a few more occurred in Cycle 24 in early 2014. KH6 was on the east end of the link at night, and Europe was on the west end, in their morning.

In KH6, the openings occurred in the late evening usually after 2200 station LST, when TEP was already in evidence over the usual paths (such as VK4), though the TEP was generally sporadic and not particularly intense or widespread. Quite strong backscatter was often heard from headings of about 195°, suggesting lots of ionization and tilted layers. Often the signals were very weak, though a great many SSB contacts were made. On a few occasions, the signals were very loud, allowing contacts with modest power and small antennas.

KH6 also saw the other side of the TPL path, as well, in Cycle 23 and again in early 2014. In these openings, the KH6 stations were on the west end of the path between 0830 and 1100 station LST, beaming around 140° and the path went into A45 and thereabouts in their late evening. Other recent examples include openings between EA8 and BV, and between E51 and ZS (Figure 15). There are many other example paths for this mode, but there are also some geographical limitations. A great many mathematically possible paths end up with one end in an ocean.

Whether going around westward or eastward, there was no evidence of the signals coming back to Earth in between the two ends of the path. These paths cover a lot of water and sparsely inhabited land. Nevertheless, it gives the impression that the signals start off as “ordinary” TEP. But, when the signal skipped off the far side lane, instead of coming back to Earth (say, in VK), some of the signal energy continued at a much shallower angle off the curved surface. This “launched” the signal into a series of high-M skips off the F2, over and over — like a whispering gallery — until the signals hit the anomaly lanes on the far end of the path over northern Africa. At that point, the far side lanes reversed the “launching” process and brought the signal back to Earth (Figure 16).

Midmorning TEP Curiosity

One interesting observation is that the east ends of the circuits, in both the eastern and western hemispheres, seem to systematically be in their evening TEP period. This necessarily means that the western ends of the paths are in midmorning. Normally, this would be too early for aTEP and too late for eTEP. Nevertheless, hundreds of contacts were made in Cycles 23 and 24. The mechanism for this effect might be associated with various observations that indicate that the ionization bubbles, such as

associated with eTEP, sometimes have very long lifetimes.¹¹ Referred to as fossilized bubbles, they may play a role in facilitating this unusual TEP connection.

Common Paths

The paths from Hawaii to the Mediterranean, southern Europe, and the Near East is well known. There have been credible reports between South America and Australia, Polynesia and India, China and the Canaries, and a number of others.

The paths here are generally constrained by the placement of the landmasses within the Earth’s oceans. Besides the fact that the stations have to be within access of the TEP ionospheric system, the paths are very long. So, from a given point at one end of the circuit, there are only a limited number of viable places at the other end of the proposed circuit. Nevertheless, some DXpeditions to carefully-chosen islands can produce designed-in opportunities.

Times of Day

Looking west, 2130-0130 station LST. Looking east, 0830-1100 station LST.

Seasons

This propagation seems to be confined to high solar activity and the equinox periods. There are indications that the April time frame is better than the October time frame.

Linking to TEP from Afar

It’s reasonable to ask just how far from the TEP lanes can one be and still connect to the various TEP-like modes. The obvious requirement is that the station must be close enough to be able to illuminate the nearside TEP ionization lanes with its signal. This, in turn, is a function of the height of the lanes themselves. For peak regions at 300 and 450 km, these distances are about 2000 and 2500 km respectively. Figure 17 shows the TEP lanes and outer boundary limit lines.

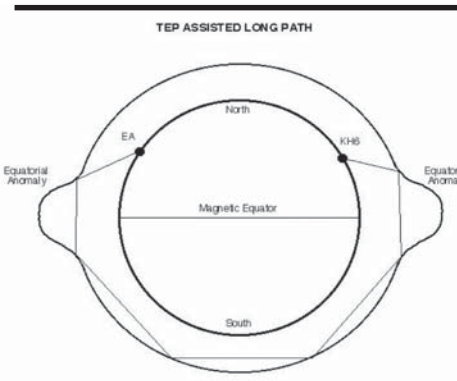


Figure 16 — TEP appears to provide launching points for high M-Factor, shallow attack-angle grazing hops that cover long distances, with higher than normal MUF and low absorption.

In principle, stations within these outer boundary lines should be able to connect directly to the TEP nearside lane.

However, it would also be possible to make a less direct connection from beyond the outer boundary using some different propagation mode to cross over the boundary from the outside. The most likely opportunity is having a sporadic E cloud in just the right place.

If the Es link brings the incoming signal down inside the outer boundary line, then it can begin a second hop. If things are properly lined up, then that second hop can become an F hop going up to the nearside TEP lane, and then complete a full TEP hop. Since single-hop Es can have a range of 1000-2000 km, this has the capacity to stretch the “TEP” range well beyond the direct connection limit. What’s more, these paths really happen, as shown in Figure 17. Note that a number of those paths actually link across the boundary line, some from quite a distance. In all likelihood, many of the paths starting inside the boundary line were also Es links.

Common Paths

In the Western Hemisphere, the most common paths are between the US and both the Pacific and South America.

Times of Day

While there are exceptions, this is dominantly an evening affair, suggesting that the TEP component is eTEP.

Seasons

In the Northern Hemisphere the Es links to the TEP system are usually seen in mid to late April, at the time when the ending of the TEP season and the beginning of the Es season overlap. In the Southern hemisphere this would be in early to middle October.

Summary

The Equatorial Ionospheric Anomaly defines the behavior of radio propagation that originates, terminates, or passes through the vicinity of the Earth’s geomagnetic dip equator. The daytime core of the EIA is the Equatorial Electrojet, a powerful electron current flowing in the E layer between 100 and 110 km, straddling the dip equator centerline between ±3° of latitude.

During the day, the electrojet and the Earth’s magnetic field produce an “electron pump” which drives E and F1 layer electrons upward in a fountain carrying them high into the F2 layer. The fountain overflow settles into two crests or pools, one centered on about 17° north and the other about 17° south of the dip equator, still in the F layer at 300 to 450 km. The ionization peaks in those two pools follow the Sun daily, but lagging behind the Sun by a few hours.

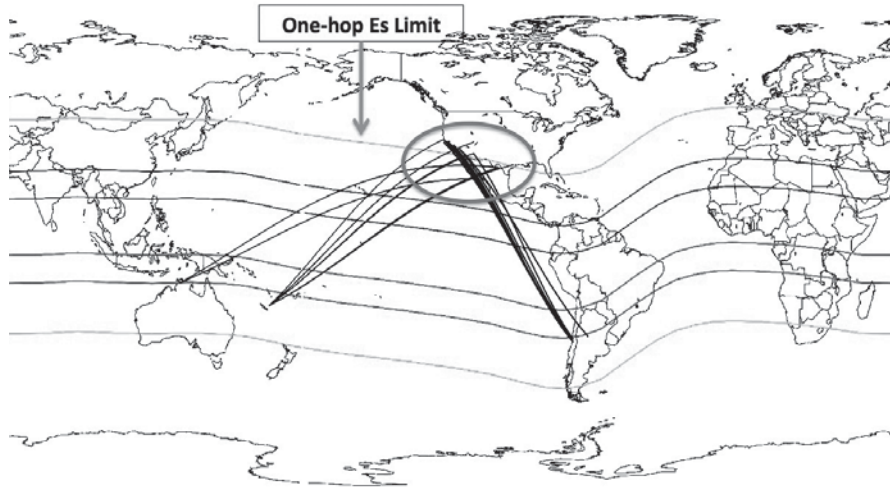


Figure 17 — The outermost lines show the nominal limits for direct TEP access to the more central ionization-lane pairs. Access from beyond the “direct” boundaries requires some additional mechanism, such as Es, to reach inside an outer boundary and link to the TEP. [G.Projector map and overlays.]

From local afternoon until sunset, these ionization pools facilitate radio propagation called afternoon TEP, or aTEP. Afternoon TEP skips signals from the ionization pool on one side of the dip equator, to the pool on the other side, allowing signals to cross over the dip equator with paths out to 7500 km.

When the Sun sets, the electrojet loses its energy source and the current ribbon abruptly stops, but a sudden last gasp sends an upward shock wave through the standing column of fountain electrons. This shock creates a series of large, flat “bubbles” of alternating layers of very-highly, and then very-weakly, ionized plasma. These bubbles are buoyant and they rise upward to great heights in the F2 layer, sometimes over 1500 km.

The bubble regions extend outward as much as 20° north and south of the dip equator. They are open at their edges. The weakly ionized layers act as ducts that can guide radio waves from one side of the dip equator to the other, providing evening TEP, or eTEP, propagation out to a total path length of about 8800 km.

The majority of this propagation is along largely north-south paths, which limits the maximum path length. However, there are variations that provide propagation across the dip equator, but with a very large east-west component as well. This Oblique TEP can produce paths to beyond 13,000 km. It generally involves a west-end station in its afternoon TEP regime and an east-end station in its evening regime.

The afternoon electron pools and nighttime plasma bubbles also support single-lane F2 skip from just one pool (either north or south), such as single-hop north-south paths across the lane. If the two stations

and the lane are all aligned with each other east and west, then an east-west single or even a double-hop F2 can occur.

In addition, there are forms of propagation that involve a mixture of two or more of these modes in different segments of the same path. One example is very long, skewed paths, which do not follow a single Great Circle path. Another variation is Transpolar Longpath or TPL, which generally are not skewed, but involve TEP twice in the path, with something else different in between. Still another variation occurs when a station, far from the dip equator, uses an Es hop to link into range for a following TEP hop.

Acknowledgements

The author wishes to express his appreciation to a number of people and programs that have made contributions to this effort, including:

Gabriel Sampol, EA6VQ, whose **dxmaps.com** database has been an invaluable source of operational data, without which this study would not have been possible.

Javi Pons Estel, LU5FF; Haroldo “DJ” Bradaschia, PY7DJ; Rémi Touzard, FK8CP; and Jon Jones, NØJK, who provided valuable insights to interesting propagation observations, and Linda Kennedy, WH6ECQ, who diligently proofread the many drafts.

The USU-GAIM team and the NASA Goddard Community Coordinated Modeling Center group provided their valuable and gracious assistance. The USU-GAIM Model was developed and made available by the GAIM team (R. W. Schunk, L. Scherliess, J.J. Sojka, D. C. Thompson, L. Zhu) at Utah State University. The Community Coordinated Modeling Center group at the

NASA Goddard Space Flight Center ran the computer models for the selected dates and times.

The various path maps were implemented using the *G.Projector* mapping program, which was written and is supported by Robert B. Schunk, NASA Goddard Institute for Space Studies. This tool was a great help in graphically combining data from the various disparate types and sources.

Jim Kennedy, K6MIO, has been licensed since 1955. He has been an avid 6-m operator for much of that time. He holds a PhD in physics from the University of Florida, and has taught astronomy and electronics at the university and college levels. For more than twenty years, he was a senior manager with the National Solar Observatory in Tucson, and later, Associate Director of the Gemini Observatory in Hilo, Hawaii.

Notes

¹R. W. Schunk, L. Scherliess, J.J. Sojka, D.C. Thompson, D.N. Anderson, M. Codrescu, C. Minter and T.J. Fuller-Rowell, *Global Assimilation of Ionospheric Measurements (GAIM)*, **Radio Sci**, **39**, RSIS02, doi: 10.1029/2002RS002794, 2004.

²C. S. Lin, T.J. Immel, H.C. Yeh, S.B. Mende, and J.L. Burch, *Simultaneous observations of equatorial plasma depletion by IMAGE and ROCSAT-1 satellites*, **J Geophys Res**, **110**, A6, 2005, pp 1978–2012.

³K. Y. Chen, H. C. Yeh, S.Y. Su, C.H. Liu and N.E. Huang, *Anatomy of plasma structures in an equatorial spread F event*, **Geophys Res Letters**, DOI: 10.1029/2000GL012805, 2012.

⁴C. S. Huang, O. de La Beaujardiere, P.A. Roddy, D.E. Hunton, J.O. Ballenthin and M. R. Hairston, *Generation and characteristics of equatorial plasma bubbles detected by the C/NOFS satellite near the sunset terminator*, **J Geophys Res: Space Phys**, **117**, A11, 2012.

⁵W. J. Burke, L.C. Gentile, C.Y. Huang, C.E. Valladares, and S.Y. Su, *Longitudinal variability of equatorial plasma bubbles observed by DMSP and ROCSAT-1*, **J. Geophys. Res.**, **109**, A12301, doi:10.1029/2004JA010583 2004.

⁶N. F. Joly, *The Dawn of Amateur Radio in the U.K. and Greece: a personal view*, Ch. 7. Project Gutenberg, 1990.

⁷J. Kennewell, and P. Wilkinson, *Transequatorial Radio Propagation*, IPS Radio and Space Services, 2004, www.ips.gov.au/Category/Educational/Other%20Topics/Radio%20Communication/Transequatorial.pdf.

⁸J. Kennedy, *50 MHz Long-Path Propagation*, Proc. 37th Conference of the Central States VHF Society, 84-105, ARRL 2003.

⁹Kenneth Davies, *Ionospheric Radio*, Peter Peregrinus Ltd., London, 1990, p 183.

¹⁰Costas Fimerelis, Private communication, 2003, see also Note 6.

¹¹P.D. Pautet, M.J. Taylor, N.P. Chapagain, H. Takahashi, A.F. Medeiros, F.T. Sao Sabbas and D.C. Fritts, *Simultaneous observations of equatorial F-region plasma depletions over Brazil during the Spread-F Experiment (SpreadFEx)*, **Ann Geophys**, **27**, 2009, pp 2371–2381, see also Note 4.

Gray Line Propagation, or Florida to Cocos (Keeling) on 80 m

N4II investigates mechanisms responsible for gray line propagation on the low bands.

Introduction

From 30 March to 13 April 2013, Chris Tran, GM3WOJ, and Keith Kerr, GM4YXI, operated as VK9CZ from the Cocos (Keeling) Islands, the DXCC entity farthest from my location in south Florida. When this DXpedition was announced in late 2012, I determined that I wanted to work VK9CZ on 80 m.

The first step was to identify the period of common darkness between us — if, in fact, one existed. A check of the sunrise (SR) and sunset (SS) times at both locations for 7 April, midway through the DXpedition, revealed the following:

VK9CZ SS = 1132Z; N4II SR = 1106Z

VK9CZ SR = 2337Z; N4II SS = 2340Z.

There was no period of mutual darkness, but I thought that the low bands might still be

a possibility at the “gray line” of my SS and VK9CZ SR, which occurred within three minutes of each other. In the past I had heard stories of enhanced propagation under such conditions from grizzled low-band veterans, and I was curious to find out if I could hear VK9CZ on 80 m at all.

Due to CC&R restrictions at my home, I chose to operate from nearby club stations. The best 80 m station available at the time was at the Boca Raton Amateur Radio Association, N4BRF. It offered a SteppIR vertical, with 60 radials, in a quiet location on the edge of the Loxahatchee National Wildlife Refuge, and a 500 W transmit power amplifier. The station did not have a dedicated receive antenna.

My first opportunity was on 3 April. Not knowing what to expect, I began monitoring 80 m CW at 2300Z (40 minutes before my

SS). At 2325Z, to my delight I heard VK9CZ calling CQ on 3507.5 kHz. There was no pile-up, and he was not working split. To my amazement I worked him on the first call, as N4II. He called CQ again and, still with no pile-up, I worked him again, this time using the club call sign N4BRF. VK9CZ called CQ again and again, until he finally faded at 2345 Z — 5 minutes after my SS, and 8 minutes after his SR. The next 80 m opportunity was on 5 April, but a large thunderstorm sat over the club station, keeping me off the air.

On 7 April, wanting to hear more, I began monitoring 80 m CW at 2315Z, 25 minutes before SS. At 2330Z, I heard VK9CZ again calling CQ on 3507.5 kHz. There still was no true pile-up. He worked several stations in an orderly, workmanlike fashion before fading at 2350Z, 10 minutes after my SS, and 13 minutes after his SR.



QX1611-Callaway01

Figure 1 — Into daylight? Some reports indicated that the received VK9CZ signal peaked to the SSW. [DX Atlas]

This experience left me stunned. Why no pileup? Why so strong? How could he be worked almost at will, from 11,450 miles away, on 80 m? Where was everyone else?

What kind of propagation made this possible?

The Investigation

My curiosity probably would have stayed idle, were it not for an item that appeared in the *ARRL Propagation Bulletin* the following week on 12 April. Bruce Smith, AC4G, wrote in to say:

“I was so excited to QSO VK9CZ on 80 m CW that I had to write in. Our QSO took place on 3 April around 2345Z when VK9CZ and my location in southern Tennessee were in sunlight

at the edge of the terminator. This had to be one of my best QSOs ever due to the level of difficulty, the distance, and no darkness at either location (so my terminator map showed).

The VK9CZ signal was S5-S7 on my transmit antenna (vertical). The signal was so strong that my separate receive antenna was not required. Since that date, I have not been able to copy their 80 m signal. I guess it was one of my luckiest days to be able to make this QSO.”

Well! I wasn’t the only one who was impressed with VK9CZ on 80 m.

More information was clearly needed, so I sent a plea to the email reflectors of the South Florida DX Association, and the Florida Contest Group, asking for information from

others in Florida. This dragnet produced claims of 16 QSOs from Florida. The VK9CZ log would ultimately indicate a total of 21, and nearly everyone was as impressed as I. I also looked at *Club Log* data, which indicated 51 QSOs with US Zone 5. This indicated that QSOs with Florida were an unexpectedly large fraction of the total, even allowing for the large number of DXers in the state.

Kai Siwiak, KE4PT, suggested that I check VK9CZ 80 m spots, and they proved quite interesting (Table 1). The first thing of note was that, even though they were spread over three separate days (3, 7, and 11 April) they were all within a very narrow time window — eight minutes. The second point of note was the spot from W1QS, in Maine, who noted that the signal came from the SE.

This second point was interesting because the only station with a directional array that replied to my email survey was Pete Rimmel, N8PR, who sent the following:

“Antenna [was] 4 phased ½-wave sloping dipoles in [a] 4-square phased arrangement and pointed SW when I worked them ... Louder than SE, and better yet on my Waller Flag receive antenna pointed SSW and rotated to the horizontal [polarization] configuration.”

Pointed SSW? Into daylight (Figure 1)? Things were getting stranger and stranger.

Carl Luetzelschwab, K9LA, asked for, and received, the VK9CZ 80 m log from GM3WOJ. This showed a total of 108 QSOs with the US, evenly split — 54 at their SR, 54 at their SS. Interestingly enough, there were no QSOs with Canada. For each QSO, K9LA looked up the US station’s location, and built a spreadsheet listing each QSO by date, time, and state. He deleted the call sign of each QSO, and sent the data to me for analysis. Table 2 shows the summarized data.

In Table 2 I defined the *opening duration* as the time difference between the first and last QSO on each day. In other words, this would be the “opening” as experienced by VK9CZ. As I experienced, the East Coast openings were brief, with the exception of two QSOs on 4 April, the rest of the openings had a duration of 14 to 20 minutes. It was also clear that the West Coast openings were of much longer duration.

I then put the number of QSOs made by each state on a map (Figure 2). It was interesting to see how the QSOs were distributed geographically, especially when compared to the meridian of the VK9CZ antipode. The VK9CZ antipode — the point on the opposite side of the Earth from VK9CZ — is in the Atlantic Ocean, just off the coast of Nicaragua. This map seemed to explain why the eastern openings were much shorter in duration than the western openings. The eastern stations were much closer to the meridian of

Table 1.
VK9CZ 80 m spots made during the openings to eastern North America. All were made within an eight-minute window, 2335-2343Z, over three days.

Date	Time	DX	From	Frequency	Note
3 Apr	2342Z	VK9CZ	N4SS	3507.5	QSX 3509.13 Gud signal into Ga.
3 Apr	2343Z	VK9CZ	K3TW	3507.5	Amazing 589 in FL! QSX 3508.6
7 Apr	2340Z	VK9CZ	N8PR	3507.5	QSX up 1
11 Apr	2335Z	VK9CZ	W4SO	3507.5	qsx up 1 great sig tonite
11 Apr	2338Z	VK9CZ	W1QS	3507.5	SE 449

Table 2.
Summary of 108 QSOs with VK9CZ on 80 m.

Date	1100-1400Z (West Coast NA) Opening Duration	QSOs	2300-2400Z (East Coast NA) Opening Duration	QSOs
20130403	-	0	0:20	13
20130404	-	0	0:03	2
20130405	0:42	7	-	0
20130406	-	0	-	0
20130407	-	0	0:19	18
20130408	-	0	-	0
20130409	1:52	20	0:14	6
20130410	1:56	16	0:14	3
20130411	0:27	11	0:16	12
Totals:	-	54	-	54

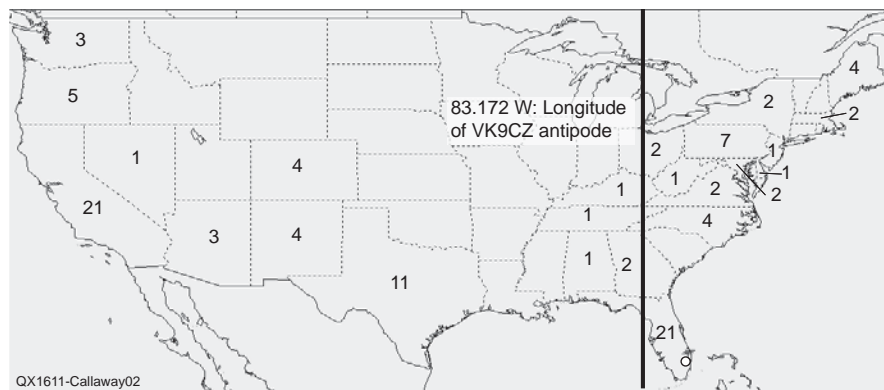


Figure 2 — VK9CZ 80 m QSOs made with North America. (Not Shown: An additional QSO made with Alaska.) QSOs east of the Mississippi occurred at or after SS (2300-2400Z); QSOs west of the Mississippi occurred at or before SR (1100-1400Z). [DX Atlas]

the VK9CZ antipode than those in the west. Many stations in the west, in fact, were so far away from the meridian that the term “gray line propagation” seemed inappropriate, and that standard short path propagation was likely responsible for their QSOs.

Next, I made a listing of the states in an approximate west-to-east order, and made a chart of QSOs made by state (Figure 3). This

chart emphasized the “dead zone” between the East (SS) and West (SR) openings, a region that did not have common darkness with VK9CZ at this time of year. Outside of this dead zone, there did not seem to be any particular advantage to be east or west; however, there was a large advantage to be in CA, TX, and FL — three southern states — even accounting for the large DXer

populations of these states.

Finally, I made a chart of the duration of the opening by state. Since there were so few QSOs per state, I modified the definition of “duration” slightly, to be the difference between the earliest and latest QSO time from that state, regardless of the day on which it occurred (Figure 4). Stations in some states in the east had very short

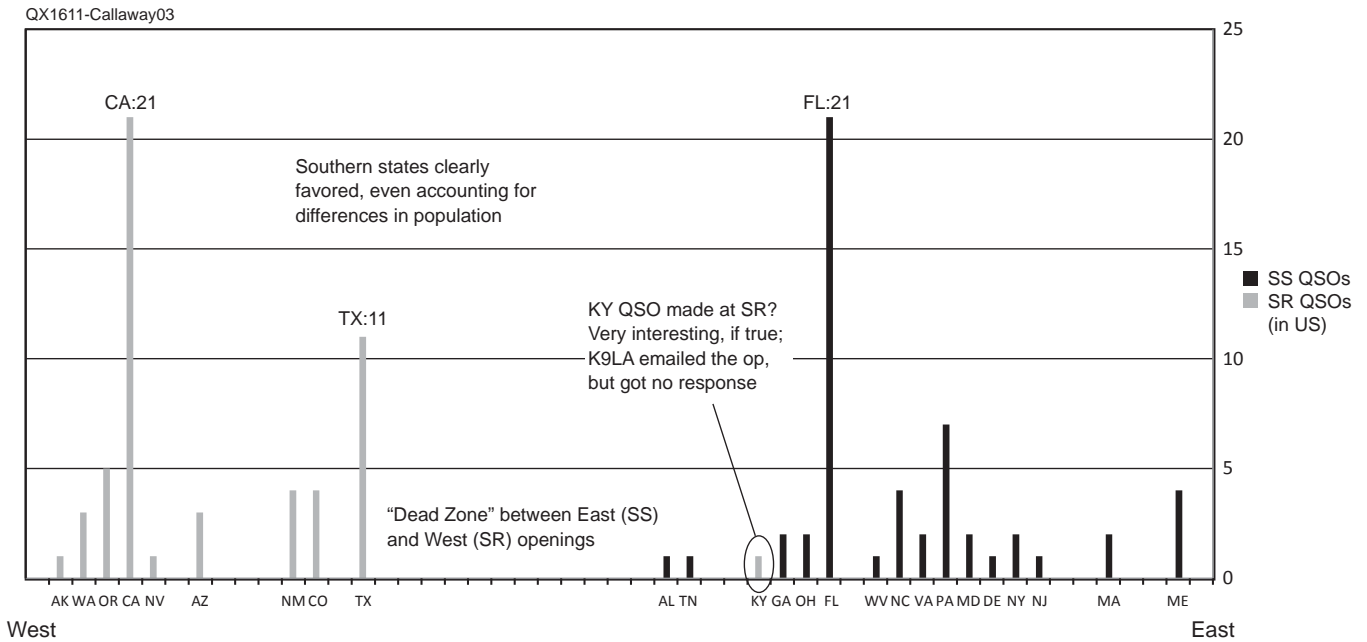


Figure 3 — VK9CZ 80 m QSOs made by state, ordered West-to-East. Southern states were favored in both SS and SR openings.

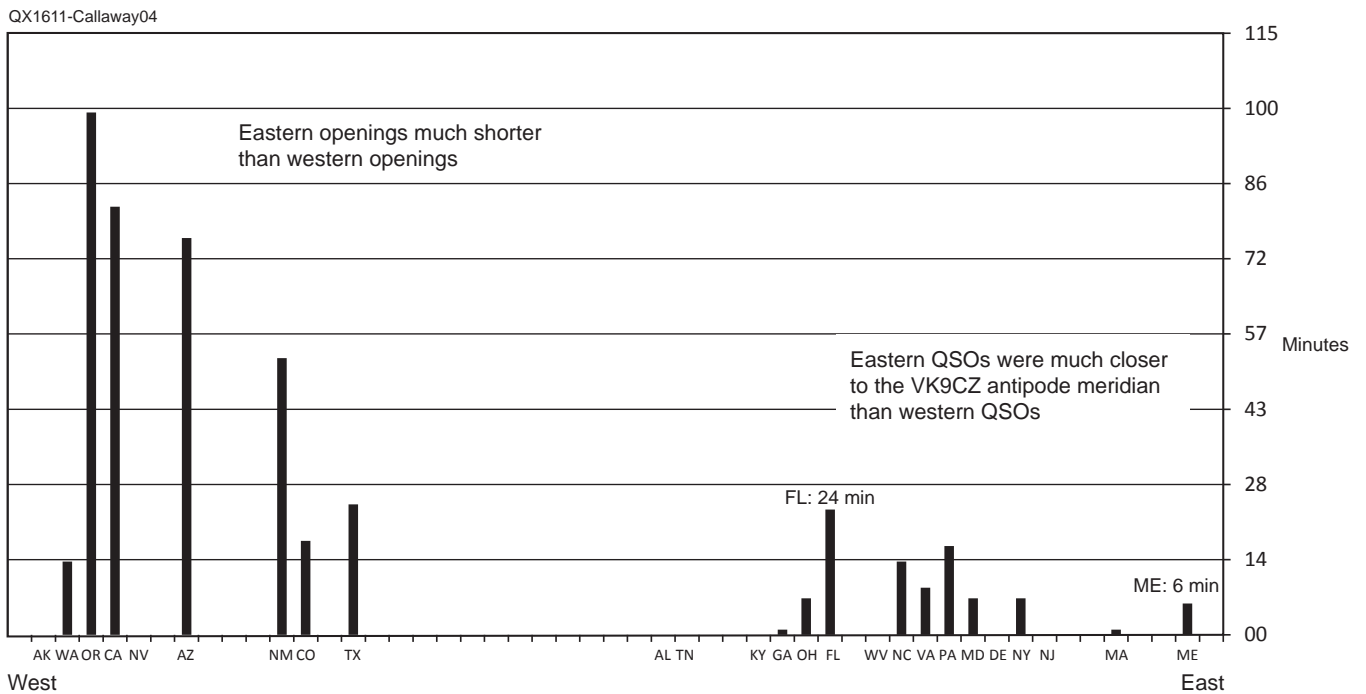


Figure 4 — Duration of VK9CZ 80 m opening by state, ordered West-to-East. The eastern openings were of much shorter duration than the western openings. Note the short duration of the Maine opening.

openings. Maine, for example, had 4 QSOs over 4 different days (by 4 different stations), and the time difference each day between the earliest and the latest QSO was only 6 minutes! Florida had the longest opening, at 24 minutes, although this could have been influenced by the relatively large number of QSOs made (21).

Insights

I now knew what had happened. The question of why it happened still remained. As I (and many others) had done in the past, when stumped on a propagation issue I asked

Carl, K9LA, for his opinion. He offered several insights.

1. Low band operators using directional receive antennas usually optimize signal-to-noise ratio (SNR), not signal strength.

This makes sense. One copies a signal best when the signal-to-noise ratio, not just the signal strength itself, is maximized. However, there is an interesting corollary in the case of gray line propagation on the low bands: When receiving, operators will have a directional bias towards the sun side of the terminator, since there is less noise

propagated from that side.

At SS, the signal may be arriving from the SSE, while the best SNR is found when the receive antenna is pointed SSW (Figure 5). The operator finds that, by turning the receive antenna slightly towards the sun side of the terminator, the signal level drops slightly, but the noise level drops more, thereby improving the SNR — and his ability to copy the DX.

Of course, the best direction for transmitting is still the direction from which the signal is arriving, leading to a second corollary: Under gray line conditions, optimum directions for low band transmit and receive antennas may be different!

This insight could explain why some ops said they copied the VK9CZ signal best when their receiving antennas were pointed to the SSW. Perhaps their signal was really coming from the SSE.

2. Propagation directly along the terminator is very unlikely and, if it did happen, would be very lossy.

One of the features of the terminator is a significant horizontal ionization gradient: There is (of course) much more ionization on the sun side than there is on the night side. This difference in ionization would refract a signal traveling along the terminator away from the sun side, and into the dark, nighttime ionosphere (Figure 6).

It's difficult to describe a physical mechanism that would trap a signal along the terminator for a trip halfway around the globe. Even if the signal were trapped by some means, the ionization levels along the terminator are quite high, which would lead

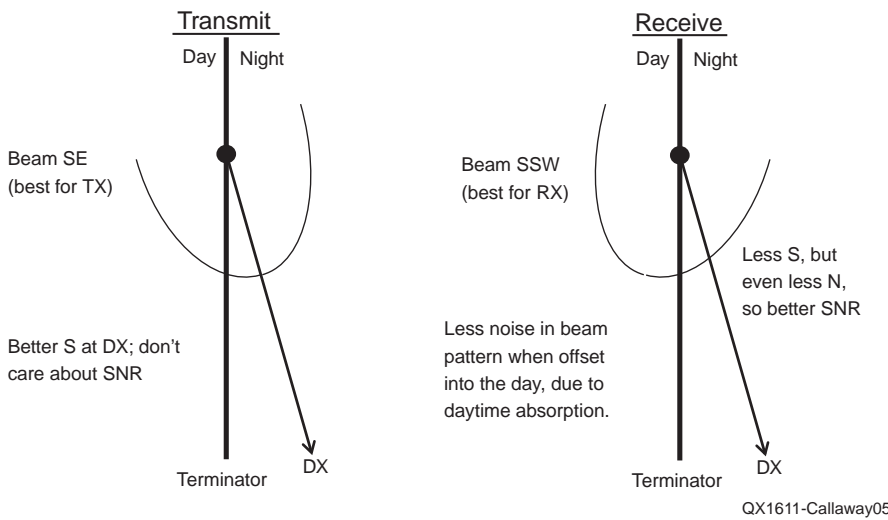


Figure 5 — The optimum transmit and receive beam headings can differ on the low bands at SR and SS, due to the lower noise arriving from the sunlit side of the terminator. The transmit antenna heading is optimized for best signal at the DX station, while the receive antenna heading is optimized for best SNR.

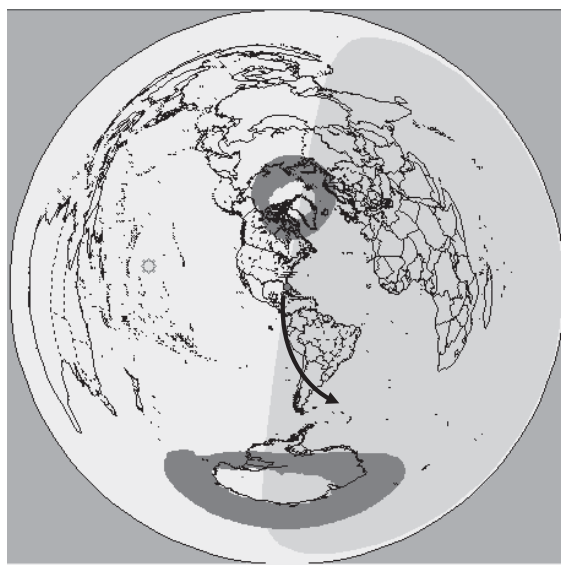


Figure 6 — Propagation along the terminator is unlikely. The horizontal ionization gradient along the terminator would refract a signal away from the terminator, into the dark ionosphere. [DX Atlas]

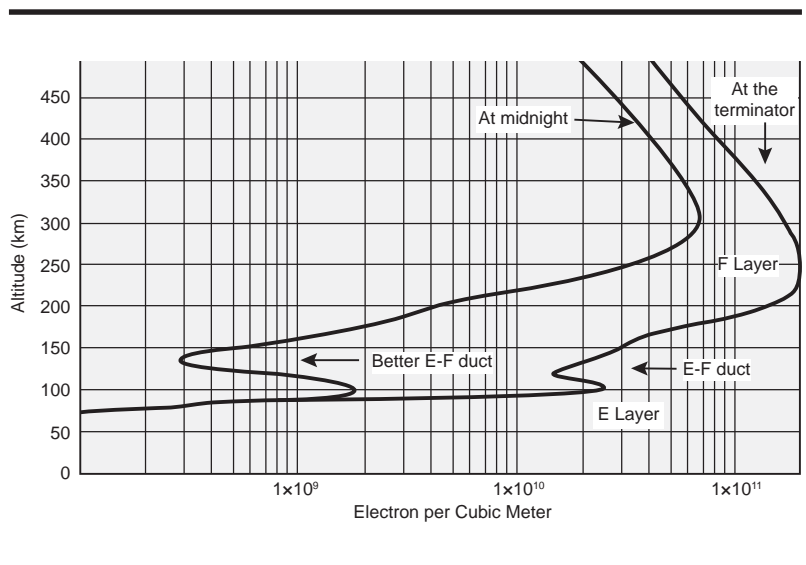


Figure 7 — The duct between the E and F layers of the ionosphere. Note the more pronounced duct at midnight, compared to the duct at the terminator. [Adapted from Robert R. Brown, NM7M, "On the SSW Path and 160-Meter Propagation," QEX, Nov/Dec 2000, pp. 3-9, Figure 1.]

to greatly increased absorption (attenuation) of low band signals when compared to the dark ionosphere.

It's also worth noting that north-south gray line propagation is "never" experienced. If it is SS, the propagation is always to someplace where it is SR, or vice-versa. One "never" has, for example, gray line propagation from North America to Brazil, when it is SS at both ends of the link. If the path for gray line propagation is along the terminator, it's difficult to identify a mechanism that enables SS-SR communication, while prohibiting SS-SS and SR-SR communication at the same time.

3. Long-distance low-band propagation almost certainly involves the duct between the E and F layers.

The path via conventional E- or F-layer hops has excessive ground loss (and ionospheric absorption) for an 11,450 km QSO on 80 m. On the low bands, the signal is refracted relatively low in the ionosphere, returning it to the ground more quickly than on the higher bands. This leads to more hops to cover a given distance, in turn leading to more ground loss. When the losses are added up, a QSO with VK9CZ on 80 m by this means seems unlikely.

However, if a signal can be injected into the region between the E and F layers of the ionosphere, the ground losses may be avoided and the resulting propagation can be relatively efficient (Figure 7). Intriguingly, the tilt of the ionosphere at SR and SS enhances the ability of a signal generated on the ground to enter the duct, so this would seem to be consistent with low-loss, long-distance gray line propagation.

At other times of the night, signals may still exit the duct and reach the ground at almost any location, if a local irregularity — a "hole" — exists in the E layer. Such irregularities are more common than not, and may play a part in so-called "spotlight" propagation, where signals are heard only in restricted, and seemingly random, geographic locations.

To experiment with this concept, I purchased *PropLab Pro 3.0*, a ray-tracing propagation simulation tool.¹ I set the tool for the date and time of the first VK9CZ opening that I experienced — 3 April 2013, 2327Z — and experimented with elevation angles with the beam heading set approximately south-southeast. The tool predicted that an 80 m signal leaving N4BRF at an elevation of 11 degrees would have one E-layer hop, then enter the E-F duct, and remain there (Figure 8). A similar analysis for Cocos (Keeling) indicated that a signal leaving VK9CZ at an elevation of 10 degrees on a heading of 210.7 degrees would go directly into the E-F duct (Figure 9).

The tool predicted that the headings needed to enter the duct were not especially critical — as long as they were into the dark side of the terminator, of course — but the elevations were required to be within a relatively narrow range. The required elevations on both sides of the link were relatively low — 11 and 10 degrees — but did not seem impractical, especially for vertical antennas located near seawater (as VK9CZ was).

4. Lowest-loss propagation for low-band signals should occur far from the sun, in the dark ionosphere, where absorption is least.

I say "should" because there is a long-standing problem with this. The N4BRF – VK9CZ Great Circle route (short path or long path) does not cross the dark ionosphere, but instead was near the terminator when these QSOs were made. This, as I have already

described, is an unlikely path. However, a path from N4BRF across the dark ionosphere never arrives at VK9CZ — it's pointed in the wrong direction. To get the signal to arrive at VK9CZ would require something to skew, or otherwise redirect, the signal traveling from N4BRF onto a Great Circle route leading to VK9CZ.

But what?

Candidate Path Summary

I now had a list of candidate paths between VK9CZ and N4BRF (Figures 10(A) – 10(D).

(A) — Short Path (12°) Great Circle Route

Improbable, as it passes through the high attenuation of the northern auroral oval, and disagrees with the beam headings observed by N8PR and W1QS.

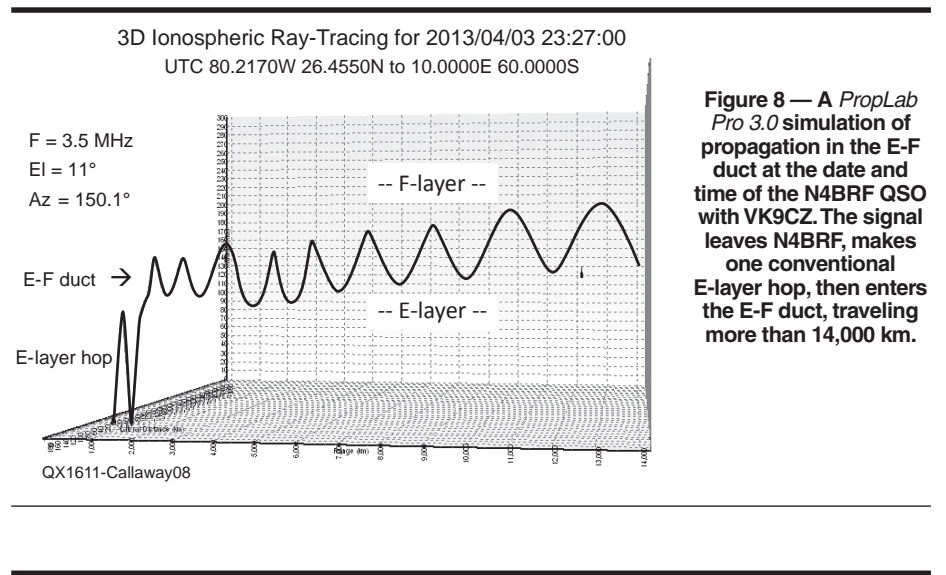


Figure 8 — A *PropLab Pro 3.0* simulation of propagation in the E-F duct at the date and time of the N4BRF QSO with VK9CZ. The signal leaves N4BRF, makes one conventional E-layer hop, then enters the E-F duct, traveling more than 14,000 km.

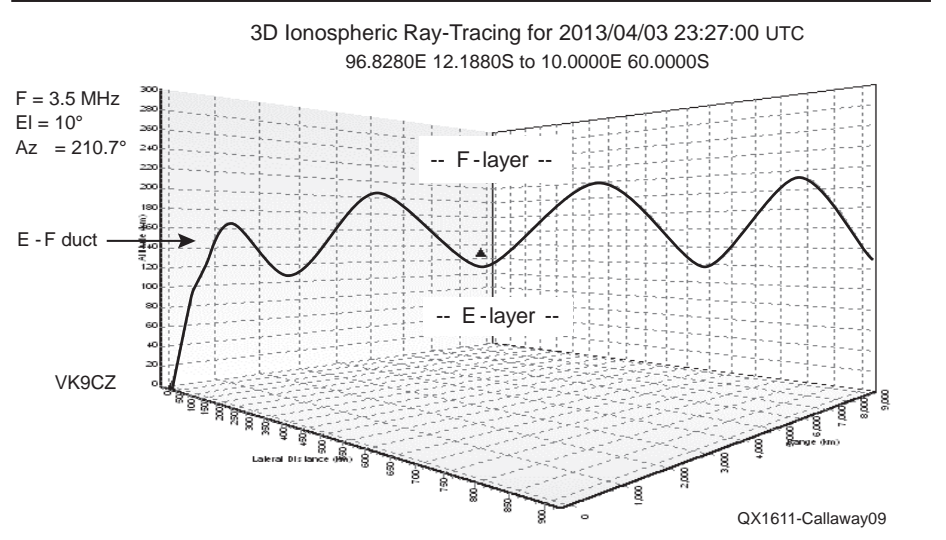


Figure 9 — A *PropLab Pro 3.0* simulation of propagation in the E-F duct at the date and time of the VK9CZ QSO with N4BRF. The signal leaves VK9CZ and immediately enters the E-F duct, traveling more than 9,000 km.

(B) — Long Path (192°) Great Circle Route

Improbable, as it passes through the high attenuation of the southern auroral oval, and stays in sunlight the entire way.

(C) — Path Along the Terminator
 Improbable, due to the high ionization (and horizontal gradient of the ionization) along the terminator; also, the E-F electron density valley is not as well developed along

the terminator, meaning that ducting is less likely here than in the dark ionosphere.

(D) — Path Through the Dark Ionosphere
 Seems the most promising, but what could cause the required skew?

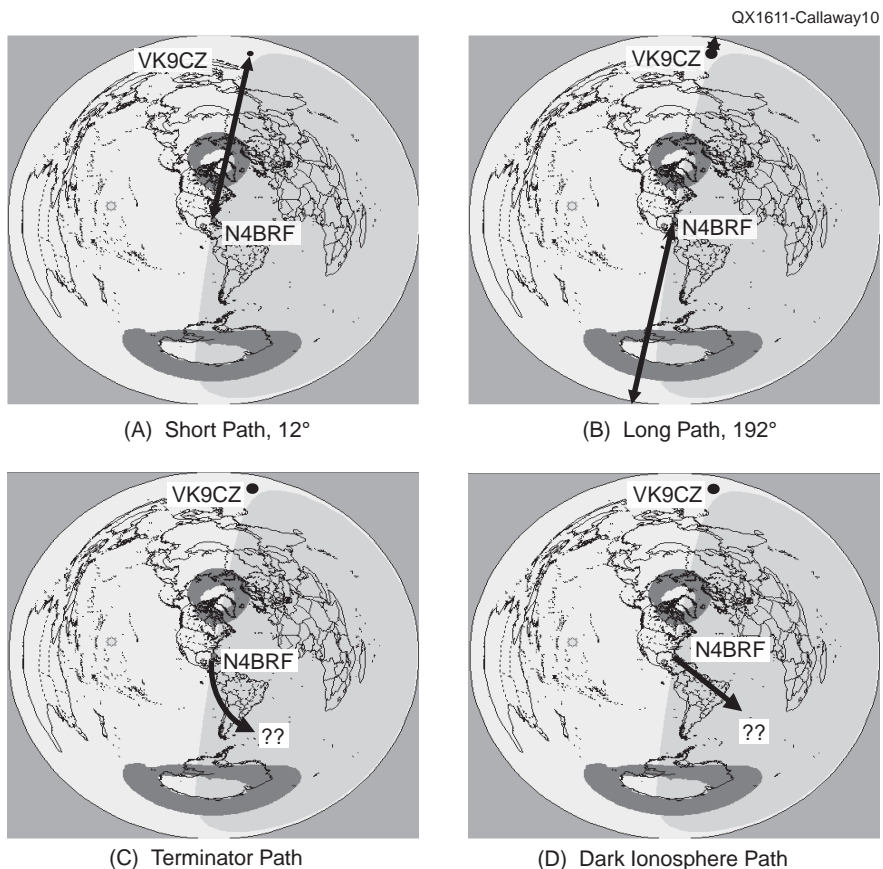


Figure 10 — Improbable routes between N4BRF and VK9CZ: (A) Short path to the north; (B) Long path to the south; (C) Path along the terminator; and (D) Path through the dark ionosphere. [DX Atlas]

The Path through the Dark Ionosphere

Old hands on the low bands know the adage, “SE at SS, SW at SR.” To identify what might cause the required skew for the path through the dark ionosphere, one starts by realizing that, if the path leaves N4BRF on a Great Circle to the SE, and arrives at VK9CZ on a Great Circle from the SW, the skewing element is most likely at the intersection of these two Great Circles.

It became clear that I needed a software package that could plot two Great Circles on a map of the globe. After some experimentation, I found one in *R*, a software environment for statistical computing and graphics.² *R* is available as Free Software under the terms of the Free Software Foundation’s GNU General Public License in source code form. It compiles and runs on a wide variety of UNIX platforms and similar systems (including FreeBSD and Linux), Windows and MacOS, and has many extension packages available via pull-down menu picks. The method I used required the “maps” and “geosphere” packages.

The Great Circle code in *R* is very simple; for example, this code draws a dashed line on a world map that follows the Great Circle leaving N4BRF at a bearing of 150 degrees:

```
[Line 1] #requires maps and
         geosphere packages
[Line 2] N4BRF <- c(-80.217,
                 26.455)
[Line 3] data(wrld)
[Line 4] plot(wrld, type='l')
[Line 5] dpN4150
         <- destPoint(N4BRF,
                     b=150, d=15000000)
[Line 6] gcN4150
         <- greatCircle(N4BRF,
                       dpN4150, n=360)
[Line 7] lines(gcN4150,
              lwd=2, lty='dashed',
              col='black')
```

Line 2 locates N4BRF on the map by longitude and latitude. Line 5 defines a destination point 15 million meters away from N4BRF, along the great circle heading of 150 degrees. Line 6 defines the Great Circle containing the locations of N4BRF and the destination point, and Line 7 draws the line on the map.

Using *R*, I made a map that had Great Circles leaving N4BRF to the SSE (I used

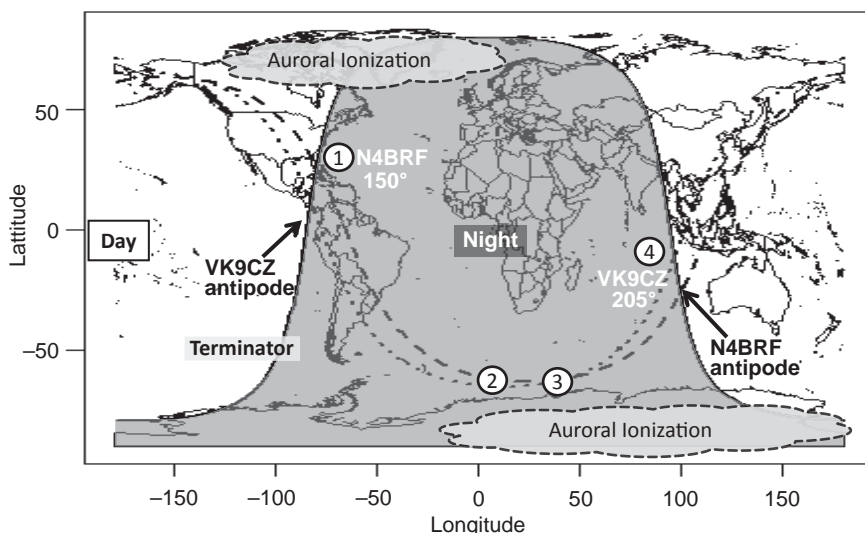


Figure 11 — The path through the dark ionosphere, with the ionization of the southern polar oval as the skewing element between N4BRF and VK9CZ. The ionization skews the signal towards the equator, i.e., to the north, from one Great Circle to the other. Dashed line: N4BRF Great Circle. Dotted line: VK9CZ Great Circle. Solid line: terminator.

DX[®] ENGINEERING

8:30 am to midnight ET, Monday-Friday
1230 to 0400 UTC March-October

8:30 am to 5 pm ET, Weekends
1230 to 2100 UTC March-October

International/Tech: 330-572-3200

8:30 am to 7 pm ET, Monday-Friday

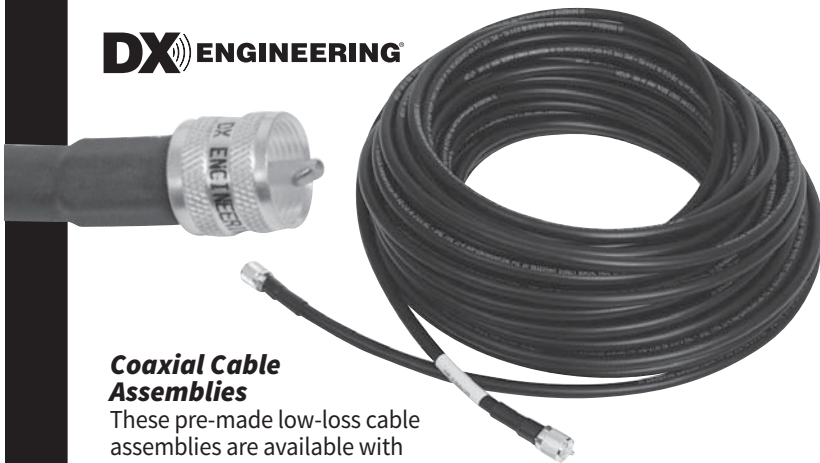
9:00 am to 2 pm ET, Saturday

Country Code: +1 Sale Code: 1612QEX

800-777-0703 | DXEngineering.com

**ORDER BY 10 PM
SAME-DAY
SHIPPING**
Mon-Fri, 10 pm ET
In-Stock Items

DX[®] ENGINEERING



Coaxial Cable Assemblies

These pre-made low-loss cable assemblies are available with DX Engineering's patented new PL-259 connectors, featuring the best qualities of both crimp-on and solder-on connectors. Use the free online Custom Cable Builder at DXEngineering.com to build assemblies made to your exact specs.

DX Engineering's coaxial cable is also available by the foot or in bulk spools.

bhi
Noise Cancellation Products



bhi Noise Cancellation Products

bhi Noise Cancellation Products harness cutting-edge digital signal processing (DSP) technology to enhance the audio quality of incoming radio signals. By removing the noise, the improved audio makes it much easier to discern distant and weak contacts. DX Engineering now carries bhi Noise Cancellation Products, plus bhi accessories like switches, cables, adapters and extension speakers.

DX[®] ENGINEERING



Footswitches

Go hands-free and speed up your operating. These new PTT footswitches from DX Engineering blend performance and value. You have three options: a budget friendly plastic model, the stalwart cast iron version, and a new style with an extra-wide pedal—perfect for enthusiastic stomps.

DX[®] ENGINEERING

Active Magnetic Loop MF/HF Receiving Antenna

The well-known RF-PRO-1B is now manufactured and sold exclusively by DX Engineering. This original Pixel loop design incorporates a high performance preamplifier for excellent broadband reception from 50 kHz to 30 MHz. Installation is easy, because it's only 38 inches in diameter. When rotated, this antenna provides deep nulls for effective reduction of directional noise and interfering signals. Ideal for Amateurs, SWLs and AM DXers, this loop also offers up to 30 dB rejection of electrostatic field noise.



150 degrees) and VK9CZ to the SSW (I used 210 degrees). The two Great Circles crossed just off the coast of Antarctica — and on the edge of the auroral oval.

The Path Skewing Element

The auroral oval, or some region of ionization associated with it, represents a candidate for the skewing element. The proposed propagation mechanism would be as follows (Figure 11).

(1) – The signal leaves N4BRF at SS, and enters the E-F duct on a Great Circle route to the SSE.

(2) – On its way to the N4BRF antipode, the signal approaches the southern auroral oval at a small (almost tangential) angle.

(3) – The horizontal ionization gradient — more ionization towards the pole, less towards the equator — present at the auroral oval refracts the signal onto a new Great Circle route, equator-ward of the previous route, still via the E-F duct.

(4) – The signal exits the E-F duct on a Great Circle route from the SSW, and reaches VK9CZ at SR.

This is probably best seen by an azimuthal plot, centered on the presumed skewing element (Figure 12). In this plot, it is clear that the required refraction by the skewing element is only a few degrees. This small amount of refraction is all that is required to bend the N4BRF signal away from the N4BRF antipode and onto the Great Circle route leading to VK9CZ.

It is interesting to consider an azimuthal plot for the path from Maine to VK9CZ (Figure 13). Due to the different path geometry, the required refraction is much greater, which may explain the very short duration of this opening. Interestingly, the portions of Canada along the terminator would require even greater refraction angles, which may explain why no Canadian QSOs were made by VK9CZ on 80 m.

These were, and are, interesting results, but what evidence can be found that refraction off polar ionization is, in fact, the correct mechanism?

One bit of support comes from the 2012 *International Reference Ionosphere* (IRI), an empirical standard model of the ionosphere used for geophysical research. Using the IRI, I made a model simulation of the E-F duct — which the IRI calls the “E valley” — for 3 April 2013 at 2330Z, along the 20° East meridian (Figure 14). The model shows that the duct is 50 to 65 km wide (top to bottom) for most of the meridian, but closes to less than 20 km at both poles. Further, the ratio of minimum to maximum ionization along the valley is approximately 0.2 for most of the meridian, but rises to nearly 1.0 at the poles — i.e., the duct goes away.

A second bit of support is more

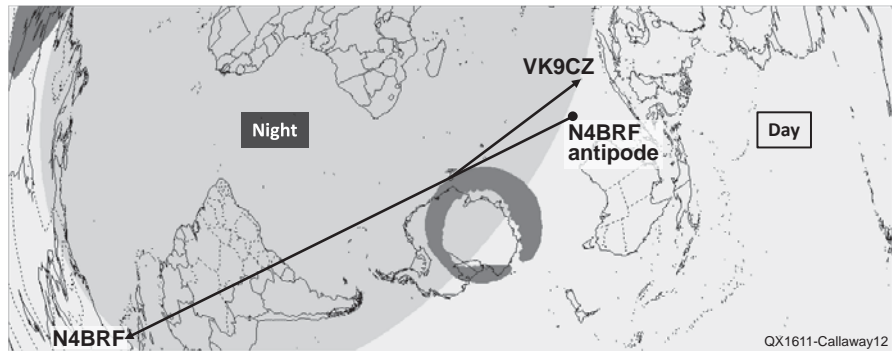


Figure 12 — An azimuthal plot of the path through the dark ionosphere between N4BRF and VK9CZ, centered on the presumed skewing element. Note the relatively small angle of refraction needed. [DX Atlas]

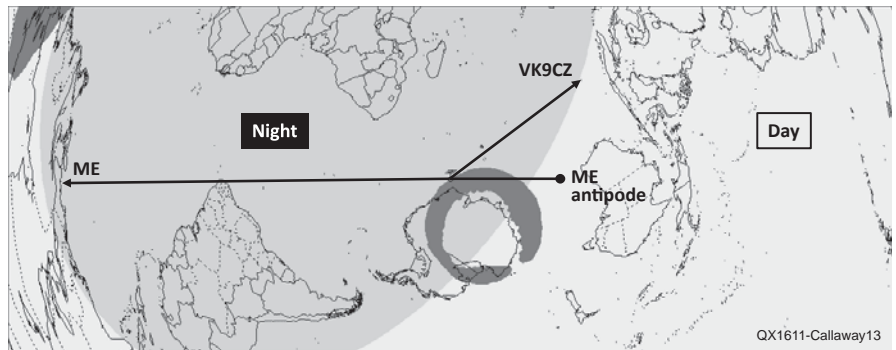


Figure 13 — An azimuthal plot of the path through the dark ionosphere between Maine and VK9CZ, centered on the presumed skewing element. Note the relatively large angle of refraction needed. [DX Atlas]

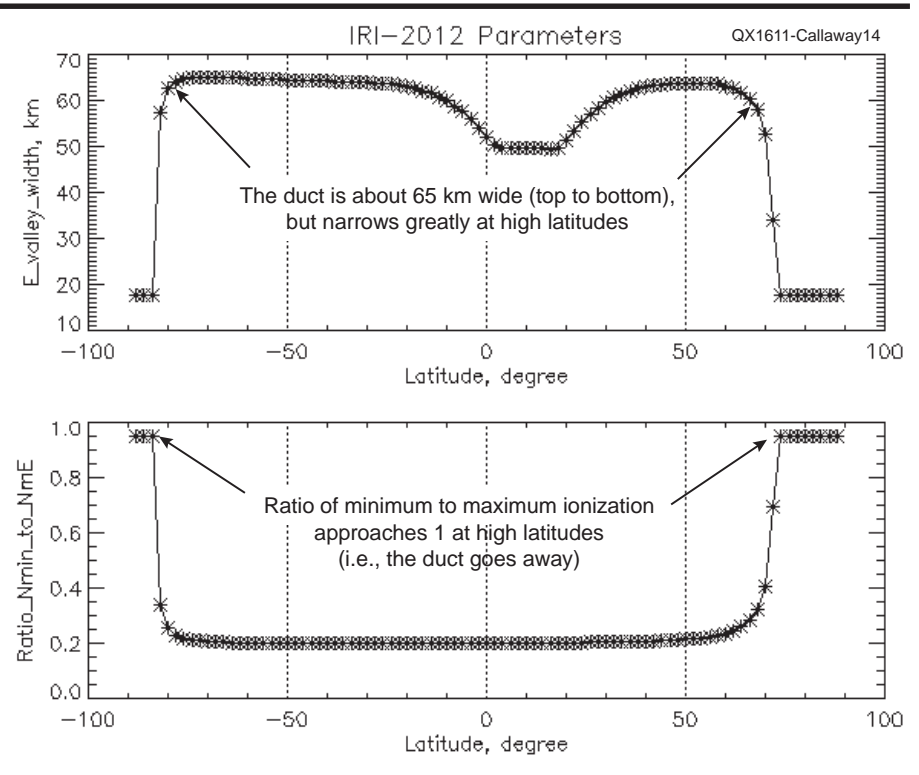


Figure 14 — Parameters of the E-F duct available in the 2012 International Reference Ionosphere model for 3 April 2013 at 2330Z, along the 20° East meridian. [omniweb.gsfc.nasa.gov/vitmo/iri2012_vitmo.html]

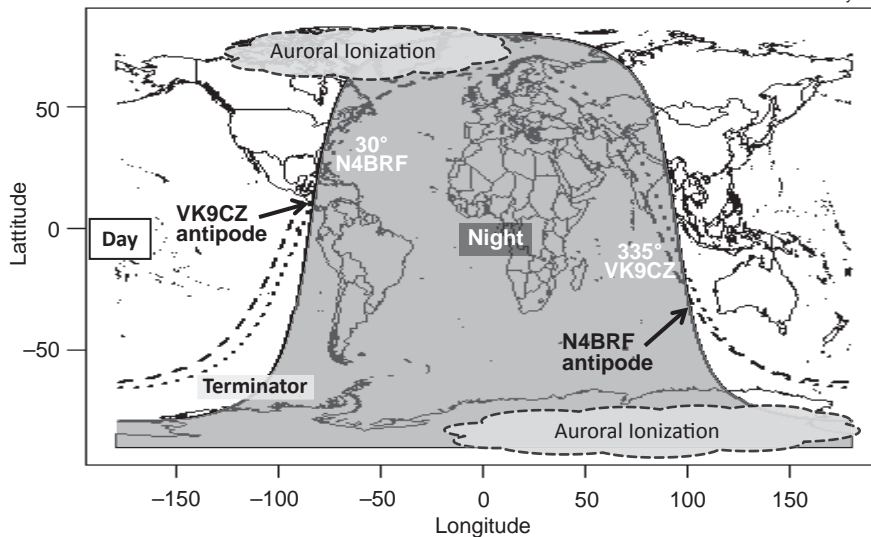


Figure 15 — The path to the north is not open because the skew required to move from one Great Circle to the other is to the north, but the ionization of the northern polar oval refracts the signal towards the equator, i.e., to the south. Dashed line: N4BRF Great Circle. Dotted line: VK9CZ Great Circle. Solid line: terminator.

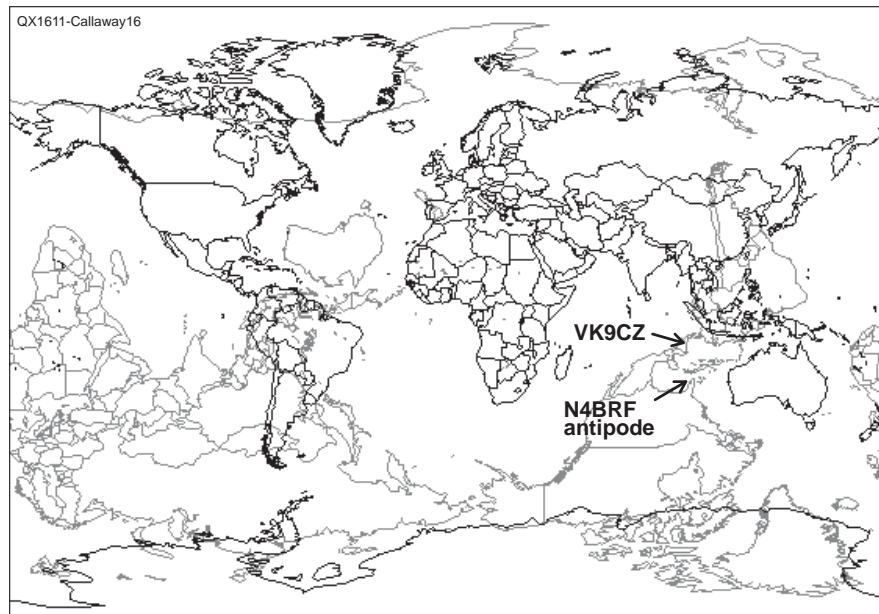


Figure 16 — Antipodes. For stations in North America, nearly all DX in Asia and Oceania is north of their antipode. This accident of geography drives the “SW at SR, SE at SS” experience. [peakbagger.com/pbgeog/worldrev.aspx]

circumstantial. While “SE at SS, SW at SR” is commonly experienced in the northern hemisphere, to my knowledge there has never been a satisfactory explanation for why one never experiences the symmetrical situation to the north. One does not experience “NE at SS, NW at SR” – at least, not in the northern hemisphere. What is so special about the southern direction?

This asymmetry is explained by the polar refraction hypothesis of gray line propagation. Consider a path to the northeast

from N4BRF, with the goal of reaching VK9CZ (Figure 15). Because VK9CZ is north of the N4BRF antipode, a signal on an N4BRF Great Circle to the north must be refracted north, towards the pole, to get on a VK9CZ Great Circle.

However, the horizontal ionization gradient at the auroral oval (greater ionization to the north, less ionization to the south) refracts the signal south, towards the equator, sending the N4BRF signal into Europe or Africa – away from the VK9CZ Great

Circles. It is only in the southern hemisphere that signals from the northern hemisphere are refracted in the correct direction.

This means that the requirement for gray line propagation for DXers in the northern hemisphere is that the DX station must be north of the DXer’s antipode. Due to an accident of geography, this requirement is met for nearly all combinations of locations in the North America and DX locations in Asia and Oceania (Figure 16). A similar relationship exists between Europe and much of Oceania.

Points in Favor of this Hypothesis

The polar refraction hypothesis of gray line propagation then has the following points in its favor.

(1) – Explains the “SE at SS, SW at SR” experience of low-band operators in the northern hemisphere for long-distance QSOs. Ionization in or near the southern auroral oval refracts signals from the source Great Circle to the destination Great Circle.

(2) – Explains why a path to the north is “never” open from the northern hemisphere. Ionization in or near the northern auroral oval refracts signals away from the needed direction.

(3) – Explains why VK9CZ favored southern stations. The required angle of refraction increases for more northerly (and easterly) stations.

(4) – Explains why north-south gray-line paths are “never” experienced. The signal travels into the dark ionosphere, away from the terminator, in a duct of better quality than that available along the terminator itself.

(5) – Predicts the “NE at SS, NW at SR” experience of low-band operators in the southern hemisphere. Take, for example, a link between southern Brazil and central Philippines (Figure 17). In this case, the ionization at or near the northern auroral oval refracts the signal from Brazil in the required direction — south, towards the equator, and onto a Great Circle leading to the Philippines. The antipode of the Brazilian station is near Okinawa, so it can employ gray line propagation for DX south of that point.

Assumptions Made in this Hypothesis

While the above may be persuasive, the polar refraction hypothesis is based on several unproven assumptions.

(1) – Auroral oval ionization is as described, and does close the E-F duct and refract the incoming signal equatorward. While the existence of the auroral oval is established fact, its function in refracting signals in the E-F duct has not been demonstrated.

(2) – The path was to the SSE, not SSW, at N4BRF. We have no data, since N4BRF used a vertical (omnidirectional) antenna.

(3) – The path was to the SSW at VK9CZ. Again, we have no data, since VK9CZ used a vertical (omnidirectional) antenna.

(4) – E-F duct propagation. While there are strong, compelling reasons for believing that long-distance low-band propagation occurs via the E-F duct — largely path loss calculations and the known structure and physics of the ionosphere — I know of no measurements taken to confirm that propagation actually occurs via this mechanism.

The TOFU Project

One way to confirm this propagation mechanism is to use time-domain techniques to determine the path delay and, therefore, its path length. The problem of gray line propagation seems particularly amenable to this type of analysis, since it is relatively predictable in both time and location, and there are specific candidate paths having predictable path delays. The Time-Of-Flight Unit (TOFU) project is an attempt to use time-domain techniques to answer this question.³

The concept of TOFU is simple. Both ends of the link are synchronized in time, via GPS. At a known time, the transmitting station sends a predetermined pseudo-random (PR) sequence (e.g., 255 bits in length) of ones and zeros. The receiving station stores what it receives in a time-stamped file. The received data can be post-processed (with, e.g., *Matlab*) by passing it through a sliding correlator and the time of maximum correlation — the “correlation peak” — determined. Since both stations are time-synchronized, once the delays through the transmitter and receiver are removed, a simple calibration, the difference between the time of the correlation peak and the time that the PR sequence was sent is the measured path delay. This delay can then be compared against those delays predicted by the various candidate propagation mechanisms.

At present the US has a 300 baud limit on digital signaling at HF, which means the minimum duration of bits in the PR sequence is 3.333 ms. Given the signal-to-noise ratios common on the low bands and the limited symbol transition times due to the limited signal bandwidth, but accounting for oversampling at the receiver, one may hope to achieve a measured path delay accuracy of better than plus or minus 1 ms, leading to a path length measurement uncertainty of plus or minus 300 km.

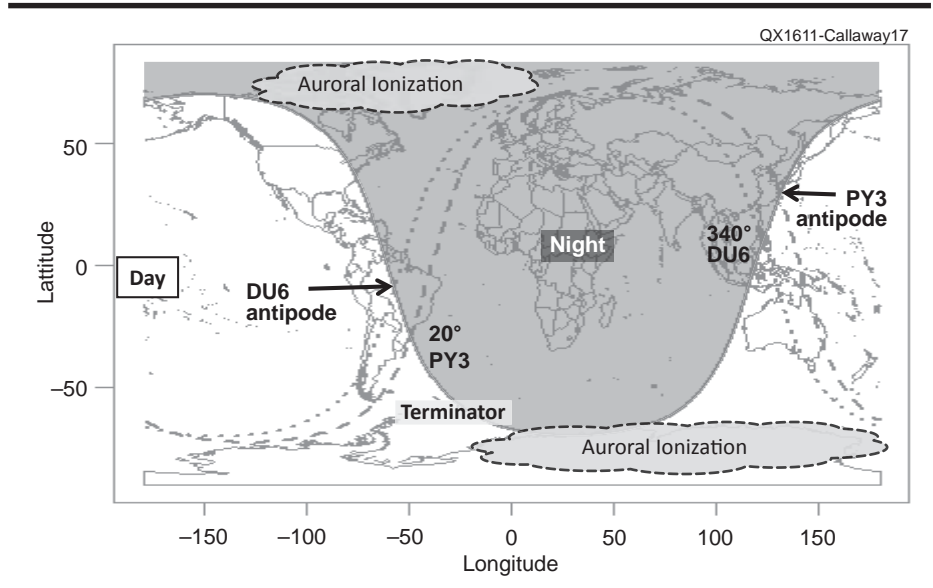


Figure 17 — The path through the dark ionosphere, with the ionization of the northern polar oval as the skewing element between PY3 (southern Brazil) and DU6 (central Philippines). The ionization skews the signal towards the equator, i.e., to the south, from one Great Circle to the other. Dashed line: PY3 Great Circle. Dotted line: DU6 Great Circle. Solid line: terminator.

Those interested in working on the TOFU project — a project still at the concept stage — should contact the author.

Conclusion and Future Work

This investigation of gray line propagation started with a surprising 80 m QSO, and is still going strong, three years later. The tentative conclusion is that polar refraction of low-band signals in the E-F duct is most likely responsible for the phenomenon, although this has yet to be confirmed experimentally.

One corollary to this hypothesis is that relatively low takeoff angles would be best to participate in gray line propagation, since they are needed to inject a signal into the E-F duct at SR and SS. Interestingly, if long-range, low-band propagation generally occurs via the E-F duct at times other than SR and SS, antennas with higher angles of radiation also may be useful, so that signals may be injected into — and detected coming out of — random E-layer inhomogeneities. Perhaps the main value of gray line propagation is that it provides a predictable time and location for an entrance into the E-F duct — SR and SS.

Experimental confirmation of the polar refraction hypothesis is a subject of future work. Also of interest is a study of the

polarization of signals received via gray line propagation. This could be done, for example, using Waller flag antennas having rotatable polarization.

Ed Callaway, N4II, received the BS degree in mathematics and the MSEE degree from the University of Florida in 1979 and 1983, respectively, the M.B.A. degree from Nova (now Nova-Southeastern) University in 1987, and the PhD degree in computer engineering from Florida Atlantic University in 2002. He holds 58 issued US patents, and is the author of several books, book chapters, and papers. Dr. Callaway is a Registered Professional Engineer and was named an IEEE Fellow in 2010. After 25 years with Motorola, in 2009 Dr. Callaway co-founded Sunrise Micro Devices, a leading provider of low-voltage, low-power wireless IP to the semiconductor industry, where he was CTO. In 2015 the company was sold to ARM, Ltd., where he is now Director of Radio Standards. Dr. Callaway holds an Amateur Extra Class license and is a Life Member of the ARRL. He is an avid DXer, and is fascinated by ionospheric propagation of all types.

Notes

¹shop.spacew.com.

²<https://www.r-project.org/>.

³Carl Luetzelschwab, K9LA, first suggested the use of time-domain techniques to me.

A More Efficient Low-pass Filter

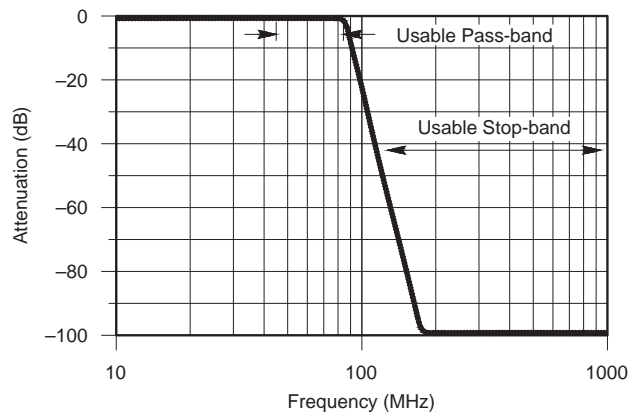
G3TMG compares Zolotarev quasi-elliptic low pass-band characteristics with the classical Chebyshev design in terms of the expected performance for lumped-element circuits, and shows a universal table of values that can be used in filters for Amateur Radio bands.

A comparison between two synthesized quasi-elliptic low-pass filters — one possessing a Chebyshev and the other a Zolotarev pass-band characteristic — is carried out in terms of the expected performance for lumped-element circuits. Two examples of the Zolotarev filter type have been constructed and tested using different, but appropriate, inductor techniques. Also, a universal table of values, which can be used for most of the Amateur Radio bands, is for the first time made available.

Introduction

A radio transmitter/amplifier combination can be a powerful source of interference. It is particularly important to protect against harmonic emission. As a consequence the output stages for both driver and amplifier equipments are most often followed by filters that provide harmonic suppression — usually for HF — using a lumped element low-pass network. When consideration is given to a modern transceiver, which allows moderately high power operation from 1.8 – 50 MHz (6 octaves), it is clearly necessary to have many switched analog output filters within the equipment — one thing that the Software Defined Radio concept hasn't yet solved.

Using stock low-pass designs^{1,2} with well-matched pass bands from dc to a predefined cut-off frequency f_c , is clearly not efficient since more than half of the low-pass bandwidth is of no practical value — the required signal frequency must lie above $f_c/2$ to provide any harmonic attenuation from the filters transition edge or ultimate stop-band.



QX1609-Cobb01

Figure 1 — Generic low-pass filter.

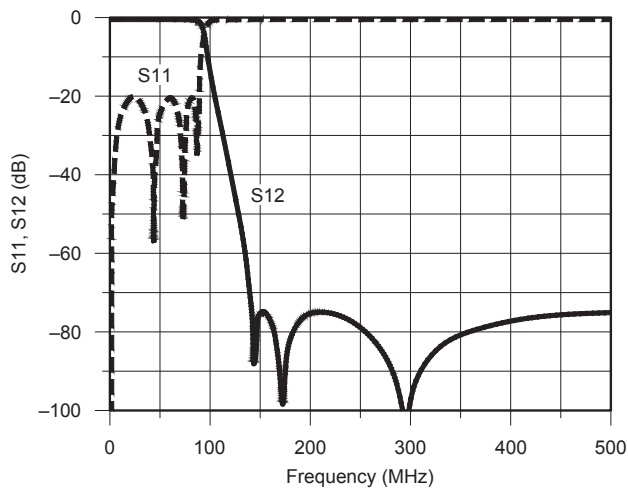
Figure 1 shows a generic low-pass filter. This is somewhat of an over simplification but that's the way it appears because the Amateur Radio bands have a small fractional bandwidth.

Available Low-pass Solutions

It is known that N^{th} order Cauer or Elliptic low-pass filters provide the fastest pass-band to stop-band roll-off rate together with a predefined minimum attenuation across the entire stop-band. They have $(N-1)/2$ or $N/2$ finite frequency transmission zeros, for even or odd orders respectively, periodically placed across the entire stop-band. An example 7th order response, shown in Figure 2, is based on the 4 m band — say 70 –

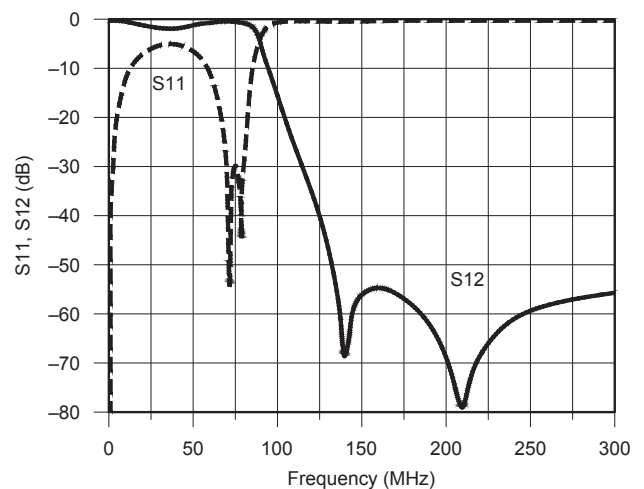
71 MHz for the sake of argument — being coincident with the second reflection zero left of the cut-off frequency so as to reduce reflection loss. Additionally, a single real frequency transmission zero (most adjacent to the transition region) is arranged to coincide with the 4 m signal 2nd harmonic of 140 MHz.

This approach needs 10 components but, except for the first transmission zero, the far out zeros do not actually contribute greatly to the transition region roll-off rate and, as can be seen, does not provide for the production of a zero at, or near, the 3rd harmonic frequency of 210 MHz. Also, and importantly, the inductance ratio within the realized network is in the region of 25:1



QX1609-Cobb02

Figure 2 — A loss-less 7th order Elliptic response.



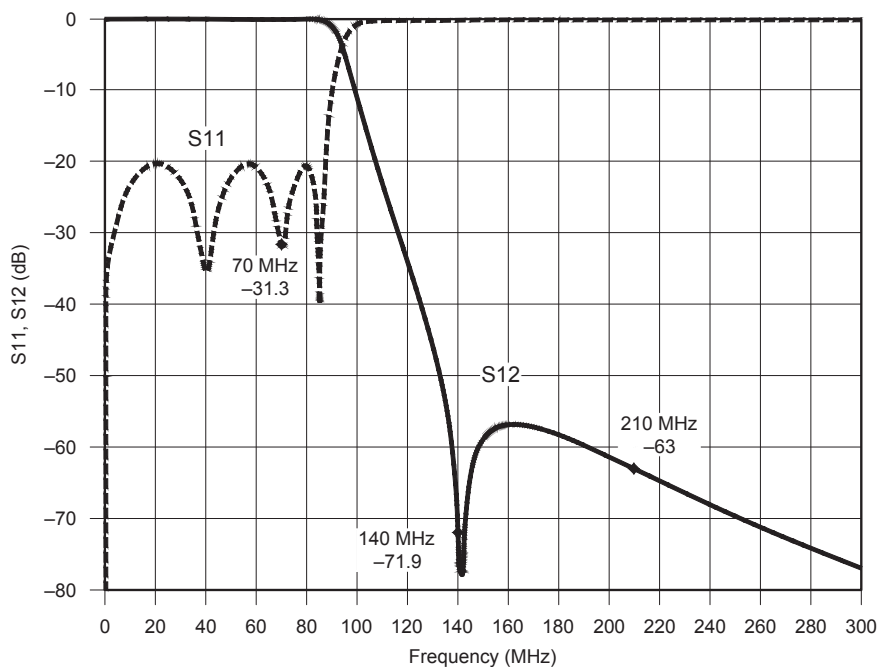
QX1609-Cobb03

Figure 3 — A 5th order response from *OptLowpass* program, tweaked and with losses.

which, for the higher HF bands, makes it quite difficult to realize the additional zeros due to mutual coupling and unintentional resonance issues. Although Elliptic designs may in many cases be impractical, one might still consider the out-of-band performance to be the state-of-the-art target.

To keep the insertion loss to a minimum, the lowest order filter together with the widest pass-band width, and the smallest number of components, is the usual approach. Generally, the solution is most often the use of a low-pass filter with Chebyshev pass-band characteristics — equi-ripple response — whose order can be further minimized when a single transmission zero is placed immediately adjacent to the filters transition region. The article³ by Ed Wetherhold, W3NQN, on this subject summarizes the work of Jim Tonne, W4ENE (formerly WB6BLD), on what has become known as the CWAZ (Chebyshev With Added Zero) low-pass filter. These filters are more often known as quasi- or pseudo-elliptic types in modern parlance.

Recently, Jim has further provided a useful solution to the harmonic rejection problem with his *OptLowpass* design program⁴ that combines the described Elliptic stop-band characteristic and a matched region only in the top half of the low-pass pass-band where it is needed. This program is currently restricted to a 5th order response but nevertheless may be considered optimal as it demonstrates firstly, a significant improvement in the general stop-band rejection when compared to the standard Chebyshev design of the same order and secondly, the provided stop-band zeros happen to nearly coincide with the



QX1609-Cobb04

Figure 4 — A 7th order CWAZ transmission response [after: Wetherhold, with losses].

2nd and 3rd harmonic frequencies. With a little adjustment — by using trimmer capacitors in the reject resonators in reality — improvements can be made by precisely tuning the stop-band notches. Typically then, Jim's solution provides for, in principle, around 65 dB of 2nd and 75 dB of 3rd harmonic protection and 54 dB generally elsewhere with just 7 components — see Figure 3. This is potentially a very good

performance with a cost of about 0.2 dB insertion loss based on practical solenoid inductors. In practice however, it is difficult to achieve the 3rd harmonic notch because the required resonating capacitance is only 7.5 pF with an inductance of nearly 80 nH. A shielded solenoid inductor of this value, designed to provide an unloaded Q of 200 (~15 mm diameter), is found to have a self capacitance of between 3 and 4 pF

— a significant proportion of the desired resonating capacitance. Compensating for this is a little on the tricky side but somewhat easier than trying to tune the ideal Elliptic!

Suppose that more stop-band attenuation, in general, is required. Well, we could try a 7th order CWAZ low-pass filter as previously described by Ed Wetherhold. Calculating the transfer function based on scaled prototype values for the 70 MHz example (with tweaks) provides for a response as shown in Figure 4. Clearly, the rejection has improved for the 2nd harmonic as compared to the circuit produced by *OptLowpass* at the cost of one more component — now 8. The 3rd harmonic band is clearly worse at 63 dB, as we might have expected with no coincident zero, but the general rejection is better, monotonically improving beyond the 3rd harmonic frequency. Taking a leaf out of Jim Tonne’s book, the rejection could still further be improved by providing a matched region only in the top half of the low-pass pass-band. How might this be done and what would be the cost?

It turns out that Jim has discovered, intentionally or otherwise, the characteristic that has become known as the Zolotarev function. This function is similar to the ubiquitous Chebyshev characteristic which has a y-valued unit amplitude cyclic behavior between x-axis values of -1 and 1 radian. In the Zolotarev case, which has an extra parameter, the first cycle about the origin can have a magnitude greater than 1. Figure 5 compares the two functions.

This issue was researched more than 40 years ago by Ralph Levy⁵ who determined a method of incorporating this characteristic into low-pass filter designs for, in principle, any order. The mathematics therein is not trivial but the basic outcome is that even ordered functions are analytic and can be generated by modifying the root locations of a conventional Chebyshev polynomial function in a predetermined geometric fashion. For these to be realizable however, it is necessary for the source and load to be unequally valued, the ratio depends on the bandwidth compression factor chosen.

Odd-ordered functions — more appropriate for low-pass filters — are unfortunately not so easily dealt with, requiring some rather knotty mathematical techniques. Nevertheless, these are of greater value since the resulting network source and load are always equal. Because of this, a simpler design methodology for any odd ordered function has been recently developed and fully described previously in *QEX*.⁶ The mathematics will not be described here but the Zolotarev With Added Zero (ZWAZ) will first be compared to that of the CWAZ, by way of example, using essentially the

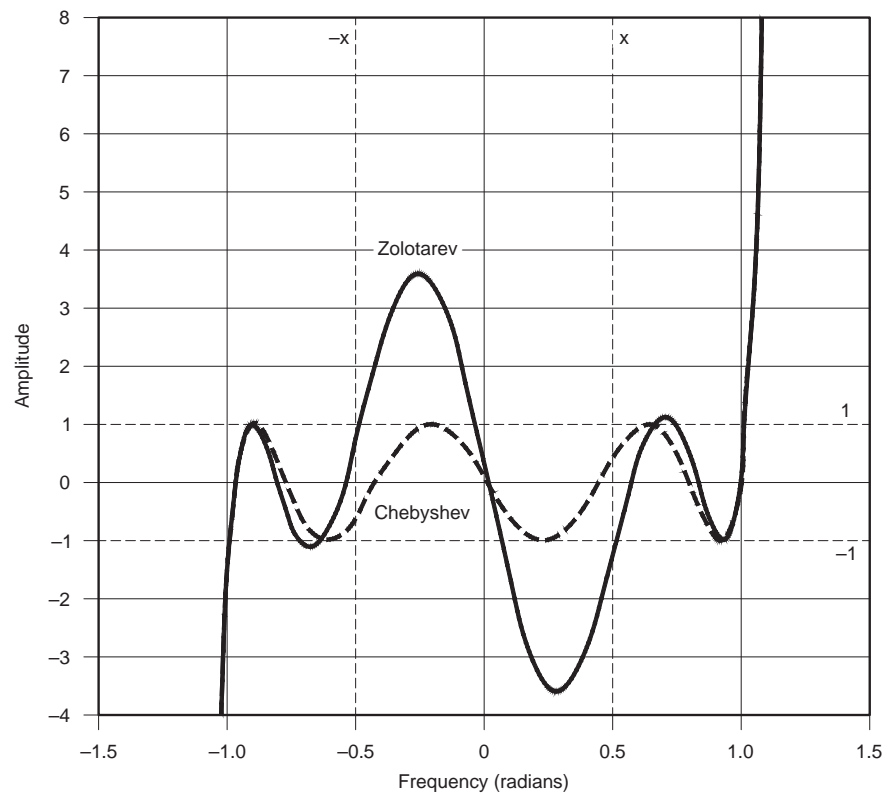


Figure 5 — A 7th order Chebyshev and Zolotarev low-pass function.

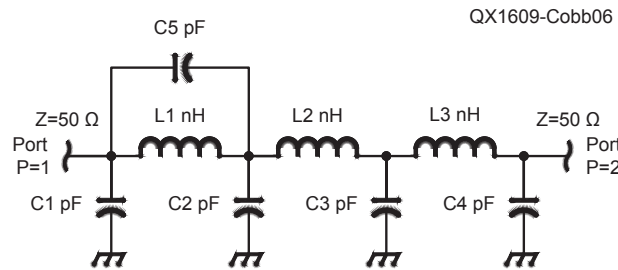


Figure 6 — Basic circuit configuration for analysis. Element values are in Table 2.

same electrical circuit. Second, a couple of practical examples will demonstrate the achievable performance using typical and appropriate inductor construction techniques.

Approximation and Synthesis of 7th Order ZWAZ Filter

To create a 7th order ZWAZ filter, we first generate a 7th order CWAZ polynomial filter function whose characteristic pole and zero singularities are then mapped

into the Zolotarev domain using a freely chosen fractional bandwidth compression factor providing a new polynomial function. Prototype lumped element component values are then extracted from the equivalent admittance polynomial and scaled in both frequency and impedance so as to produce the necessary component values.

Two filters using the common network configuration (Figure 6), have been selected for comparison, one with Chebyshev and the other with Zolotarev pass-band characteristics

with a chosen bandwidth compression factor of 35%. It is common practice, particularly for high power filter designs, to select the cut-off frequency based on minimizing the in-band insertion-loss, by positioning the transmission band center to be coincident with one of the filter reflection zeros. Therefore, both filter types will have distinctly different cut-off frequencies because the reflection zeros will be differently distributed. However, both have the same pass-band equi-ripple value of 0.044 dB corresponding to a maximum in-band return loss of 20 dB. The values determined for each design are shown in Table 1.

Observe that the ZWAZ design has the property of low inductance values with a smaller variation, at approximately 1/2, and some 10% less respectively, when compared with the CWAZ design. This is a distinct practical advantage when consideration is given to parasitic issues such as self resonance, mutual coupling and Q so that realization of the far out rejection can be more easily achieved.

Analysis and Comparison

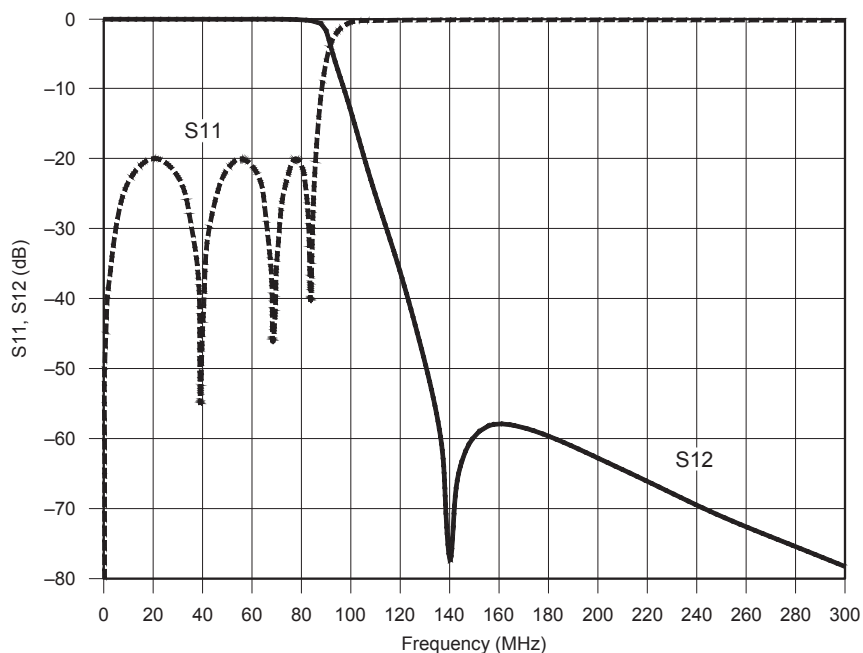
The networks so described can be analyzed in any one of the many freely available circuit simulators — *QUCS*, *Ansoft Designer SV*, *Elsie*, etc. Assuming that good quality capacitors would be the norm, the main contributor to in-band loss would be the inductors whether realized using air cored solenoid or ferrite cored toroidal coils. Toroids may be preferred particularly for the lower bands so that adequately small parasitic coupling within the network can be achieved without shielding. Shielded solenoids can also provide sufficiently low couplings for the higher frequency bands. To this end, a practical value of $Q=200$ for solenoids and $Q=150$ for toroids have been used for the simulations presented here.

Figure 7 shows the transmission/reflection behavior for the Chebyshev valued network, the equi-ripple performance being demonstrated by the familiar multi-lobed, equal amplitude return loss characteristic across the full passband. It should be noted that with the transmission zero placed at the 2nd harmonic frequency, a stop band non-harmonically related lobe amplitude of 58 dB and approximately 64 dB of attenuation at the 3rd harmonic (210 MHz) is achieved. Also, the second reflection zero corresponds closely to the nominal signal band (70 MHz) exactly as the Wetherhold CWAZ design showed previously in Figure 4.

Figure 8 shows the simulated transmission/reflection behavior for the Zolotarev valued network. Here we can clearly see the effect of incorporating the Zolotarev pole/zero distribution such that the equi-ripple performance is limited to a portion in the

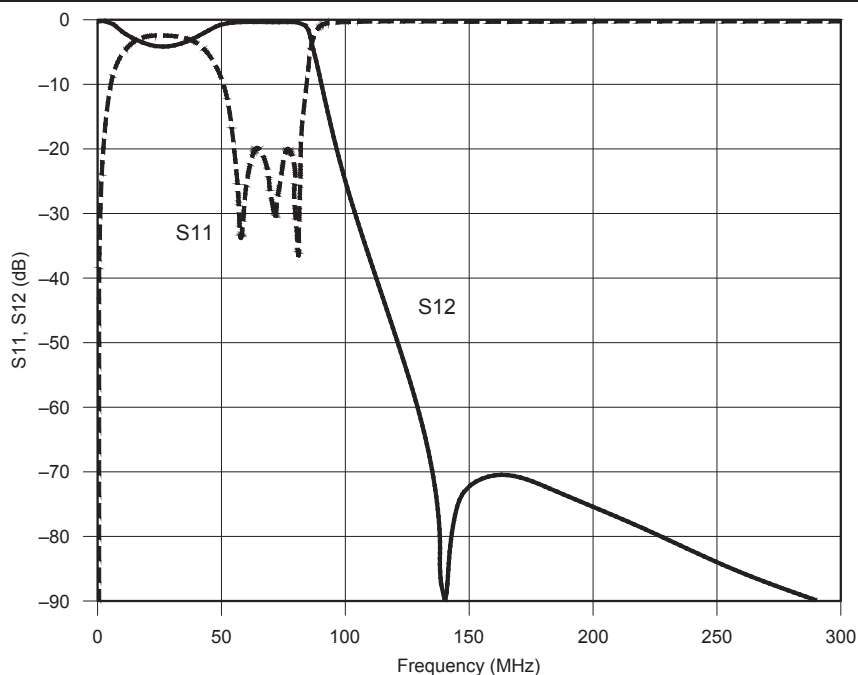
Table 1
Element values for the two filter types: (C, pF; L, nH, frequency, MHz).

Type	C1	C2	C3	C4	C5	L1	L2	L3	fc
CWAS	26.9	65.6	73.6	38.1	13.5	95.8	154.7	135.7	84.8
ZWAZ	64.0	196.0	225.8	77.25	21.4	60.6	52.6	76.8	81.5



QX1609-Cobb07

Figure 7 — Chebyshev transmission/reflection response.



QX1609-Cobb08

Figure 8 — Zolotarev transmission/reflection response.

upper 35% of the pass-pass. It is also seen that, with the single transmission zero placed at the 2nd harmonic frequency, a stop-band non-harmonically related lobe amplitude of 71 dB together with approximately 77 dB of attenuation at the 3rd harmonic is provided. Also, observe that the second reflection zero also corresponds to the desired 70 MHz band and that attenuation monotonically increases beyond the stop-band lobe unlike the ideal Elliptic filter.

As one might expect, there is a price to be paid for this apparent performance improvement. Figure 9 shows the comparative pass-band insertion-loss for both filter types examined together with the transition/stop-band attenuation characteristics.

From the design data, it is possible to quantify some practical aspects of realizability. For example, as mentioned earlier in respect of problems relating to the design realization of an ideal Elliptic filter, the inductance ratio for both Chebyshev and Zolotarev filters are considerably better. Additionally, the average value of the required inductors is also important as it is an indicator of the probable parasitic issue — larger inductors generally have larger self capacitance. To this end, these values are summarized in Table 2.

Since the Zolotarev approach is perceived as having significant benefits, the necessary component values have been calculated for most of the Amateur Radio bands and made available for the first time in Table 3.

Practical Testing of ZWAZ Designs

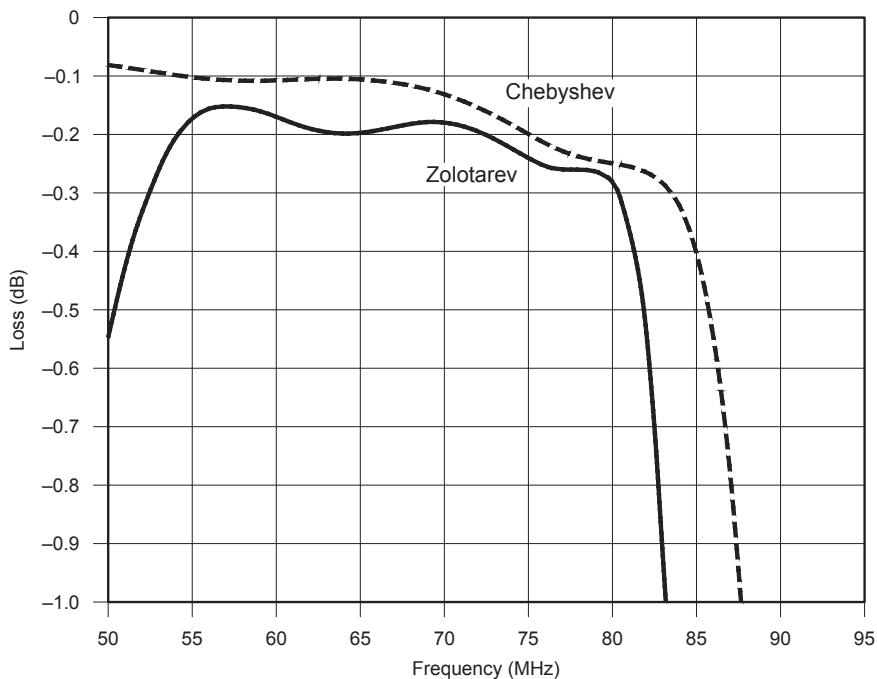
To demonstrate realizability, two design examples in different bands, have been constructed and tested against predicted performance. Component values have been selected from Table 3 and built using one of two commonly used inductor techniques. Both builds used ceramic surface mount capacitors so that the desired values were made up of parallel combinations of 2% tolerance parts. Some allowance was made for stray or parasitic capacitance.

In the first instance, a design chosen for the original 70 MHz band of interest was realized using the typical VHF technique of shielded air-cored solenoid inductors with a designed Q of 200 (Figures 10a and 10b). The measured result for transmission loss, 0.28 dB, is close to the target function, 0.19 dB, although the cut-off frequency is in error by approximately -1.5 MHz due to component tolerances and tuning inaccuracies. Good stop-band lobe definition with a peak attenuation ~71 dB is achieved with quite simple mechanical screening arrangements.

In the second instance, a design chosen for 60 m operation uses toroidal inductors with a designed Q of ~200. In this case,

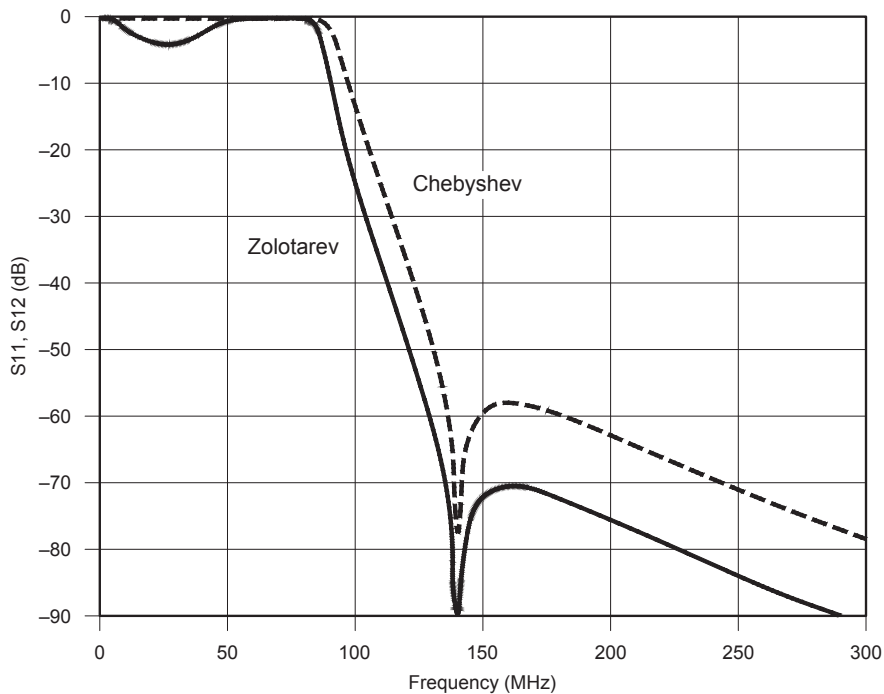
Table 2
Ratio and average values for inductive elements.

Parameter	CWAZ	ZWAZ
Inductance ratio	1.614	1.460
Average inductance (nH)	128.7	63.3



QX1609-Cobb09a

(A)



QX1609-Cobb09b

(B)

Figure 9 — (A) Insertion loss for ZWAZ (solid) and CWAZ (dashes). (B) — ZWAZ (solid) and CWAZ (dashes) shows rejection at 160 MHz for the ZWAZ is 70.7 dB, and for CWAZ is 58.2 dB.

Table 3

ZWAZ component values for the 2 to 160 m Amateur Radio bands: (C, pF; L, nH; frequency, MHz).

Band, m	f0	C1	C2	C3	C4	C5	L1	L2	L3	fc
160	1.9	2360	7240	8340	2850	790.7	2240	1940	2840	2.21
80	3.65	1230	3770	4340	1490	411.6	1170	1010	1480	4.24
60	5.3	847.7	2600	2990	1020	283.4	802.7	696.7	1020	6.15
40	7.1	632.8	1940	2230	763.8	211.6	599.2	520.1	759.3	8.24
30	10.1	444.8	1360	1570	536.9	148.7	421.2	365.6	533.8	11.7
20	14.2	316.4	969.0	1120	381.9	105.8	299.6	260.0	379.7	16.5
17	18.1	248.2	760.2	875.8	299.6	83.0	235.0	204.0	297.9	21.0
15	21.2	211.9	649.0	747.7	255.8	70.9	200.7	174.2	254.3	24.6
12	24.2	185.7	568.6	655.0	224.1	62.1	175.8	152.6	222.8	28.1
10	29	154.9	474.5	546.6	187.0	51.8	146.7	127.3	185.9	33.7
6	51	88.1	269.8	310.8	106.3	29.5	83.4	72.4	105.7	59.2
4	70.2	64	196	225.8	77.2	21.4	60.6	52.6	76.8	81.5
2	145	31	95	109.3	37.4	10.4	29.3	25.5	37.2	168.3

the frequency response has little error with respect to that of the target function. However, the measured transmission loss of 0.88 dB is not acceptable in comparison with the target function value of 0.15 dB. The cores used are Amidon T68-2 (red) iron powder types, which, from the manufacturer's data, claims a considerably better Q than the 50 or so, implied from the measured result.

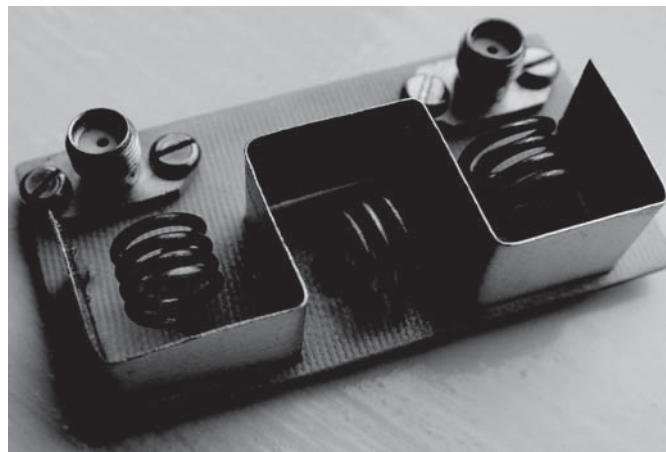
Subsequently, the inductor Q's were measured individually and found to be 250 or greater mitigating the choice of core type. The problem was ultimately traced to some of the capacitors. All of the 1000 pF, 1206 style surface mount components used were found to have a poor Q value of between 40 or 50 when measured at 5 MHz. As a consequence all of the capacitors were replaced by the more usual Silver Mica types having measured Q's of >600 at the test frequency.

This filter was re-measured after re-assembly and found to be now totally compliant with the simulated data with a more usable insertion-loss value of 0.17 dB – see Fig 11(A) and (B). Also note that the stop-band attenuation lobe is in good agreement with the predicted value of ~71 dB. Impressive is the fact that the stop-band attenuation exceeds the measurement noise floor (~85 dB) to well over 30 MHz without additional inductor shielding.

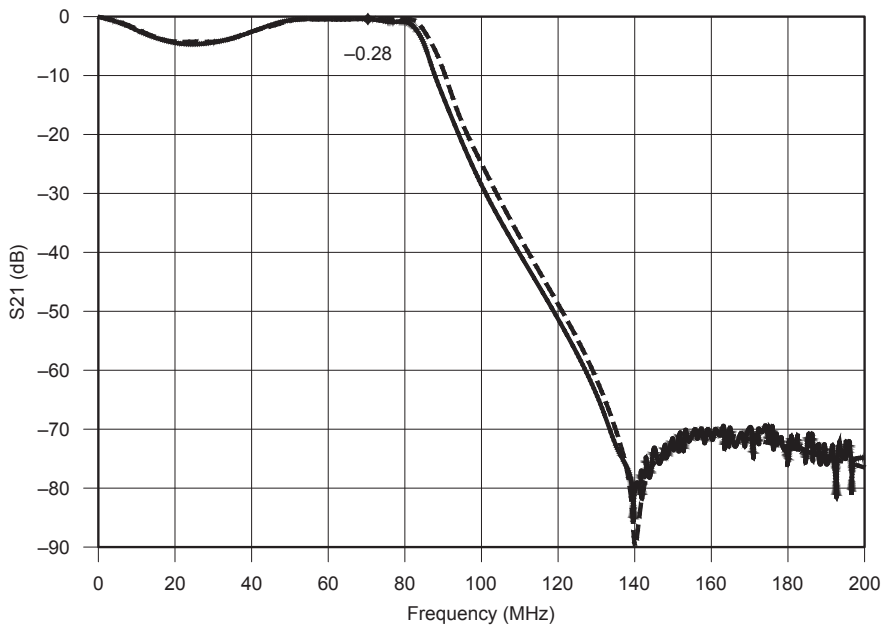
Conclusion

Two low-pass filter types (CWAZ and ZWAZ) have been synthesized and compared as an evaluation of a preferred output filter for power amplifiers in general. The ZWAZ filter is demonstrated to be significantly better, by design and realization, in terms of both harmonic and general stop-band attenuation, as compared to the CWAZ filter. In fact, the transition rate and the ultimate stop-band attenuation beyond the 3rd harmonic frequency all exceed that of the ideal Elliptic filter.

The two test samples generally show good agreement with the target design



(A)



QX1609-Cobb10b

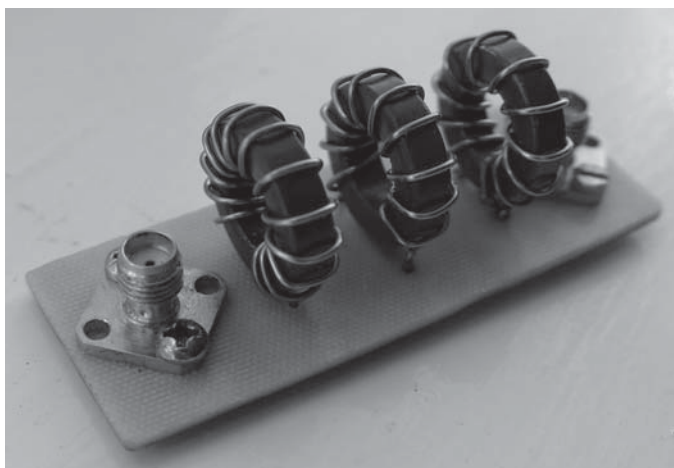
(B)

Figure 10 — (A) A 4 m band Zolotarev low-pass filter test piece construction. (B) — The 4 m band Zolotarev low-pass filter S21 test result – measured (solid), predicted (dashed). [Gary Cobb, G3TMG, photo]

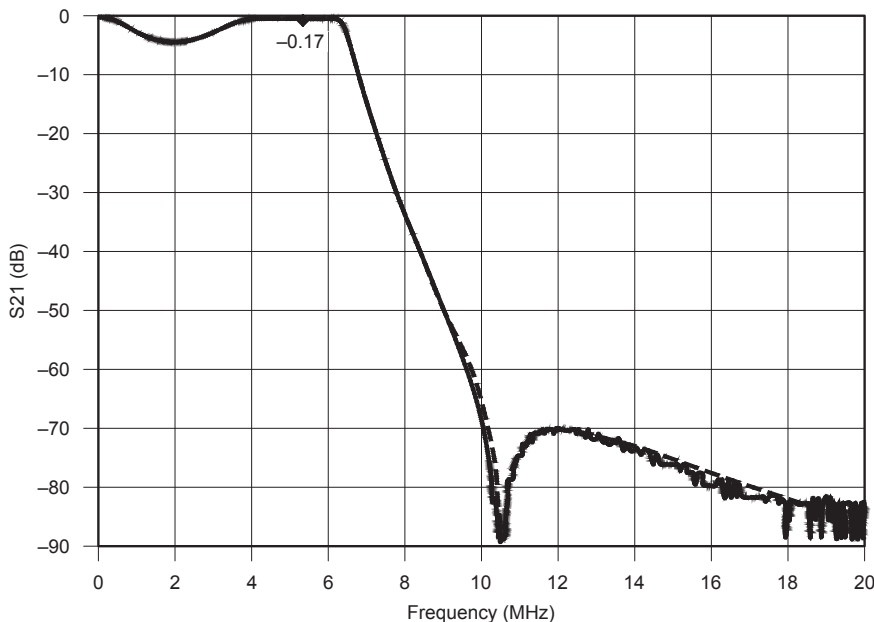
characteristic without significant deviation the synthesized component values. The HF filter sample illustrates the need not only to ensure that the inductors are of adequate design in terms of achievable Q but proper consideration should be given to selecting good quality capacitors for the operational frequency chosen.

Gary Cobb, G3TMG, has held the same call sign since he was first licensed in 1964. He holds a BA degree in Mathematics, an MSc in Microwave Physics, and is a Life

Member of the IEEE. His early professional career development took place in the defense industry where he designed high resolution microwave antenna interferometry systems. Later, research activities moved toward the realization of adaptive arrays for ship-borne radio communications in a Navy environment. Gary spent the last 20 years in military and commercial satellite payload engineering, developing output multiplexers, multi-port amplifiers and filter techniques appropriate for high-power geostationary systems. Now retired, Gary operates CW and SSB on HF and VHF amateur bands with a special interest in sporadic-E during the summer months.



(A)



(B)

QX1609-Cobb11b

Figure 11 — (A) A 60 m band Zolotarev low-pass filter test piece construction. (B) — The 60 m band Zolotarev low-pass filter S21 test result – measured (solid), predicted (dashed). [Gary Cobb, G3TMG, photo]

Notes

¹Radio Society of Great Britain, *Radio Communications Handbook*, all editions since 1938. Available from your ARRL dealer or the ARRL Bookstore, ARRL item no. 2040. Telephone 860-594-0355, or toll-free in the US 888-277-5289; www.arrl.org/shop; pubsales@arrl.org.

²(In all editions since 1926), *The ARRL Handbook for Radio Communications*, 2016 Edition. Available from your ARRL dealer or the ARRL Bookstore, ARRL item no. 0413 (Hardcover 0420). Telephone 860-594-0355, or toll-free in the US 888-277-5289; www.arrl.org/shop; pubsales@arrl.org.

³E. Wetherhold, W3NQN, "Second-Harmonic-Optimized Low-Pass Filters", *QST*, Feb 1999, pp 44-46.

⁴J. Tonne, W4ENE, *OptLowpass*, www.TonneSoftware.com.

⁵R. Levy, "Generalized Rational Function Approximation in Finite Intervals Using Zolotarev Functions", *IEEE Trans, MTT*, Vol 18, Dec, 1970, pp 1051-1064.

⁶G. Cobb, G3TMG, "Zolotarev Low-pass Filter Design", *QEX*, Jul/Aug, 2016, pp 23-29.

We Design And Manufacture To Meet Your Requirements

*Prototype or Production Quantities

800-522-2253

This Number May Not Save Your Life...

But it could make it a lot easier! Especially when it comes to ordering non-standard connectors.

RF/MICROWAVE CONNECTORS, CABLES AND ASSEMBLIES

- Specials our specialty. Virtually any SMA, N, TNC, HN, LC, RP, BNC, SMB, or SMC delivered in 2-4 weeks.
- Cross reference library to all major manufacturers.
- Experts in supplying "hard to get" RF connectors.
- Our adapters can satisfy virtually any combination of requirements between series.
- Extensive inventory of passive RF/Microwave components including attenuators, terminations and dividers.
- No minimum order.

NEMAL
Cable & Connectors
for the Electronics Industry

NEMAL ELECTRONICS INTERNATIONAL, INC.

12240 N.E. 14TH AVENUE

NORTH MIAMI, FL 33161

TEL: 305-899-0900 • FAX: 305-895-8178

E-MAIL: INFO@NEMAL.COM

BRASIL: (011) 5535-2368

URL: WWW.NEMAL.COM

High-Accuracy Prediction and Measurement of Lunar Echoes

K1JT describes a series of recent lunar echo measurements at 144 and 432 MHz, and tests his new EMEcho software to predict and measure Doppler shift, frequency spread, and polarization of EME signals using amateur equipment.

1. Introduction

For me, one of the fascinations of amateur Earth-Moon-Earth (EME) communication is the range of interesting physics that accompanies it. Motivated in part by a need to test a new software program called *EMEcho*, and also by a desire to see how well I could predict and measure the phenomena of Doppler shift, frequency spread, and polarization of EME signals using amateur equipment, I recently made an extensive series of lunar echo measurements at 144 and 432 MHz. This paper describes how the measurements were made and presents a selection of results.

Doppler shifts of EME signals are caused by continuous changes in the total line-of-sight distance between a transmitter, reflecting or scattering spots on the lunar surface, and a receiver. The relevant rates of change are usually dominated by Earth rotation, which at the equator amounts to about 460 m/s. As a consequence, two-way Doppler shifts can be as large as ± 440 Hz at 144 MHz, ± 4 kHz at 1296 MHz, and ± 30 kHz at 10 GHz. Different reflection points on the lunar surface produce slightly different Doppler shifts, so the echo of a monochromatic signal is spread out over a small and predictable frequency range. The full range of spread can be as large as 4 Hz at 144 MHz and 300 Hz at 10 GHz. However, at VHF and UHF a majority of reflected power is returned from a region near the center of the lunar disk, so the observed half-power Doppler spread is always considerably less than the full limb-to-limb amount.

A smooth moon would produce a specular reflection that preserves linear polarization and reverses the sense of circular polarization. A rough moon (on the scale of one wavelength) would produce diffuse echoes and significant depolarization; cross-polarized return echoes might be just a few dB weaker than the dominant polarization. At VHF and UHF frequencies the circumstances are closer to the specular limit. Received echoes should be almost fully polarized, and with linear polarization they should have a polarization angle that depends on geographic locations of the transmitter and receiver and the amount of ionospheric Faraday rotation.

Together with our knowledge of solar-system dynamics, the relevant physics is such that EME Doppler shifts can be calculated with high accuracy (parts in 10^{10} , or better) for any time and any terrestrial location. Maximum Doppler spread across the full lunar disk is also predictable. Faraday rotation depends on latitude, moon elevation, time of day, solar activity, and ionospheric “weather”; the resulting effects are generally not predictable in detail. For optimum efficiency, EME operators must know about and take account of this full range of phenomena, both predictable and otherwise.

2. Equipment Setup

I used single-station echo tests to measure Doppler shift, frequency spread, and polarization during the moon pass of January 2-3, 2015. My equipment was that of the 144 MHz EME station at K1JT and

the 432 MHz station at W2PU, the Princeton University Amateur Radio Club. The two stations are configured in a similar way. Both have four dual-polarization Yagis — 4x2Mxp28’s at 144 MHz¹ and 4x15LFA-JT’s at 432 MHz.² Both stations use a single low-loss feed line for transmitting and separate LNAs and receive feed lines for each polarization. The receivers use dual-channel down-converters to produce four baseband signals, *I* and *Q* (in-phase and quadrature) for each polarization. WSE converters by SM5BSZ³ were used at 144 MHz, and the IQ+ receiver by HB9DRI⁴ at 432 MHz. Four-channel sound cards (M-Audio Delta44) digitize the *I/Q* signals at 96000 samples per second, and in normal EME operation all further processing takes place in the computer programs *Linrad*⁵ and *MAP65*⁶. For this echo experiment my new program *EMEcho* was used in place of *MAP65*. Transmitter power was about 500 W at the antenna, at each station.

2.1 EMEcho Software

EMEcho is a new program designed to make reliable tests of lunar echoes from an amateur EME station. It goes beyond the Echo mode available in *WSJT* in two important ways. Doppler calculations are done with state-of-the-art accuracy, based on the Jet Propulsion Laboratory’s DE405 planetary ephemeris.⁷ In addition, *EMEcho* takes full advantage of a dual-polarization system by measuring the polarization as well as the frequency and strength of echo signals.

The basic echo-testing cycle is similar

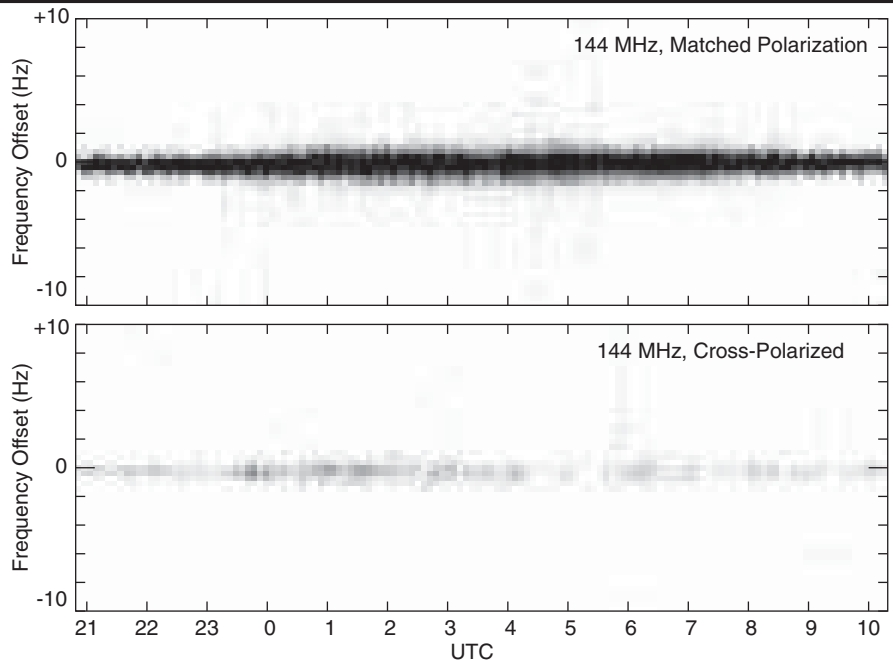


Figure 1 — Measured echo power at 144 MHz as a function of frequency offset and time. Upper: linear polarization angle matched to that of the echo. Lower: orthogonal linear polarization.

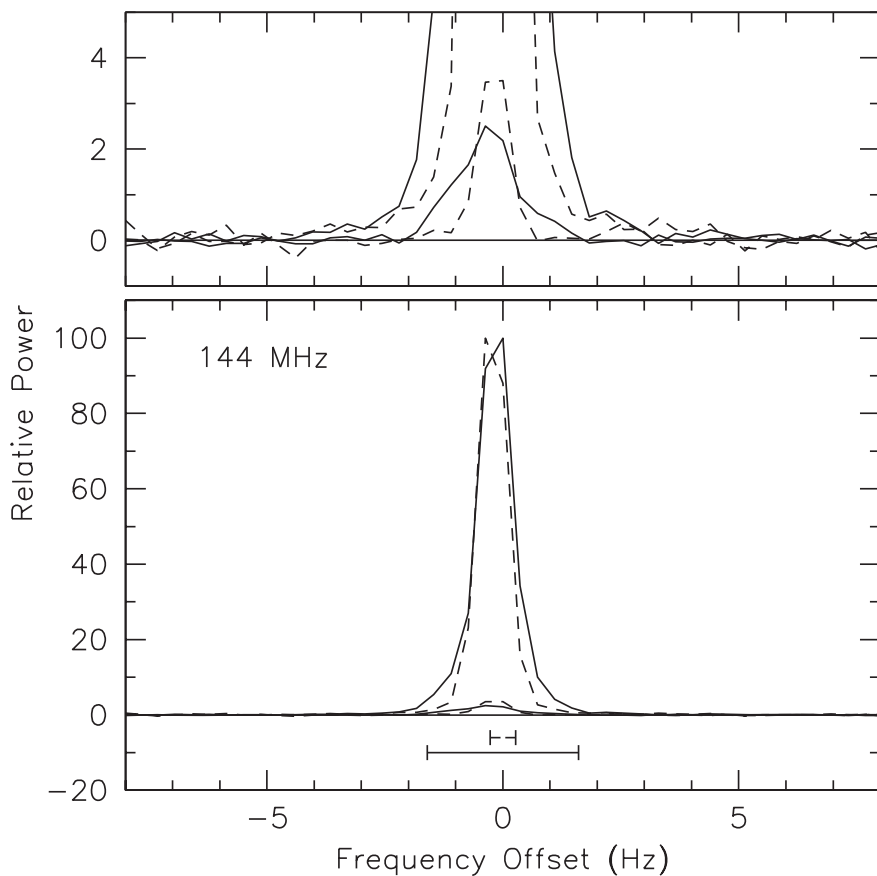


Figure 2 — Frequency structure of echoes at 144 MHz near meridian transit (solid line) and near 2130 UTC, a time of minimum libration rate (dashed line). The upper panel uses an expanded vertical scale to show the weakest spectral features. Horizontal bars in the lower panel indicate the full range of predicted Doppler spread. The pair of curves with intensity a few percent of maximum show the measured cross-polarized power, which in this case may be mostly a result of minor alignment imperfections in the K1JT antenna. Horizontal bars in the lower panel indicate the full limb-to-limb ranges of predicted Doppler spread.

to that used in program *WSJT*. The cycle repeats every six seconds, starting at 0, 6, 12, ... seconds of a UTC minute. A fixed-frequency tone is transmitted for 2.3 s, the echo is received and recorded about 2.5 s later, and the spectrum is computed, displayed, and (if desired) recorded in a disk file. In a dual-polarization *MAP65*-compatible system, spectra can be displayed for both the matched linear polarization and the orthogonal polarization.

3. Measurements

A six-second measurement cycle means that some 8400 2.3-second pulses were transmitted at each station over the full moon pass. A few of the return echoes were rejected for failing a simple interference test; the remainder were averaged in groups of 10 to produce about 800 sets of polarized spectra. Measurements are reported here for both 144 and 432 MHz. They include frequency profiles of the echoes with bin spacing 0.37 Hz, Doppler shifts accurate to around 0.1 Hz, and polarization angles accurate to a few degrees.

3.1 Doppler Shift and Doppler Spread

Figure 1 is a grayscale plot showing matched-polarization and cross-polarized echo strengths as a function of frequency and time. No *ad hoc* frequency adjustments have been made; the plotted “Frequency Offset” is that of the received spectrum relative to the predicted Doppler shift. The Doppler shift, in turn, is based on station location, UTC according to the internet-synchronized computer clock, and the JPL DE405 planetary ephemeris. The grayscale chosen for Figure 1 is logarithmic, so as to emphasize the weakest features.

It’s easy to see that the frequency width of return echoes is greater in the middle of the run than near either end. These differences are consistent with the predicted dependence of Doppler spread during the course of a moon pass. Further details of this effect can be seen in Figure 2, where spectra have been averaged over about an hour near the times of minimum and maximum libration rate. Dashed curves represent the echo profile around 2130 UTC, shortly after moonrise, while solid curves are the average spectral profile around 0330 UTC, near lunar culmination.

Figures 3 and 4 display the corresponding results obtained at 432 MHz. Again the measured frequency offsets are essentially zero (within the measurement uncertainties). Doppler spreads are rather more than 3 times larger than at 144 MHz, owing to the higher frequency and the somewhat larger size of the lunar reflecting region. Cross-polarized echo signals are essentially undetectable in

the grayscale plot and only barely visible in the expanded view (upper panel) of Figure 4. It is interesting to see that at both frequencies the weak wings of the spectral profile extend out to the full calculated limb-to-limb Doppler spread — as they should, with adequate sensitivity. These effects have been noted before by EME operators.^{8,9}

I consider the Doppler calculations used in this paper to be the best achievable with today’s knowledge of solar system dynamics. The JPL DE405 ephemeris represents a numerically integrated model of the solar system based on several hundred years of astronomical observations, radar observations of planets out as far as Saturn, and tracking observations of many interplanetary spacecraft. Positions and velocities of the Earth and Moon (and many other solar system objects) are tabulated in a data file suitable for numerical interpolation. Doppler calculations in *EMEcho* include the following steps:

1. Convert geodetic coordinates of the antenna to geocentric coordinates, accounting for the Earth’s oblateness.
2. Convert UTC to UT1 and to LAST (local apparent sidereal time). Note that UTC runs at an essentially constant rate defined by the average of many atomic clocks, plus occasional leap seconds. UT1 represents the actual measured rotation of the Earth. UTC and UT1 can differ by up to ± 0.9 s.
3. Compute 3-dimensional position and velocity of the antenna with respect to center of Earth.
4. Convert UTC to ET (Ephemeris Time), accounting for all leap seconds up to the present.
5. Interpolate the DE405 ephemeris to obtain the 3-dimensional position and velocity of center of moon relative to center of Earth.
6. Combine results of items 3 and 5 to get position and velocity of antenna with respect to moon.
7. Calculate Doppler shift from the line-of-sight component of velocity obtained in item 6.

Achieving the accuracies required to produce the results presented in Figures 1 through 4 requires knowledge of antenna coordinates to better than one km and clock accuracy better than one second. The transmitter frequency in the antenna’s reference frame must also be specified accurately: for example, 144.118 MHz rather than 144 MHz. The Doppler calculations must avoid certain shortcuts and approximations that have typically been used in amateur EME-related software, including my own programs *WSJT* and *MAP65*.

Figure 5 illustrates some potential consequences of ignoring one or more of the

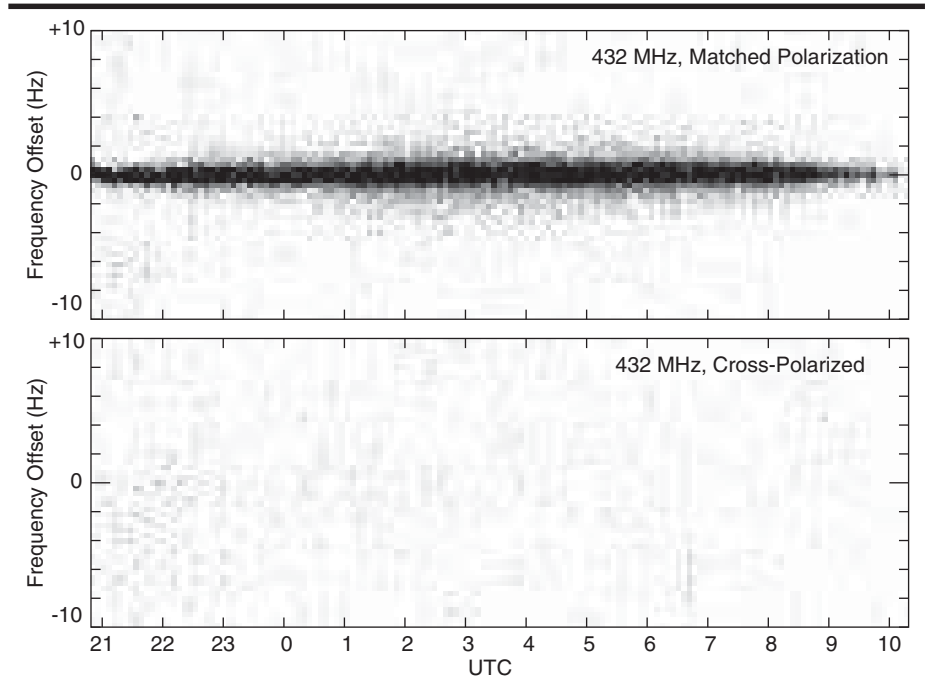


Figure 3 — Measured echo power at 432 MHz as a function of frequency offset and time. Upper: linear polarization angle matched to that of the echo signal. Lower: the orthogonal linear polarization.

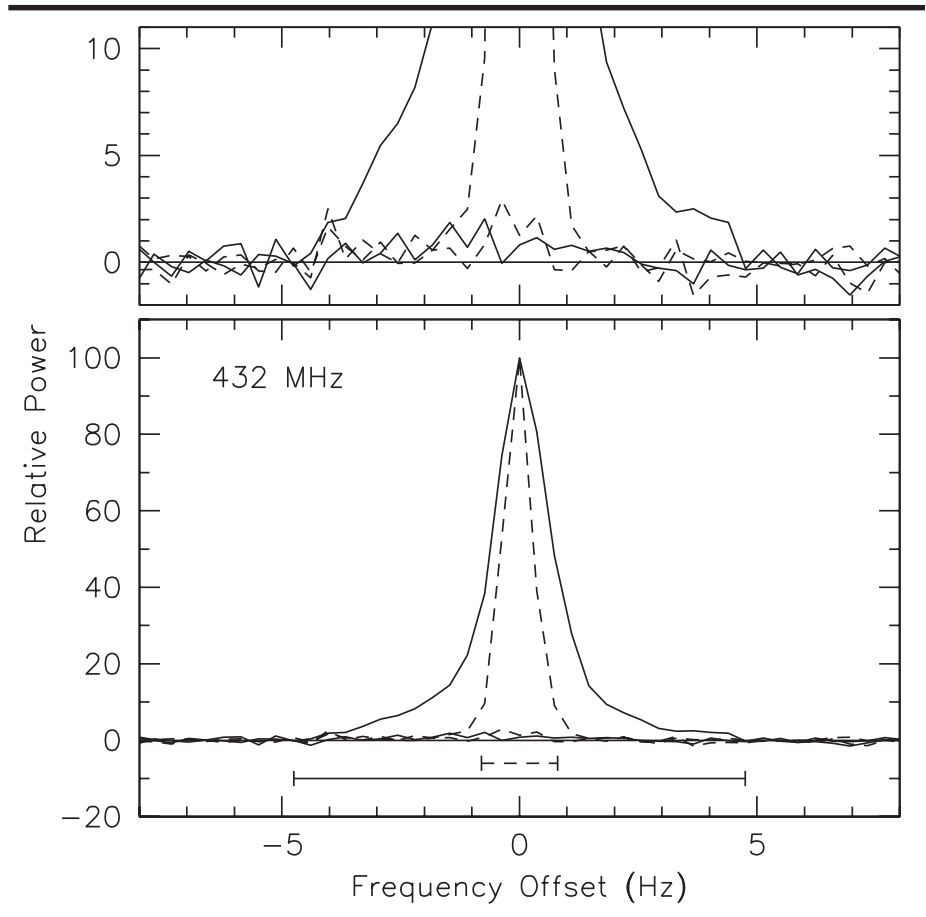


Figure 4 — Frequency structure of echoes at 432 MHz near meridian transit (solid line) and near 2130 UTC, a time of minimum libration rate (dashed line). The upper panel uses an expanded vertical scale to show the weakest features. Horizontal bars in the lower panel indicate the full limb-to-limb ranges of predicted Doppler spread.

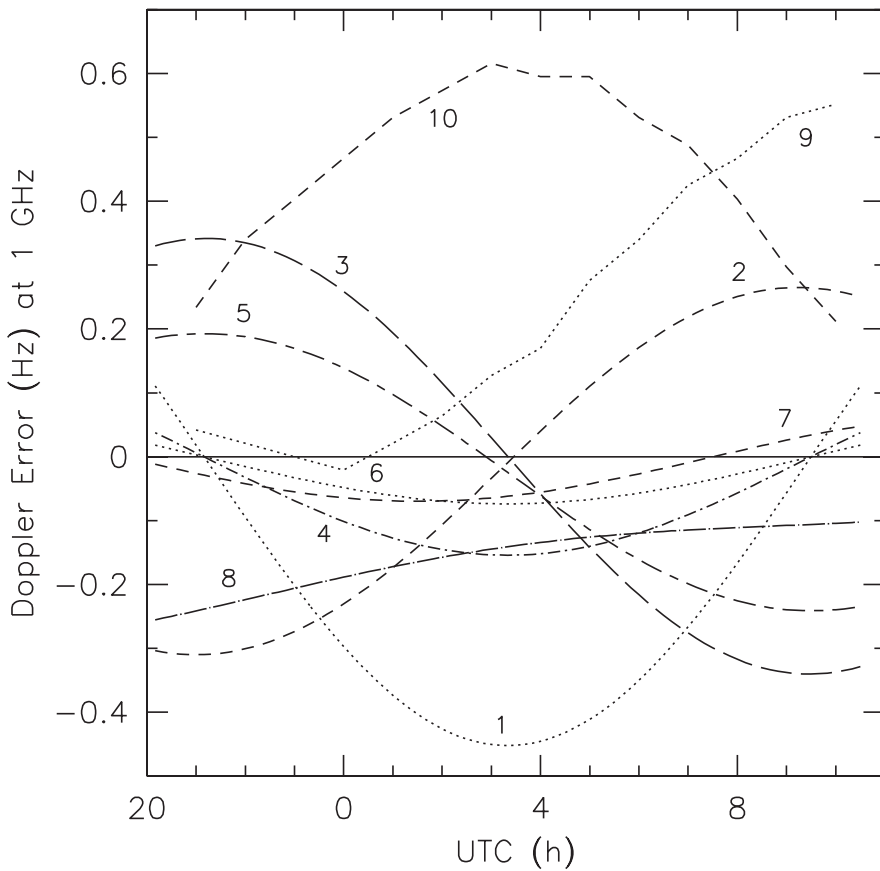


Figure 5 — Examples of contributions that might affect the accuracy of computed Doppler shifts.

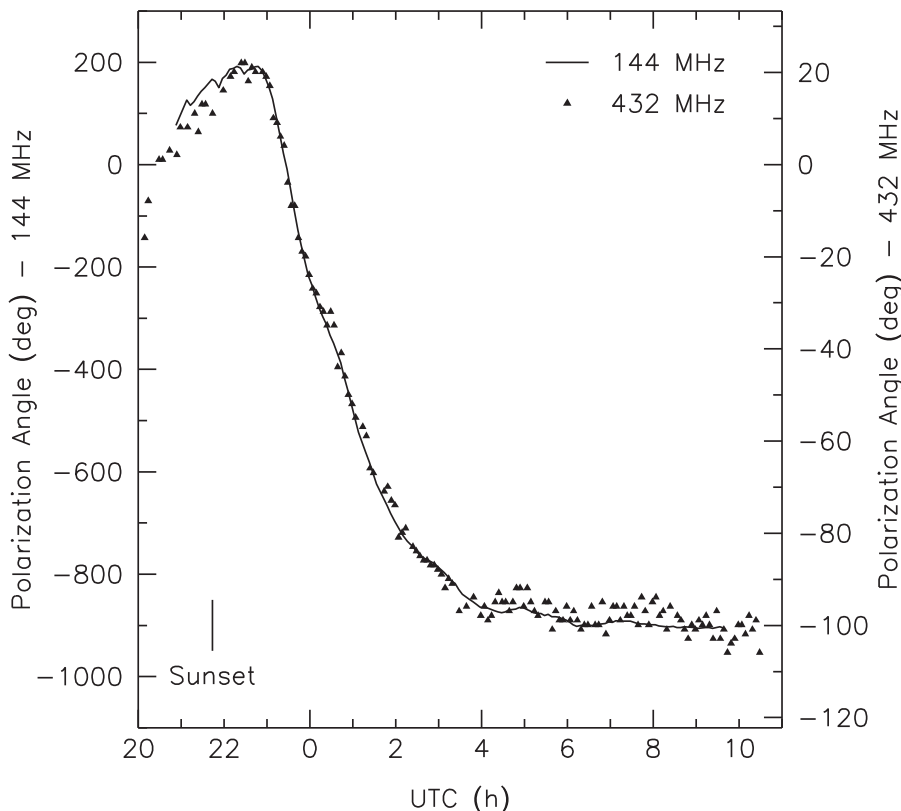
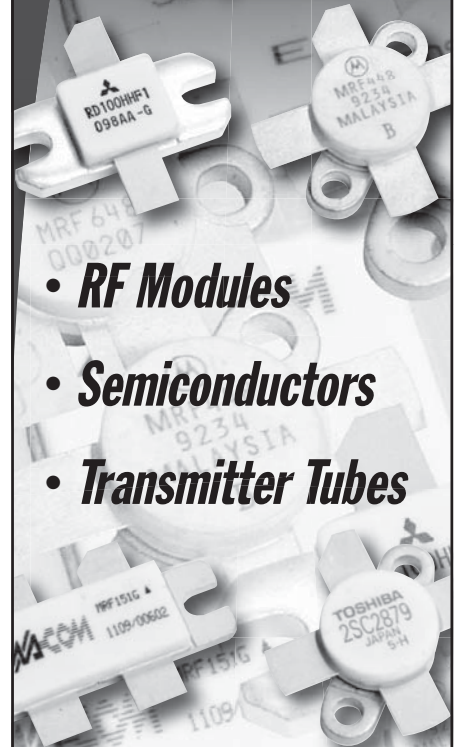


Figure 6 — Measured polarization angles at 144 MHz (left scale) and 432 MHz (right scale).

From **MILLIWATTS**
To **KILOWATTS**SM
*More Watts per Dollar*SM

In Stock Now!
Semiconductors
for Manufacturing
and Servicing
Communications
Equipment



- **RF Modules**
- **Semiconductors**
- **Transmitter Tubes**

Se Habla Español • We Export

Phone: **760-744-0700**
Toll-Free: **800-737-2787**
(Orders only) **800-RF PARTS**
Website: **www.rfparts.com**
Fax: **760-744-1943**
888-744-1943
Email: **rfp@rfparts.com**



RF PARTSTM
COMPANY
*From Milliwatts to Kilowatts*SM

warnings mentioned above. To produce this graph I used GPS-measured coordinates of the W2PU antenna and calculated Doppler shifts at a nominal frequency of 1.0000 GHz, at frequent intervals from moonrise to moon set on January 2-3, 2015, the date of my echo-test observations. The horizontal straight line at zero represents my supposed state-of-the-art calculation. The ten numbered curves show the differential effects of various

changes, omissions, or assumptions in the Doppler calculation, as follows:

1. Antenna moved 1 km East.
2. Antenna moved 1 km North.
3. Antenna moved to 1 km higher elevation.
4. UTC clock error +1 s.
5. Frequency changed to 1.0001 GHz.
6. Time difference UT1-UTC ignored.
7. Nutations ignored.
8. Calculation of moon position based on a closed-form series expansion rather than interpolation of the DE405 ephemeris.
9. Doppler calculation made by program *EME Planner*, by VK3UM.¹²
10. Doppler calculation made by program *EME System*, by F1EHN.¹¹

I call particular attention to several points relating to Figure 5. First, the Doppler calculations in *EME Planner* and *EME System* are very good — in this example, accuracies better than 1 Hz at 1 GHz, through a full moon pass. Note that in order to obtain this accuracy you must start with very accurate station coordinates: a six-digit Maidenhead locator is not good enough. Your computer clock must be synchronized to UTC and your software must be updated with the latest leap seconds. And you must use the actual transmitter frequency, not just the frequency of the band edge, for example. Careful use of *EME Echo* should give Doppler predictions even better than those of *EME Planner* and *EME System*, accurate to about 1 Hz at 10 GHz.

3.2 Polarization

In addition to Doppler shift and Doppler spread, my experiment yielded polarization measurements at both 144 and 432 MHz. The polarized spectra recorded on disk were averaged over five-minute intervals. The resulting polarization angles are plotted in Figure 6. A solid line connects sequential measurements at 144 MHz. As shown by the scale at left, these angles increased gradually from about 60 degrees to 200 degrees in the two hours around local sunset. The angles then decreased through some 1080 degrees — three full turns — over the next five hours. Subsequent angles decreased only slightly more from 0400 UTC (an hour before local midnight) until moon set, about two hours before sunrise.

Polarization angles measured at 432 MHz are plotted as filled triangles in Figure 6, using the scale at right. Note that the left and right scales are in the ratio of 9 to 1. The close tracking of the scaled results at the two frequencies is an excellent confirmation that Faraday rotation scales inversely as the square of frequency.

4 Conclusion

Program *EME Echo* requires a *MAP65*-compatible EME station and was written mainly for my personal use. However, all of its features except the dual-polarization capability have been incorporated into *WSJT-X*, the latest program version in the *WSJT* project.¹² *WSJT-X* also offers a number of features such as automatic rig control and Doppler tracking, which make it especially attractive for amateur EME communication on any band.

Joe Taylor was first licensed as KN2ITP in 1954, and has since held call signs K2ITP, WA1LXQ, W1HFV, VK2BJX and K1JT. He was Professor of Astronomy at the University of Massachusetts from 1969 to 1981 and since then Professor of Physics at Princeton University, serving there also as Dean of the Faculty for six years. He was awarded the Nobel Prize in Physics in 1993 for discovery of the first orbiting pulsar; leading to observations that established the existence of gravitational waves. After retirement he has been busy developing and enhancing digital protocols for weak-signal communication by Amateur Radio, including JT65 and WSPR. He chases DX from 160 meters through the microwave bands.

Notes

- ¹www.m2inc.com.
- ²Joe Taylor, K1JT, and Justin Johnson, GØKSC. *Dubus*, 4/2014, p 53.
- ³www.sm5bsz.com/linuxdsp/optrx.htm.
- ⁴www.linkrf.ch/.
- ⁵www.sm5bsz.com/linuxdsp/linrad.htm.
- ⁶physics.princeton.edu/pulsar/K1JT/map65.html.
- ⁷ftp://ssd.jpl.nasa.gov/pub/eph/planets/fortran/userguide.txt.
- ⁸www.sm5bsz.com/sm5frh/sm5frh.htm.
- ⁹physics.princeton.edu/pulsar/K1JT/EME2010_K1JT.pdf.
- ¹⁰www.vk3um.com/eme%20planner.html.
- ¹¹www.f1ehh.org/.
- ¹²physics.princeton.edu/pulsar/K1JT/wsjsx.html.

Down East Microwave Inc.

We are your #1 source for 50MHz to 10GHz components, kits and assemblies for all your amateur radio and Satellite projects.

Transverters & Down Converters, Linear power amplifiers, Low Noise preamps, coaxial components, hybrid power modules, relays, GaAsFET, PHEMT's, & FET's, MMIC's, mixers, chip components, and other hard to find items for small signal and low noise applications.

We can interface our transverters with most radios.

Please call, write or see our web site www.downeastmicrowave.com for our Catalog, detailed Product descriptions and interfacing details.

Down East Microwave Inc.
19519 78th Terrace
Live Oak, FL 32060 USA
Tel. (386) 364-5529

Letters to the Editor

Measuring Propagation Attenuation Using a Quadcopter (May/June 2016)

Dear Editor,

The [Glenn Elmore, N6GN] article in the May/June issue of *QEX* was an excellent example of experimental measurements of the attenuation between two local antennas on 10 m when the height of one antenna is varied. Figure 5 in the article shows excess path loss above the expected free space path loss for antenna separations from 1000 ft to 10 mi. The author attributes the excess loss to the ground pushing the angle of peak radiation upward, and possibly additional loss due to intervening absorbers, such as trees, terrain and buildings.

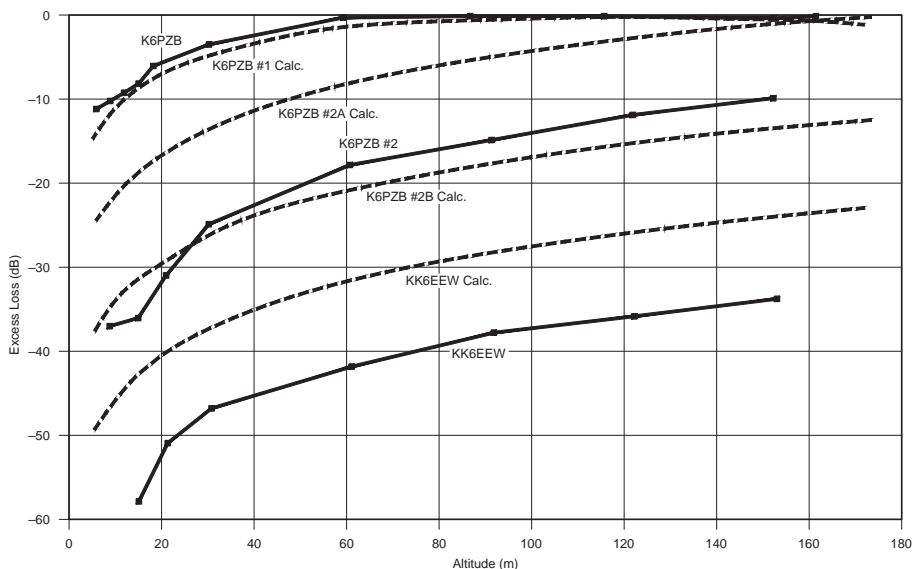
This note shows that most of the excess loss is primarily due to the interaction of lossy ground with the propagating electromagnetic (EM) wave. In free space EM energy falls off by 6 dB as you double the distance between two antennas. However, for local propagation with two antennas within a few wavelengths of lossy flat ground, a doubling of the separation distance decreases the signal by ~12 dB if everything else is kept the same.

I used the equations in this letter to predict the excess loss for several of the stations shown in Figure 5 of the *QEX* article. Since the variable height transmitting antenna was vertically polarized, I used only those receiving stations that were also vertically polarized. The conversion of vertical to horizontal polarization adds another uncertainty that I wished to avoid. I assumed

a flat average ground with $\epsilon_r = 13$ and $\sigma = 0.005$ S/m. Figure A shows three different sets of observations as the antenna height is varied from 5 to 150 m. The measurements designated K6PZB#1 were done at a separation distance of 1000 ft in a local park. The K6PZB antenna was a vertical dipole with the end a few feet above ground. The solid lines show the measurements, while the dashed lines are the predicted excess loss for two vertically polarized antennas. The two results closely agree. A slight adjustment of the lossy ground parameters could obtain a more precise agreement.

The measurements showed a slight dip at 140 to 160 m for the K6PZB#1 measurements. The theoretical calculations also show a decrease for altitudes above 140 m when you use the full reflection coefficient model.

The K6PZB#2 measurements done on a different day are shown as a solid line. In this case, K6PZB was setup on the top of a 100 ft hill 3 mi away with a line of sight view to the park. I ran two different estimates of the excess loss. In K6PZB#2A dashed line, I assumed that the hill was isolated feature on a flat plain. This would put the antenna about 3 wavelengths above the height of local ground. In K6PZB#2B dashed line, I assumed that the hill was a gradual rise from the park, which would place the antenna a few tenths of a wavelength above ground for the propagation path near the receiving antenna. These two results bound the measurements, but the gradual increase in height model is closer. While I don't know



QX1609-LettersA

From **MILLIWATTS**
To **KILOWATTS**

More Watts per Dollar



Transmitting & Audio Tubes



**COMMUNICATIONS
BROADCAST
INDUSTRY
AMATEUR**

Immediate Shipment from Stock

3CPX800A7	4CX1000A	810
3CPX1500A7	4CX1500B	811A
3CX400A7	4CX3500A	812A
3CX800A7	4CX5000A	833A
3CX1200A7	4CX7500A	833C
3CX1200D7	4CX10000A	845
3CX1200Z7	4CX15000A	6146B
3CX1500A7	4CX20000B	3-500ZG
3CX3000A7	4CX20000C	3-1000Z
3CX6000A7	4CX20000D	4-400A
3CX10000A7	4X150A	4-1000A
3CX15000A7	572B	4PR400A
3CX20000A7	805	4PR1000A
4CX250B	807	...and more!

Se Habla Español • We Export

Phone: **760-744-0700**

Toll-Free: **800-737-2787**

(Orders only) **RF PARTS**

Website: **www.rfparts.com**

Fax: **760-744-1943**

888-744-1943

Email: **rfp@rfparts.com**



the topography between the two locations, I would suspect that the hill is not an isolated feature.

The KK6EEW location is about 10 miles distant and the article notes it is not line-of-sight. The predicted excess loss is about 10 dB less than the actual loss shown as a solid line. There are probably diffraction effects from the intervening topography, which are contributing to the higher excess loss.

The shape of the predicted and measured excess loss curves agree in all three cases. In two of them it is possible to get good agreement with the measured loss using reasonable assumptions about the local terrain. It seems likely that most of the excess loss shown in Figure 5 is due to the interaction between the electromagnetic (EM) wave and lossy ground.

The equations to calculate excess path loss for two antennas elevated above flat lossy ground are as follow. The antennas are separated by a distance d and the height of their centers above ground are h_1 and h_2 . There are two components to the path loss between the antennas: the free space path loss given by $20\log_{10}(4\pi d/\lambda)$ and the path loss due to the interaction between the electromagnetic wave and ground, which we will call excess path loss (EPL).

The following calculation is based on the Method of Images. This set of equations assumes a flat lossy ground, and $d > 5(h_1 + h_2)$, which implies they are valid for reflection angles less than 10 degrees.

$$P_{diff} = \frac{2h_1h_2}{d\lambda}, \text{ and } R_{slope} = \frac{h_1 + h_2}{d}.$$

P_{diff} is the path length difference between the direct and reflected waves in wavelengths, R_{slope} is the slope of the reflected wave and should be less than 0.2 for these equations, and λ is the wavelength in the same units as d and h .

A horizontally polarized antenna will reflect 99% of the EM wave for these grazing reflection angles, but it inverts the phase

by 180 degrees. The excess path loss EPL_H for horizontally polarized antennas is,

$$EPL_H = 20\log_{10} \left(\sqrt{\left\{1 - \cos(2\pi P_{diff})\right\}^2 + \left\{\sin(2\pi P_{diff})\right\}^2} \right).$$

A vertically polarized antenna will refract some of the EM wave into the ground where it is dissipated as heat. The reflected wave will be reduced in amplitude and phase shifted depending on the reflection angle. The reflected magnitude R_{mag} and reflected phase R are calculated for average ground, and for the 10 m band, but provide good estimates of excess path loss from 80 m through 6 m.

$$R_{mag} = 1 - 7.35488R_{slope} + 22.0086R_{slope}^2 - 33.3939R_{slope}^3$$

$$R_{\phi} = -\pi + 1.12604R_{slope} - 8.01175R_{slope}^2 + 55.8017R_{slope}^3$$

The excess path loss EPL_V for a vertically polarized antennas may be computed by

$$EPL_V = 20\log_{10} \left(\sqrt{\left\{1 + R_{mag} \cos(R_{\phi} - 2\pi P_{diff})\right\}^2 + \left\{R_{mag} \sin(R_{\phi} - 2\pi P_{diff})\right\}^2} \right).$$

These equations have been checked against the 2015 version of the Numerical Electromagnetic Code. The excess path loss calculations agree within 1 dB for horizontally polarized antennas and 2 dB for vertically polarized antennas. — *John Grebenkemper, KI6WX, ARRL Technical Advisor.*

[The author replies]

John, thanks for taking the time to compare and comment. Just a bit of detail for your own consideration. As it turns out, K6PZB#2 and W6SFH are both an a fairly isolated hill. While there might be a bit of gradual slope, I need to consult a more accurate map than I have readily available, but I expect that the ground is within 30 feet or less of constant until the last 1/4 mi to W6SFH's hill where it rises pretty rapidly. His call book address and that of N6GN are close to describing the two locations, though the park is actually about 1/4 mi east of N6GN, and K6PZB#2 was about 600 ft NW of W6SFH.

KK6EEW's antenna factor is a bit of an unknown and could possibly account for the 10 dB. He was using a 5 foot whip (the only one, I failed to notice that the graphics in the article had all stations using this antenna) with a high-Z preamp. But as I understand it, that preamp is a source follower so has no voltage gain. One would think that the com-

bination that it would be pretty similar to a dipole but that hasn't been carefully measured. For it to have 10 dB gain doesn't fit with what I think is inside it. I asked him to see if he could at least compare 10 m response with a dipole or quarter-wave whip some time but haven't yet heard of the results.

Still, for a fairly spur-of-the-moment pair of measurements it is gratifying that it matches theory so well. I'm still pondering the relation of this "lossy ground" interpretation to the foliage/obstruction loss we see at 70 cm (per the video referenced in the article). I've been considering this was due to vegetation/obstructions above the ground surface rather than the actual ground itself. I wouldn't expect 70 cm and 10 m to have identical ground effects so maybe they shouldn't be compared this way.

Again, thanks for the added thoughts and discussion. It's interesting stuff! — *Best, Glenn Elmore, N6GN.*

(July 16, 2016)

Dear Editor

I look forward to my QEX every two months. Most of the articles impress me with their analysis, while some seem to be beyond my current technical grasp, and many of them way beyond. But, that is one of the factors that keep me interested and stretches me.

In most issues I see the request for submission of articles. Oh, how I wish I could submit something. Please keep up the good work. — *Gordon Duff, KA2NLM, Chapel Hill, NC.*

Send your QEX Letters to the Editor to, ARRL, 225 Main St., Newington, CT 06111, or by fax at 860-594-0259, or via e-mail to qex@arri.org. We reserve the right to edit your letter for clarity, and to fit in the available page space. "Letters to the Editor" may also appear in other ARRL media. The publishers of QEX assume no responsibilities for statements made by correspondents.



Statement of Ownership, Management, and Circulation
POSTAL SERVICE® (All Periodicals Publications Except Requester Publications)

1. Publication Title QEX	2. Publication Number 0 8 8 6 - 8 0 9 3	3. Filing Date October 1, 2016
4. Issue Frequency Bi-Monthly: Jan/Mar/May/July/Sept/Nov	5. Number of Issues Published Annually 6	6. Annual Subscription Price \$24.00
7. Complete Mailing Address of Known Office of Publication (Not printer) (Street, city, county, state, and ZIP+4®) 225 Main Street, Newington, Hartford County, CT 06111-1494		Contact Person Yvette Vinci Telephone (include area code) 860.594.0257
8. Complete Mailing Address of Headquarters or General Business Office of Publisher (Not printer) 225 Main Street, Newington, CT 06111-1494		

9. Full Names and Complete Mailing Addresses of Publisher, Editor, and Managing Editor (Do not leave blank)
 Publisher (Name and complete mailing address)
American Radio Relay League, Inc., 225 Main Street, Newington, CT 06111-1494

Editor (Name and complete mailing address)
Kazimierz "Kai" Siwiak, 225 Main Street, Newington, CT 06111-1494

Managing Editor (Name and complete mailing address)
Kazimierz "Kai" Siwiak, 225 Main Street, Newington, CT 06111-1494

10. Owner (Do not leave blank. If the publication is owned by a corporation, give the name and address of the corporation immediately followed by the names and addresses of all stockholders owning or holding 1 percent or more of the total amount of stock. If not owned by a corporation, give the names and addresses of the individual owners. If owned by a partnership or other unincorporated firm, give its name and address as well as those of each individual owner. If the publication is published by a nonprofit organization, give its name and address.)

Full Name	Complete Mailing Address
American Radio Relay League, Inc.	225 Main Street, Newington, CT 06111-1494

11. Known Bondholders, Mortgagees, and Other Security Holders Owning or Holding 1 Percent or More of Total Amount of Bonds, Mortgages, or Other Securities. If none, check box None

Full Name	Complete Mailing Address

12. Tax Status (For completion by nonprofit organizations authorized to mail at nonprofit rates) (Check one)
 The purpose, function, and nonprofit status of this organization and the exempt status for federal income tax purposes:
 Has Not Changed During Preceding 12 Months
 Has Changed During Preceding 12 Months (Publisher must submit explanation of change with this statement)

PS Form 3526, July 2014 (Page 1 of 4 (see instructions page 4)) PSN 7530-01-000-9931 PRIVACY NOTICE: See our privacy policy on www.usps.com

13. Publication Title		14. Issue Date for Circulation Data Below	
QEX		Sept/Oct 15-July/Aug 16	Sept/Oct 2016
15. Extent and Nature of Circulation		Average No. Copies Each Issue During Preceding 12 Months	No. Copies of Single Issue Published Nearest to Filing Date
a. Total Number of Copies (Net press run)		6958	6900
b. Paid Circulation (By Mail and Outside the Mail)	(1) Mailed Outside-County Paid Subscriptions Stated on PS Form 3541 (include paid distribution above nominal rate, advertiser's proof copies, and exchange copies)	4456	4392
	(2) Mailed In-County Paid Subscriptions Stated on PS Form 3541 (include paid distribution above nominal rate, advertiser's proof copies, and exchange copies)	0	0
	(3) Paid Distribution Outside the Mails Including Sales Through Dealers and Carriers, Street Vendors, Counter Sales, and Other Paid Distribution Outside USPS®	1249	1187
	(4) Paid Distribution by Other Classes of Mail Through the USPS (e.g., First-Class Mail®)	577	461
c. Total Paid Distribution (Sum of 15b (1), (2), (3), and (4))		6282	6043
d. Free or Nominal Rate Distribution (By Mail and Outside the Mail)	(1) Free or Nominal Rate Outside-County Copies included on PS Form 3541	59	58
	(2) Free or Nominal Rate In-County Copies included on PS Form 3541	0	0
	(3) Free or Nominal Rate Copies Mailed at Other Classes Through the USPS (e.g., First-Class Mail)	86	69
	(4) Free or Nominal Rate Distribution Outside the Mail (Carriers or other means)	83	82
e. Total Free or Nominal Rate Distribution (Sum of 15d (1), (2), (3) and (4))		228	209
f. Total Distribution (Sum of 15c and 15e)		6509	6252
g. Copies not Distributed (See Instructions to Publishers #4 (page #3))		449	648
h. Total (Sum of 15f and g)		6958	6900
i. Percent Paid (15c divided by 15f times 100)		96.50%	96.66%

* If you are claiming electronic copies, go to line 16 on page 3. If you are not claiming electronic copies, skip to line 17 on page 3.



Statement of Ownership, Management, and Circulation
(All Periodicals Publications Except Requester Publications)

16. Electronic Copy Circulation	Average No. Copies Each Issue During Preceding 12 Months	No. Copies of Single Issue Published Nearest to Filing Date
a. Paid Electronic Copies		
b. Total Paid Print Copies (Line 15c) + Paid Electronic Copies (Line 16a)		
c. Total Print Distribution (Line 15f) + Paid Electronic Copies (Line 16a)		
d. Percent Paid (Both Print & Electronic Copies) (16b divided by 16c × 100)		


I certify that 50% of all my distributed copies (electronic and print) are paid above a nominal price.

17. Publication of Statement of Ownership

If the publication is a general publication, publication of this statement is required. Will be printed in the **November/December 2016** issue of this publication. Publication not required.

18. Signature and Title of Editor, Publisher, Business Manager, or Owner

Date

 Publisher

10/1/16

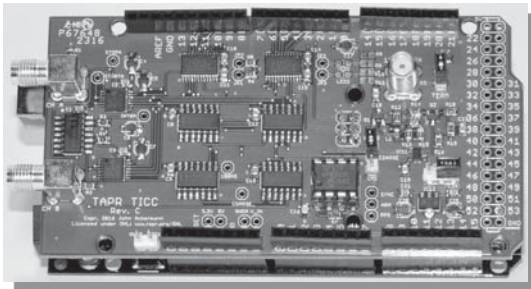
I certify that all information furnished on this form is true and complete. I understand that anyone who furnishes false or misleading information on this form or who omits material or information requested on the form may be subject to criminal sanctions (including fines and imprisonment) and/or civil sanctions (including civil penalties).



20M-WSPR-Pi is a 20M TX Shield for the Raspberry Pi. Set up your own 20M WSPR beacon transmitter and monitor propagation from your station on the wspnnet.org web site. The TAPR 20M-WSPR-Pi turns virtually any Raspberry Pi computer board into a 20M QRP beacon transmitter. Compatible with versions 1, 2, 3 and even the Raspberry Pi Zero!

TAPR is a non-profit amateur radio organization that develops new communications technology, provides useful/affordable hardware, and promotes the advancement of the amateur art through publications, meetings, and standards. Membership includes an e-subscription to the *TAPR Packet Status Register* quarterly newsletter, which provides up-to-date news and user/technical information. Annual membership costs \$25 worldwide. Visit www.tapr.org for more information.

NEW!



The **TICC** is a two channel counter that can time events with 60 **picosecond** resolution. It works with an Arduino Mega 2560 processor board and open source software. Think of the most precise stopwatch you've ever seen, and you can imagine how the TICC might be used. The TICC will be available from TAPR in early 2017 as an assembled and tested board with Arduino processor board and software included.

TICC
High-resolution 2-channel Counter



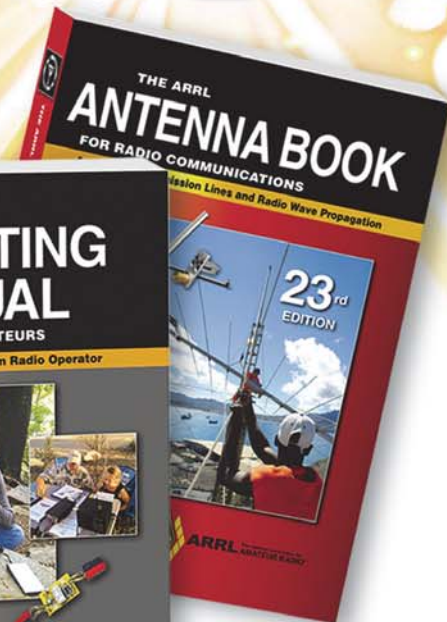
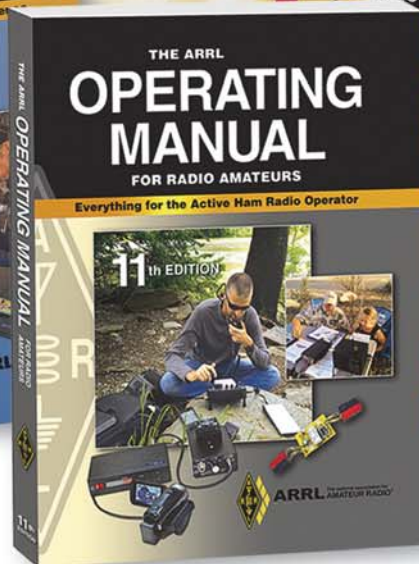
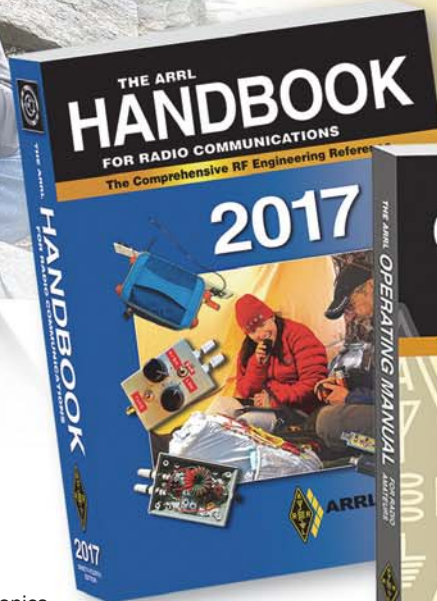
TAPR

PO BOX 852754 • Richardson, Texas • 75085-2754
Office: (972) 671-8277 • e-mail: taproffice@tapr.org
Internet: www.tapr.org • Non-Profit Research and Development Corporation

The POWER of 3

Three Books Every
Radio Amateur Should Have

3



NEW! ARRL Handbook 2017 Edition

The **ARRL Handbook** is the standard for applied theory and practical information concerning the fundamentals of radio electronics and wireless communications. It's filled with the most up-to-date knowledge representative of the wide and ever-expanding range of interests among radio amateurs. There are hands-on projects for all skill levels, from simple accessories and small power supplies, to legal-limit amplifiers and high-gain antennas.

New projects and information

- High-Performance IF and Dual-band Preamp Project
 - RTL-SDR Receiver Project
 - 30, 17 and 12 Meter Antenna Projects
 - Raspberry Pi Network Server/Client for Antenna Rotators
- Handbook 2017 Edition. Book and CD-ROM

Hardcover. ARRL Item No. 0635.

Bonus Offer! Only \$49.95* Retail ~~\$59.95~~

Softcover. ARRL Item No. 0628. Retail **\$49.95**

NEW! ARRL Operating Manual 11th Edition

The **ARRL Operating Manual** is the most comprehensive guide to Amateur Radio operating — everything you need to get involved, get active, and get on the air. Each topic has been written and updated by experienced hams. They are happy to share what they have learned so that you can get involved too.

Includes

- Basic Station and Operating Techniques
- Radio Clubs and Public Service
- On-Air Activities and Radiosport
- Resources for the Active Ham

Operating Manual 11th Edition.

Softcover. ARRL Item No. 0598. **Only \$24.95**

ARRL Antenna Book 23rd Edition (2015)

Everything you need to design your own complete antenna system.

The **ARRL Antenna Book** covers antenna theory, design and construction, and practical treatments and projects. Includes hundreds of antenna designs: wire, vertical, portable and mobile, and new high-performance VHF/UHF Yagi designs.

Antenna Book 23rd Edition. Book and CD-ROM

Hardcover. ARRL Item No. 0390.

Bonus Offer! Only \$49.95* Retail ~~\$59.95~~

Softcover. ARRL Item No. 0444. Retail **\$49.95**

*Actual dealer prices may vary. Shipping and handling charges apply. Sales Tax is required for all orders shipped to CT, VA, and Canada. Prices and product availability are subject to change without notice.



www.arrl.org/Power-of-3

Toll-Free US 888-277-5289,
or elsewhere +1-860-594-0355

Quicksilver Radio

Portable Power Solutions



Portable to go or backup in the shack. Includes powerpoles, bright easy to read voltmeter, & lighted switch. Different models in stock.

Portable EmComm Stations



Ready to Go. Our new Hammo-Can™ line is a complete VHF-UHF station in a box. New! Get them with or without radios installed. Fits most FM mobiles & several HF radios, too. Powerpoles, USB & lighter socket included.

Play-Series™



Customize your new Ham shack or Go Kit with our meters and power modules. Easy to install and connect with your existing setup.

Happy Holidays From Your Friends at Quicksilver Radio!

More Ham Radio stuff than anybody. Something for every Ham in the house.



Low Loss Coax



Poor quality coax can easily eat up half of your signal or more. We carry a wide variety of high quality low loss feedline. And it's 100% USA made!

Powerpole Connectors

The standard for DC power connections. Power distribution, pre-built cables, mounts & more.



Get All Your Ham Radio Holiday Gifts From Quicksilver Radio. Safe and Secure Ordering at:

www.qsradio.com



